Myoglobin expression improves T cell metabolism and antitumor effector function

Inaugural-Dissertation

For the attainment of the academic degree

Doctor of Natural Sciences (Dr. rer. Nat.)

Submitted to

Faculty of Mathematics and Natural Sciences

Heinrich-Heine-University, Düsseldorf

Submitted by

Julia Otto

From Neuss, Germany

Düsseldorf, 21.01.2026

Conducted at:

Institute of Molecular Medicine II

Heinrich-Heine-University, Düsseldorf

Printed with the permission of the Faculty of Mathematics and Natural Sciences of Heinrich-Heine-University, Düsseldorf

Supervisor:

1. Prof. Dr. Philipp Lang, Institute of Molecular Medicine II

2. Prof. Dr. Ingo Drexler, Institute of Virology

Day of the oral defence: 27.05.2026

During this thesis the following papers have been published:

1. ´Deep Transfer Learning Approach for Automatic Recognition of Drug Toxicity and Inhibition of SARS-CoV-2`, Werner and Kronberg *et al*., Viruses, 2021 [1]
2. ´A Hybrid Soluble gp130/Spike-Nanobody Fusion Protein Simultaneously Blocks Interleukin-6 *trans*-Signaling and Cellular Infection with SARS-CoV-2`, Ettich *et al*., Journal of Virology, 2022 [2]
3. ´Constitutive Activation of gp130 in T Cells Results in Senescence and Premature Aging`, Rafii *et al*., Journal of Immunology 2023 [3]
4. ´Bispecific soluble cytokine receptor-nanobody fusions inhibit Interleukin (IL-)6 trans-signaling and IL-12/23 or tumor necrosis factor (TNF) signalling`, Gesiorowski and Ettich *et al*., Journal of Biological Chemistry, 2023 [4]
5. ´The purinergic receptor P2X7 as a modulator of viral vector-mediated antigen cross-presentation`, Longo *et al*., Frontiers in Immunology, 2024 [5]
6. ´ Myoglobin expression improves T-cell metabolism and antitumor effector function` Werner *et al*., Journal for ImmunoTherapy of Cancer, 2025 [6]
7. ´Controlling mitochondrial membrane architecture via MIC60 determines viral replication to promote anti-viral immunity`, Katahira *et al*., Cell Reports, 2025 [7]
8. ´ Optimized arenaviruses with tumor-tropic mutations promote safe anti-tumor efficacy via sustainable immune modulatory properties`, Lang, Holnsteiner and Machlah *et al*., Cell Reports Medicine, 2025 [8]

This dissertation is based on the publication ´Myoglobin expression improves T-cell metabolism and antitumor effector function` in the Journal for ImmunoTherapy of Cancer from 2025 [6].

The authors contributed as followed: Julia Otto with 20%, Dr. Haifeng Xu with 15%, Georgios Theodorakis with 5%, Ichiro Katahira with 5%, Dr. Mitrajit Ghosh with 4%, Dr. Michał Gorzkiewicz with 4%, Luisa de Sousa Santos with 3%, Dr. Ann Kathrin Bergmann with 3%, Prof. Dr. Max Anstötz with 3%, Anne Busch with 3%, Dr. Diran Herebian with 3%, Prof. Dr. Sascha Dietrich with 3%, PD Dr. Carsten Berndt with 3%, Prof. Dr. Ertan Mayatapek with 3%, Prof. Dr. Aleksandra Pandyra with 4%, Prof. Dr. Dirk Brenner with 4% and Prof. Dr. Philipp Lang with 15%.

Table of Content

List of abbreviations

Abbreviation	Full description
·OH	hydroxyl radical
$^1O_2$	singlet oxygen
2-DG	2-Deoxy-D-glucose
AA	Antimycin A
ACT	adoptive cell transfer
ADAP	Adhesion and Degranulation-promoting Adapter Protein
ADC	anti-drug conjugate
ADP	adenosine diphosphate
Akt	Protein kinase B
ALL	acute lymphoblastic leukemia
AMPK	Adenosine Monophosphate-activated Kinase
AP-1	Adaptor Protein 1
Apaf-1	apoptotic protease-activating factor-1
APC	Antigen presenting cells
Arp2/3	Actin-related protein 2/3 complex
ATP	adenosine triphosphate
BAD	Bcl-2 associated agonist of cell death
Bad	Bcl-2-associated death promoter
BAK	Bcl-2 homologous antagonist/killer
BAX	Bcl-2-like protein 4
BCL10	B-cell lymphoma/leukemia 10
Bcl	B-cell lymphoma
BCR	B cell receptor
BID	BH3-interacting domain death agonist protein
BiTE	bispecific T cell engager
BOK	Bcl-2-related Ovarian Killer
BRCA	Breast cancer, early onset
CAD	Caspase-Activated DNase
CAFs	Cancer associated fibroblasts

CAR	chimeric antigen receptor
CARDs	caspase recruitment domains
CARMA1	Caspase Recruitment Domain-containing Membrane-Associated Guanylate Kinase Protein 1
CCR7	C-C chemokine receptor type 7
CD	Cluster of differentiation
CD40L	CD40 ligand
CD62L	L-selectin
Cdc42	Cell division control protein 42 homolog
CEACAM1	carcinoembryonic antigen-related cell adhesion molecule 1
Chk1	Checkpoint Kinase 1
CIT	checkpoint immune therapy
CLIP	class II-associated invariant chain peptide
CO_2	carbon dioxide
CoA-SH	Coenzyme A-SH
CoQ	Coenzym Q; ubiquinone
$COQH_2$	ubiquinol
CREB	cAMP response element binding protein
CRS	Cytokine release Syndrome
CSCs	cancer stem cells
CTL	cytotoxic T cells
CTLA-4	Cytotoxic T-Lymphocyte Antigen 4
CXCR4	C-X-C chemokine receptor type 4
Cyt	Cytochromes
DAG	Diaglycerin
DCs	dendritic cells
ECM	extra cellular matrix
Elk-1	ETS-like protein 1
EMT	epithelial mesenchymal transition
EndMT	endothelial to mesenchymal transition
EOMES	Eomesodermin
ER	endoplasmic reticulum

Erk	extracellular signal-regulated kinase
Ery	Erythrocruorins
ETC	electron transport chain
FAD	flavin-adenin-dinukleotid
$FADH_2$	reduced form of flavin-adenin-dinukleotid
FCCP	Carbonyl cyanide-p-trifluoromethoxyphenylhydrazone
FDA	Food and Drug Administration
FMN	flavin mononucleotide
Foxp3	Forkhead-Box-Protein P3
G_1	first cell growth phase
G_2	secound growth phase
Gads	GRB2-related adapter downstream of Shc
GAP	GTPase-activating protein
GATA3	GATA-binding protein 3
G-CSF	Granulocyte Colony-Stimulating Factor
GDP	guanosine diphosphate
GEF	Guanine nucleotide exchange factor
GSH	Glutathione
GSSG	glutathione disulfide
GTP	guanosine triphosphate
Gzm	Granzyme
H_2O	water
H_2O_2	hydrogen peroxide
HBV	hepatitis B virus
Hcy	Hemocyanins
Heme	Hemoglobin
HIF	hypoxia induced factor
HPV	papillomavirus
HRE	hypoxic response elements
ICAD	Inhibitor of Caspase-Activated DNase
iCAFs	inflammatory cancer associated fibroblasts
ICAM-1	intercellular adhesion molecule 1

ICANS	immune effector cell-associated neurotoxicity syndrome
ICI	immune checkpoint inhibition
IFNGR1	Interferon-γ receptor 1
IFN	Interferon
IgG1	Immunoglobulin G1
IKK	IκB Kinase
IL	Interleukin
IL-2R	Interleukin-2 receptor
IL-7R	interleukin-7 receptor
IP_3	Inositol-1,4,5-triphosphat
irAEs	immune-related adverse events
ITAM	immunoreceptor tyrosine-based activation motifs
ITIM	immunoreceptor tyrosine-based inhibition motifs
iT_{reg}	induced regulatory T cells
ITSM	immunoreceptor tyrosine-based switch motif
IκBα	Inhibitor of κBα
JAK	Janus Kinase
JNK	Jun kinase
Keap1	Kelch-like ECH associated protein 1
KLRG1	killer cell lectin-like receptor subfamily G member 1
KRAS	Kirsten rat sarcoma viral oncogene homolog
KSR	kinase suppressor of Ras
LANUV	State Agency for Nature, Environment and Consumer Protection
LAT	linker for activation of T cells
Lck	Lymphocyte-specific protein tyrosine kinase
LDH	lactate dehydrogenase
Leg	Leghemoglobin
LFA-1	lymphocyte function-associated antigen 1
LT-α	Lymphotoxin alpha
M	mitosis
mAbs	monoclonal antibodies

MALT1	Mucosa-Associated Lymphoid Tissue Lymphoma Translocation Protein 1
MAPK	Mitogen-Activated Protein Kinase
Mb	Myoglobin
MbO_2	oxymyoglobin
MEK1	MAPK/ERK kinase 1
MHC	Major Histocompatibility Complex
MIC	MHC class I polypeptide–related gene
MMP1	matrox metalloproteinase 1
mTOR	mechanistic Target of Rapamycin
myCAFs	myofibroblastic cancer associated fibroblasts
NAD	Nicotinamide adenine dinucleotide
NADH	Nicotinamide adenine dinucleotide plus hydrogen
Nck	Non-catalytic region of tyrosine kinase adaptor protein
NFAT	Nuclear Factor of Activated T cells
NF-κB	Nuclear Factor kappa-light-chain-enhancer of activated B cells
NKG2D	Natural Killer Group 2 member D
NK cells	natrual killer cells
NKT cells	natural killer T cells
NNT	nicotinamide nucleotide transhydrogenase
Nox	NADPH oxidase
Nrf2	nuclear factor erythroid 2-related factor 2
nT_{reg}	natural Treg cells
$O_2^{\cdot -}$	Superoxide anion radical
OBP	oxygen binding protein
OCR	Oxygen Consumption rate
ORAI1	Calcium release-activated calcium channel protein 1
OTOT	on-target off-target
OXPHOS	oxidative phosphorylation
PD-1	Programmed cell death protein 1
PDK1	phosphoinositol-dependent kinase 1
PD-L	Programmed Death Ligand

PEP	phosphoenolpyruvate
PER	proton efflux rate
PH	Pleckstrin Homology
PI3K	Phosphoinositide-3 kinase
PIP_2	phosphatidylinositol 4,5-bisphosphate
PIP_3	phosphatidylinositol-3,4-5-triphosphate
PKC-θ	protein kinase C-θ
PLC-γ	Phospholipase C-γ
Prx	Class III peroxidase
PTEN	Phosphatase and tensin homolog
Raf	Rapidly Accelerated Fibrosarcoma kinase
Rap1	Ras-proximate-1 or Ras-related protein 1
Ras	Rat sarcoma virus
RB	retinoblastoma
Rheb	Ras homolog enriched in brain
RIAM	Rap1-GTP-interacting adapter molecule
RORγT	Retinoic acid-related orphan receptor gamma T
ROS	reactive oxygen species
Rot	Rotenone
S	DNA replication phase
SASP	senescence-associated secretory phenotype
scFv	single-chain variable fragment
SDH	Succinat Dehydrogenase
SH2	Src Homology 2 domain
SHIP	SH2-containing inositol phosphatase
SHP	SH2-containing phosphatase
SHP-2	Src homology region 2 domain-containing phosphatase-2
SKAP	Src kinase-associated phosphoprotein
SLECs	short lived effector cells
SLP-76	SH2 domain-containing leukocyte protein of 76 kDa
SOD	superoxide dismutase
Src	Sarcoma

SRE	Serum-Response-Element
SRF	Serum-Response-Factor
STAT	Signal Transducer and Activator of Transcription
STIM1	Stromal Interaction Molecule 1
TAA	tumour-associated antigen
TAP	transporter associated with Antigen Processing
TCA	tricarboxylic acid
TCF-1	T cell factor-1
T_{cm}	Central memory T cells
TCR	T cell receptor
T_{eff}	Effector T cells
T_{em}	effector memory T cells
TEM	transmission electron microscopy
T_{FH}	follicular T helper cells
TGF-β	Transforming Growth Factor Beta
Th	T helper cell
TILs	Tumor infiltrating lymphocytes
Tim-3	T-cell immunoglobulin and mucin-domain containing-3
TM	transmembrane
TME	tumor microenvironment
TNF	Tumor necrosis factor
TNFR	Tumor necrosis factor receptor
TOX	thymocyte selection-associated HMG box
TRAF	TNF Receptor-Associated Factor
TRAIL-R2	TNF-Related Apoptosis-Inducing Ligand Receptor 2
T_{rm}	tissue-resident memory T cells
TRUCKS	T cells redirected for antigen-unrestricted cytokine-initiated killing
Trx	Thioredoxin
Trx_{ox}	oxidized Thioredoxin
TrxR	Thioredoxin reductase
Trx_{red}	reduced Thioredoxin
TSC	Tuberous Sclerosis Complex

U.S.	United States
Vav1	Vav guanine nucleotide exchange factor 1
VEGF	vascular endothelial growth factor
V_H	variable heavy chain
VHL	von Hippel-Lindau
V_L	variable light chain
WASp	Wiskott-Aldrich syndrome protein
WHO	World Health Organisation
WIP	WASp-interacting protein
ZAP-70	ζ chain-associated protein 70
ZETT	Central Institution for Animal Research and Scientific Animal Welfare
α	alpha
α-SMA	α-smooth muscle actin
β	beta
γ	Gamma
δ	Delta
ζ	Zeta

1. Summary

The tumor microenvironment (TME) is frequently hypoxic and characterized by a scarcity of nutritional resources including a shortage of glucose. As effector T cells have high energy demands, tumor metabolism can contribute to T cell dysfunction and exhaustion. Overcoming hypoxic conditions and improving the antitumor effector function of T cells represents a key challenge in the treatment of solid tumors. In the present study, we investigate whether intracellular oxygen availability can improve metabolic fitness and effector functions of T cells in solid tumors. We demonstrate that Myoglobin (Mb) overexpression in T cells not only boost oxidative phosphorylation (OXPHOS), but also increases the glycolytic activity and tricarboxylic acid (TCA) metabolites, resulting in elevated adenosine triphosphate (ATP) levels. This metabolic reprogramming is accompanied by structural remodelling of the mitochondria, including elongated and denser cristae and therefore indicating enhanced metabolic capacity. Mb expression further supports the differentiation in effector T cells, increases proliferation and reduces the expression of hypoxia induced factor (HIF)-1α, a key transcriptional factor regulating hypoxic response elements (HRE), *in vitro*. Additionally, Mb-expressing T cells exhibit a reduced exhaustive phenotype and appear to display prolonged survival and homeostasis, thereby improving their antitumor potential *in vivo*. Interestingly, despite the higher oxygen availability, Mb-expressing T cells show increased reactive oxygen species (ROS) scavenging capacity, maintaining redox balance and supporting effector function without compromising survival. We further demonstrate that Mb expression increases the production of effector cytokines, such as Interferon (IFN)-γ, Tumor necrosis factor (TNF)-α and Granzyme (Gzm) B, leading to an enhanced cytotoxicity against tumor cells both *in vitro* and *in vivo*.

Adoptive transfer of Mb-overexpressing cytotoxic T cells into syngeneic tumor models significantly reduced the tumor growth and improved the T cell infiltration and persistence. These effects were observed in two different tumor models and with reduced T cell numbers, highlighting the translational potential for adoptive T cell therapies. Further, Mb-expression also remodels the TME by reducing epithelial-mesenchymal transition (EMT)-associated marker, suggesting a potential role in limiting metastatic progression.

While Mb reduced exhaustion-associated transcription factors such as thymocyte selection-associated HMG box (TOX), the expression of the surface markers Programmed cell death protein 1 (PD-1) and T-cell immunoglobulin and mucin-domain containing-3 (Tim-3) was

unexpectedly significantly increased *in vivo*. Therefore, Mb-expressing T cells were combined with PD-1 checkpoint inhibition, resulting in a significant reduction in tumor growth. All in all, our data suggest that Mb-expression promotes metabolic resilience, effector differentiation and antitumor effector function under hypoxic conditions and providing therefore a promising strategy for improvement of T cell-based immunotherapies.

2. Introduction

Cancer is still a leading cause of death worldwide, with approximately 20 million new cases and 9.7 million deaths in 2022, according to the World Health Organisation (WHO) [9]. The most prevalent cancers in 2020 are breast cancer, lung cancer and colon and rectum cancer with 2.26 million, 2.21 million and 1.93 million new cases, respectively [10]. These numbers are supposed to increase in the future. Over 35 million new cases are expected in the year 2050, which corresponds to an increase of 77% [9].

Normal mammalian cells are characterised by maintaining physiological homeostasis, genomic stability and regulated metabolic activity and the ability to undergo apoptosis, as a protective mechanism when their normal function is compromised [11, 12]. This process can be triggered by various factors, such as DNA damage, mitochondrial dysfunction, or the presence of specific cytokines released by Th cells during an immune response [13-15]. Cells that contain gene deletions or mutations and evade apoptosis face the risk of transforming into tumor cells, potentially leading to cancer. Key examples include tumor suppressor genes such as p53, which regulates cell division and induces apoptosis, retinoblastoma protein (RB), which controls the cell cycle, and phosphatase and tensin homolog (PTEN), which inhibits cell proliferation [16-18]. Additionally, oncogenes can emerge from mutated proto-oncogenes, which normally regulate cell division, like Kirsten rat sarcoma viral oncogene homolog (KRAS), a gene that controls cell growth and division [19].

Over 100 different types of cancer are known which affect humans, often named after the organs in which they originate. A key distinction among different cancer types is whether they are so-called ‘hot’ and ‘cold’ tumours, which differ in their levels of tumour-infiltrating lymphocytes (TILs). In hot tumours, a higher presence of TILs triggers a more robust initial immune response compared to cold tumors [20]. The strength of this immune response, along with the stage of tumor progression, plays a significant role in determining the likelihood of successful treatment [20].

Cancer can be triggered or influences by biological factors. Increasing age represents one of the major risk factors, as the cellular capacity for DNA damage repair and epigenetic regulation, among other things, decline over time. However, cancer can also already occur during childhood. In addition, genders also play a decisive role in cancer incidence and progression [21]. Variations of hormone levels between men and women contribute to differences in both the susceptibility to and the frequency of non-gender specific cancers [22]. A cohort study

reports that the incidence of thyroid cancer is approximately 4.39 times higher in woman compared to men, which is partly due to excess of the thyroid-stimulating hormone (TSH) [22, 23]. Furthermore, environmental factors can influence the risk of developing cancer, like the infection with human papillomavirus (HPV) or hepatitis B virus (HBV), which leads to uterine cancer and liver cancer, respectively [24, 25]. In addition, lifestyle factors such as alcohol consumption and tobacco smoking further contribute to cancer risks, particularly for liver and lung cancer [10].

Mutations or DNA damages are leading cause of forming rapidly proliferating tumor cells, undergoing continuous changes. These changes pose a major challenge for cancer therapy, as they enable the tumor to evade the immune response and to continue growing. Thereby, new blood vessels are formed for better oxygen and nutrients support. With fast growing tumors these vessel formation is unstructured driven by the secretion of pro-angiogenetic factors such as vascular endothelial growth factor (VEGF) [26]. Rapidly proliferating cells require large amounts of energy and nutrients, leading to an increased uptake of resources from the surrounding microenvironment [27]. This creates a hypoxic environment that negatively affects TILs, leading to their exhaustion and loss of function [27]. As a result, tumor cells can no longer be effectively controlled by TILs [27]. An approach pursed in research is to overcome hypoxia and enhance the effector function of TILs. Especially, cytotoxic T cells, which can induce apoptosis in target cells by secreting perforins to permeabilize the cell membrane, are highly influenced by hypoxic conditions. A dysfunction or loss of T cell function allows tumor cell to rapidly proliferate and to evade the immune system [28]. Hypoxia poses a significant challenge: the lack of oxygen is associated with HIF-1α which leads to reprogramming of the T cells metabolism conducting the promotion of long-term exhaustion and cytotoxic T cell function loss [29]. Boosting the T cell metabolism can prolong the function and endurance in hypoxic tumor milieu because of higher energy availability despite oxygen deficiency. However, strong metabolic activation may also lead to increased formations of reactive oxygen species (ROS), which negatively impact T cell function [30]. To benefit from an induced metabolism, ROS scavenging might be as well a key player to cure cancer.

Therefore, we introduce the small oxygen binding protein (OBP) Mb into cytotoxic T cells to overcome hypoxic conditions and boosting T cell metabolism and effector functions in the tumor microenvironment (TME) of solid tumors. Mb is a small molecule predominantly in muscle cells with a higher affinity to oxygen than haemoglobin [31]. It is known for its oxygen transport and storage capacity [31]. T cells are known for its metabolomic changes due to its

cell division. Thereby they are switching from oxidative phosphorylation (OXPHOS) to aerobe glycolysis for an increased availability of biosynthetic building blocks to support cell division [32]. In turn, lactate production can inhibit T cell effector function, cytokine production and promote exhaustion [33].

Conventional tumor therapies such as surgery, radiation and chemotherapy have been historically used for the treatment of several cancer types, but also are impacting healthy cells leading to side effects. Modern therapies offer promising approaches, addressing many limitations of conventional therapies. Boosting the body's own immune system, mainly cytotoxic T cells, in order to achieve a highly specific pattern of action is one strategy. Cytotoxic T cells induce apoptosis in the corresponding target cells by means of the T cell receptor (TCR) binding the corresponding peptide: Major Histocompatibility Complex (MHC)-I by releasing perforins and granzymes [34]. This natural mechanism can be enhanced during different therapies. To boost T cell effector function checkpoint immune therapy (CIT) directed against exhaustion molecules on the T cell side or exhaustion ligands on the tumor side is used [35]. Also, adoptive cell transfer (ACT) has proven to be a promising approach [36]. One treatment option is the introduction of chimeric antigen receptors (CAR) in T cells, whereby the single-chain variable fragment (scFv) of the variable heavy (V_H) and light (V_L) chain of a monoclonal antibody are connected with signalling domains of the TCR [37]. Although, CART cells achieved a breakthrough in haematological malignancies, they are limited in their ability to combat solid tumors [38]. Physical barriers complicate the infiltration of CART cells in the tumor tissue. Further, the immunosuppressive TME including hypoxic conditions promoting exhaustion [39]. Therefore, novel T cell–based therapeutic strategies are urgently needed to overcome the remaining challenges in effective cancer treatment.

2.1. Hallmarks of Cancer

Due to different genotypes and phenotypes cancer is a highly complex disease. For more precise definition Robert A. Weinberg and Douglas Hanahan introduced the hallmarks of cancer. Originally six hallmarks were defined in 2000, expanded to ten in 2011 and 14 in 2022, respectively [40-42]. They are defined as characteristic features and abilities that are acquired through the cancer during malignant transformation and describe the development of cancer as a multi-stage process. Cancer is a disease in which cells acquire genetic mutations, leading to uncontrolled cell division and a failure to undergo apoptosis. To achieve this state the cells

exhibit hallmarks in order to be cancerous. ´*Self-sufficiency in growth signals*´, the first hallmark describes the ability of growing without external signals [40]. Here, cancer cells produce autocrine signals, by permanently activating signalling pathways, without relying on external growth factors [43]. Further, the tightly controlled cell division is switched off by alterations of important proteins leading to uncontrolled cell division [43]. Next, ´*Insensitivity to anti-growth signals*´ describes the resistance to tumor suppressor proteins that normally inhibit cell division [40]. The division of cells is controlled through the cell cycle, which is divided in a first cell growth phase (G_1), a DNA replication phase (S), a second growth phase (G_2) and the final cell division through mitosis (M) [44]. Resting cells remain functional in the quiescent G_0 phase and do not enter the cell cycle [44]. The progression through the cell cycle is tightly regulated by a series of checkpoints, like Checkpoint Kinase 1 (Chk1) that monitor the integrity of the genome and ensure that damaged DNA is repaired before replication or mitosis [45]. In cancerous cells, however, mutations are developed in the proteins recognizing DNA damage, leading to checkpoint failure and the propagation of genetic errors to daughter cells. [46]. ´*Evading programmed cell death*´, is the loss of the ability of self-destruction through apoptosis [40]. Defective cells undergo apoptosis in case of damaged or the loss of function in order to protect tissue homeostasis [47]. ´*Limitless replicative potential*´ further defines that cancer cells do not die after reaching the Hayflick limit, which is defined as around 40-60 divisions until a cell undergoes apoptosis [40]. With each cell division chromosomes lose parts of their Telomere structures, which works as a cap on the ends of the chromosomes protecting the DNA. By activating Telomerase in cancerous cells and prolonging the caps these cells get immortal [48]. ´*Sustained angiogenesis*´ is the formation of new blood vessels for oxygen and nutrients transport in the cancer [40]. The release of signal proteins, like VEGF under hypoxic conditions, which can bind to the receptors on endothelial cells leads to the malformed and tortuous blood vessels in the cancer [26]. Next, ´*Tissue invasion and metastasis*´ describes the metastasis to the surrounding tissues [40]. Therefore, cancerous cells have to enter the circulation of the lymphatic system by the loss of adhesion molecules like E-Cadherin, the reorganisation of the cytoskeleton or the acquisition of a more migrant phenotype (increasing C-X-C chemokine receptor type 4 (CXCR4)) allowing them to actively invade in surrounding tissues [49]. In 2011 ´*Deregulating cellular energetics*´ was added, describing the change of metabolism from highly efficient OXPHOS to inefficient glycolysis despite the presence of oxygen [41]. In order to compensate the negative energy balance, cancer cells burn a lot of glucose, known as Warburg effect. The glycosylation provides cancer cells with by-products such as amino acids and lipids which are essential for cell growth and cell division [32].

´Avoiding immune destruction´ describes the escape of the immune system in which cancerous cells can downregulate receptors for recognition on their cell surface or producing proteins to inhibit the immune cells directly [41]. For example, they can upregulate Programmed death-ligand (PD-L) 1, which binds PD-1 on leucocytes suppressing them or downregulate MHC-I presentation to not be recognized by cytotoxic T cells [50]. Next, *´Genome instability and mutation´* describes the unstableness of the genome resulting in a constant stream of alterations like mutations, duplications, deletions or chromosomal restrictions [41]. DNA repair mechanisms defects leading to uncontrolled changes in the DNA. These alterations can either be neutral, reducing the cancer cell fitness or beneficial for the cancer cell survival. However, the genomic instability is highly adaptable in curse of selection processes. Mutations in tumor suppressor genes such as Breast cancer, early onset (BRCA) 1 and BRCA2 can lead to these alterations [51]. *´Tumor-promoting inflammation´* describes the secretion of proinflammatory cytokines that support tumor growth and progression rather than protective immune functions [41]. This local inflammation allows the cancerous cells to spread more easily and break the extracellular matrix (ECM) barrier [52]. Lastly in 2022 four new hallmarks were added. *´Unlocking phenotypic plasticity´* defines the overcoming of terminal differentiation through dedifferentiation, blocked differentiation, or trans differentiation in cancerous cells [42]. This allows the cells to escape developmental limits. Next, *´Nonmutational epigenetic reprogramming´* describes the changes in gene activity without altering the DNA sequence [42]. It is a mechanism in normal development. The basis is often changing in the chromatin with for example methylations of the DNA. This influences the whole sections of the chromosomes and their transcription [53]. Next, *´Polymorphic microbiomes´* describes the influence of the microbiota in health and disease [42]. It has been shown that changes in the gut microbiome also have strong influence on cancer development. The microbiome has been shown to import nutrients into the body as part of metabolic homeostasis [54]. Last, *´Senescent cells´* is defined as the growth-arrest to protect the body against cancer [42]. But senescent cells can also promote cancer through the senescence-associated secretory phenotype (SASP) by secreting cytokines, chemokines and growth factors [55]. This promotes proinflammatory processes whereby changes in the tissue structure or immune invasion are possible outcomes [55].

2.2. Glycolysis

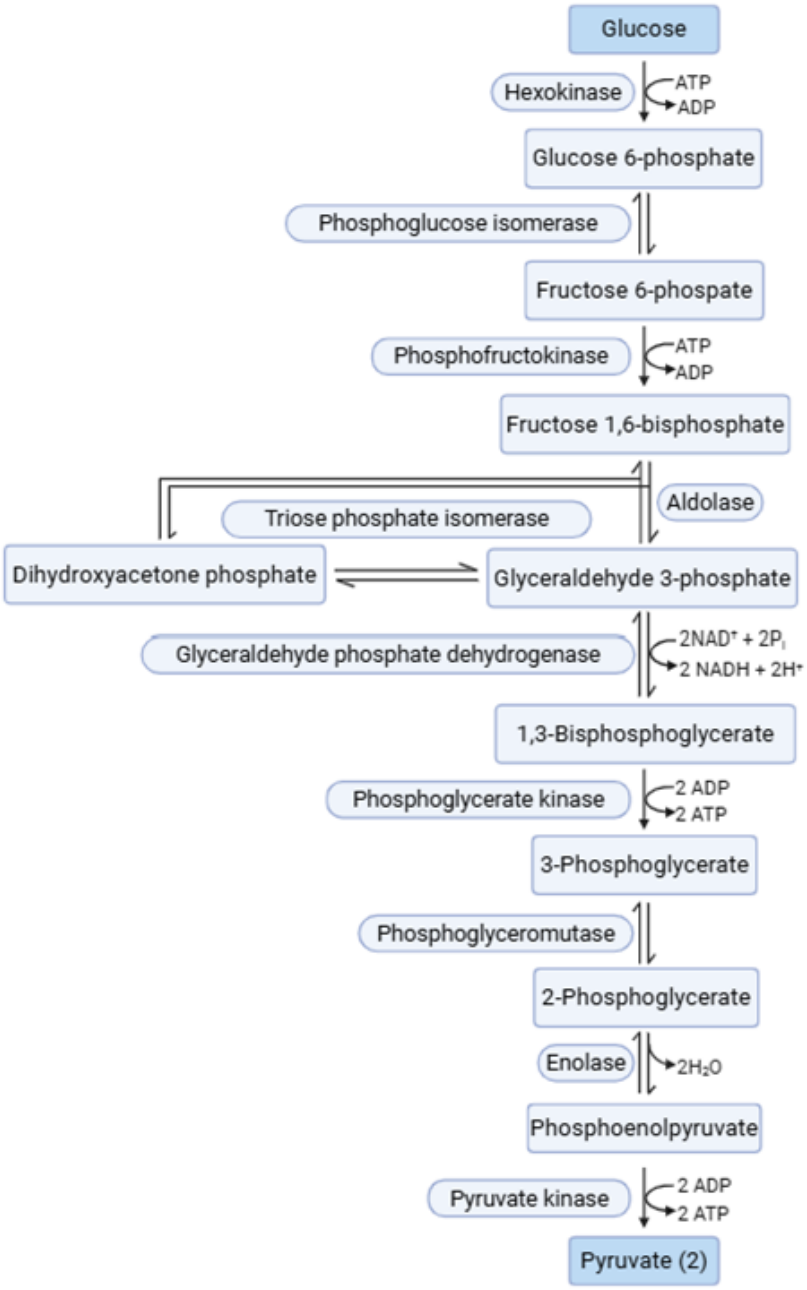

Figure 1: The glycolytic pathway. Schematic illustration of the glycolytic pathway, whereby glucose is transverted through a series of ten enzymatic steps into two molecules of pyruvate. The glycolysis yields two molecules of ATP and two molecules of NADH per molecule of glucose. Adapted from Chandel, 2021 [56].

The glycolysis is a highly conserved metabolic process to convert Glucose into Pyruvate, generating energy in form of ATP and Nicotinamide adenine dinucleotide plus hydrogen (NADH) in the Cytosol [57]. ATP is an energy source supporting many processes on the cellular level. By splitting off a phosphate group, energy is released and ATP is converted to a lower

energy form known as Adenosine diphosphate (ADP) [58, 59]. Nicotinamide adenine dinucleotide (NAD) can bind two H^+ ions for the higher energy form, by splitting of the H^+ ions in the electron transport chain (ETC) driving ATP synthase to convert ADP + P_i to ATP [56, 57]. The glycolysis can occur under both aerobic and anaerobic conditions in the cytoplasm, serving as a crucial source of energy for cells, especially under limiting oxygen conditions [32]. In this process, glucose, a six-carbon sugar, is catalysed with the loss of two ATP molecules to ADP in two Pyruvate molecules with the profit of four ATP and two NADH+H^+ [56, 57]. The cyclic glucose is converted into linear glucose 6-phosphate by the enzyme hexokinase by cleavage of one phosphate group through the loss of ATP to ADP. This reaction can be blocked by the inhibitor 2-Deoxy-D-glucose (2-DG) [60]. A further rearrangement takes place by means of phosphoglucose isomerase to Fructose 6-phosphate, which is converted to Fructose 1,6-bisphosphate by a further cleavage of a phosphate group through the loss of ATP to ADP under the enzyme phosphofructokinase [56]. After the three-step reaction that transverses glucose into fructose 1,6-biphosphate, the six-carbon sugar is split by fructose bisphosphate aldose into the two three-carbon sugars dihydroxyacetone phosphate and glyceraldehyde 3-phosphate. Both structures contain a phosphate group and can be interconverted by the enzyme triose phosphate isomerase [56]. Glyceraldehyde-3-phosphate dehydrogenase transforms glyceraldehyde 3-phosphate + NAD + P_i into 1,3-bisphosphoglycerate + NADH + H^+ [56]. The resulting 1,3-bisphosphoglycerate then undergoes phosphate group cleavage by phosphoglycerate kinase, yielding one ATP molecule [56]. The product 3-Phosphoglycerate is further converted to 2-phosphatoglycerate by phosphoglycerate mutase, followed by removal of an water (H_2O) molecule by the enolase enzyme, resulting in the product phosphoenolpyruvate (PEP) [56]. Finally, the pyruvate kinase cleaves off the last phosphate group, yielding in the production of one molecule of ATP and the intermediate product pyruvate [56]. Under anaerobic conditions pyruvate is converted with lactate dehydrogenase (LDH) and NADH + H^+ into the reduced NAD^+ and Lactate [56]. On the other hand, aerobic conditions lead to a further breakdown of pyruvate in the TCA cycle [32].

2.3. Tricarboxylic acid (TCA) cycle

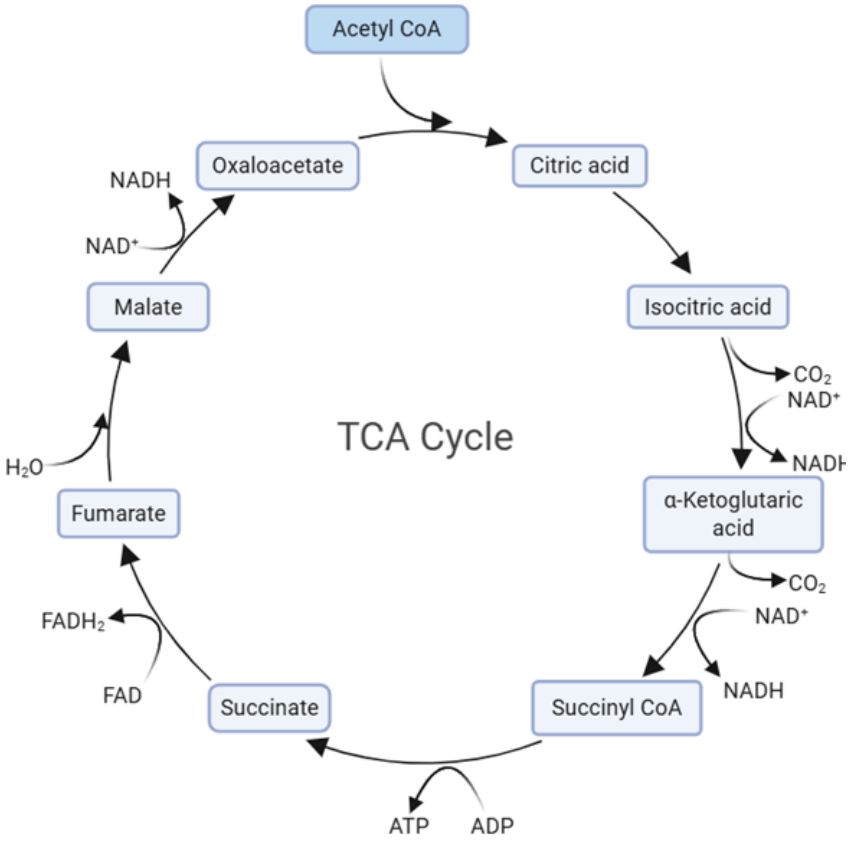

Figure 2: The TCA cycle. Schematic illustration of the TCA cycle, in which Acetyl-CoA is oxidized to CO_2 while generating NADH and $FADH_2$, as well as GTP and ATP. Adapted from Arnold *et al.*, 2023 [61].

TCA is a well conserved metabolomic process in the matrix of the mitochondria under aerobic conditions [61]. The cycle of biochemical reactions is used for oxidative degradation of organic substances for the purpose of energy production [61]. The intermediate product Pyruvate is transverted by pyruvate dehydrogenase with Coenzyme A-SH (CoA-SH) and NAD^+ to a two-carbon sugar Acetyl-CoA with the by-products of NADH + H^+ and carbon dioxide (CO_2) [62, 63]. Next Citrate synthase combines Acetyl-CoA and four-carbon sugar Oxaloactetate into the six-carbon sugar Citrate with the import of one water H_2O molecule and the loss of CoA-SH [61]. Further, Citrate is converted by Aconitase in a two-step reaction over cis-Aconitate to D-isocitrate [61]. Next, Isocitrate dehydrogenase converts the product into the five-carbon sugar α-ketogluterate and NADH + H^+ resulting in the loss of one CO_2 molecule [61]. α-ketogluterate, NAD+ and CoA-SH are transverted by α-ketogluterate dehydrogenase into NADH + H^+, CO_2 and the four carbon-sugar Succinyl-CoA [61]. Next, Succinyl-CoA synthetase converts Succinyl-CoA into Succinate by obtaining a guanosine triphosphate (GTP) molecule from

guanosine diphosphate (GDP) and P_i and by splitting off the CoA-SH region [61]. Succinate is converted into Fumarate by Succinat Dehydrogenase (SDH), during which two protons are transferred to flavin-adenin-dinukleotid (FAD), forming its more energetic reduced form of flavin-adenin-dinukleotid ($FADH_2$) [63]. FAD is a coenzyme involved in electron transfer within the ETC [61]. Next, Fumarate and H_2O are converted by Fumerase to Malate, which is further transformed by Malate dehydrogenase in Oxalacetat while obtaining NADH + H^+ [61]. Acetyl-CoA enters the cycle by combining Oxalacetat, thereby initiating a new cycle round [61]. The energy rich Coenzymes NADH + H^+ and $FADH_2$ will further be used for the generation of approximately 2.5 and 1.5 ATP molecules in the ETC [61].

2.4. Oxidative phosphorylation (OXPHOS)

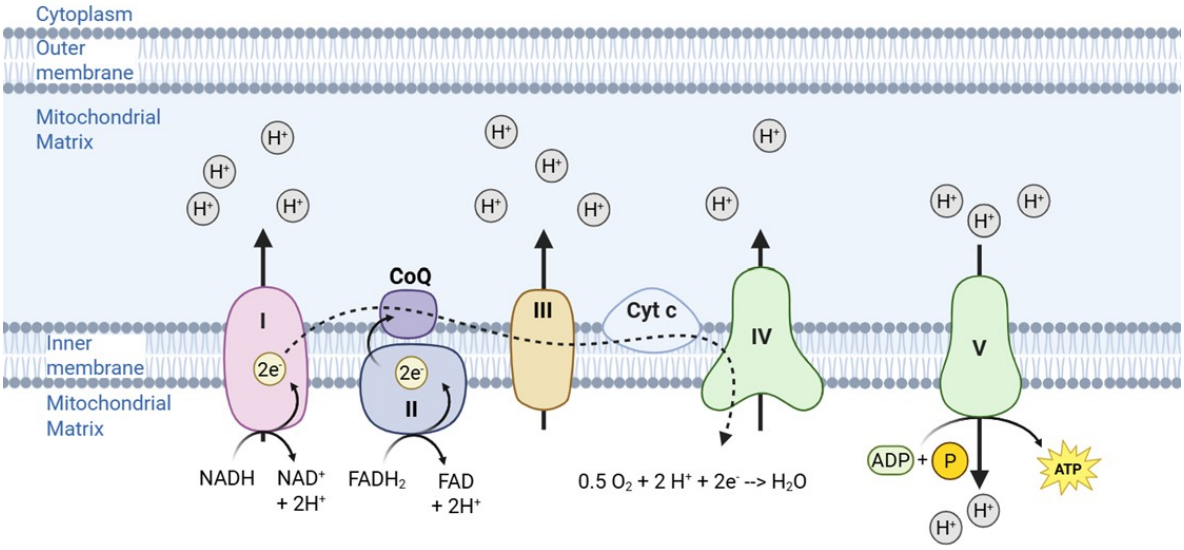

Figure 3: The five complexes of the ETC. Schematic illustration of the electron transfer through complexes I to IV and the associated pumping of protons across the inner mitochondrial membrane. This proton gradient drives ATP synthesis through Complex V, while electrons reduce molecular oxygen to water. Adapted from Zhao *et al*., 2019 [64].

The ETC is a series of protein complexes which transfer electrons for energy production located in the inner mitochondrial membrane. Here, electrons drive across an electrochemical gradient, which results in the excitation of ATP synthesis [65]. ETC consists of five main complexes. Thereby, electrons are transported across this series in the membrane, thus each electron donor

pass on electrons to higher redox potential. Each reaction is releasing energy for the stimulation of pumping protons in the intermembrane space to generate the proton gradient across the membrane [66]. The large L-shaped Complex I, a multi-subunit NADH ubiquinone oxidoreductase oxidizes NADH generated from the TCA to NAD^+ by reducing flavin mononucleotide (FMN) to $FMNH_2$ [67]. The electrons are further transported along Fe-S cluster to reach ubiquinone (Coenzyme Q (CoQ)) [67]. This electron flow leads to changes in the redox state and confirmation of complex I [67]. Four hydrogen ions are pumped in the intermembrane space and CoQ is reduced to ubiquinol ($COQH_2$) [68]. Rotenone is an inhibitor of complex I by inhibiting the transfer of electrons to CoQ [69]. Complex II, so called SDH, has four subunits (SDHA, SDHB, SDHC and SDHD) encoded by nuclear DNA [70]. Likewise, in the TCA cycle SDH oxidizes succinate to fumarate, while in OXPHOS it transfers electrons from succinate to ubiquinone via an Fe-S cluster [71]. The multiunit Complex III, so called cytochrome c reductase reduces cytochrome (Cyt) c by oxidation of CoQ. Also, four protons are pumped in the intermembrane space [72]. Antimycin A is an inhibitor of complex II by blocking the proton transport from CoQ to Cyt c [73]. Together with Rotenone (Rot) they shut down the ETC completely. In this case complex III can leak electrons resulting in superoxide formation [74]. Next, Complex IV, so called cytochrome c oxidase, removes four electrons from four molecules of cyt c resulting in reaction with H_2O [75]. Last, Complex V, known as ATP synthase, an ion channel in the mitochondrial matrix used the proton flux back generated through the mitochondrial gradient. By rotation the γ subunit of the ATP synthase, a conformational change is generated which leads to the reaction of $ADP + P_i + 2H^+ \rightarrow ATP\ H_2O + 2H^+$. [76]. Oligomycin A inhibits the ATP synthase by blocking the subunit F_O of the proton channel reducing the electron efflux [77]. Because of the proton leak, a mitochondrial decoupling occurs rather than a complete shutdown. Carbonyl cyanide-p-trifluoromethoxyphenylhydrazone (FCCP) acts as an uncoupling agent by transporting hydrogen ions through the mitochondrial membrane [78]. In seahorse analysis, the use of FCCP allows for the precise measurement of maximal respiration [79].

2.5. Tumor microenvironment (TME)

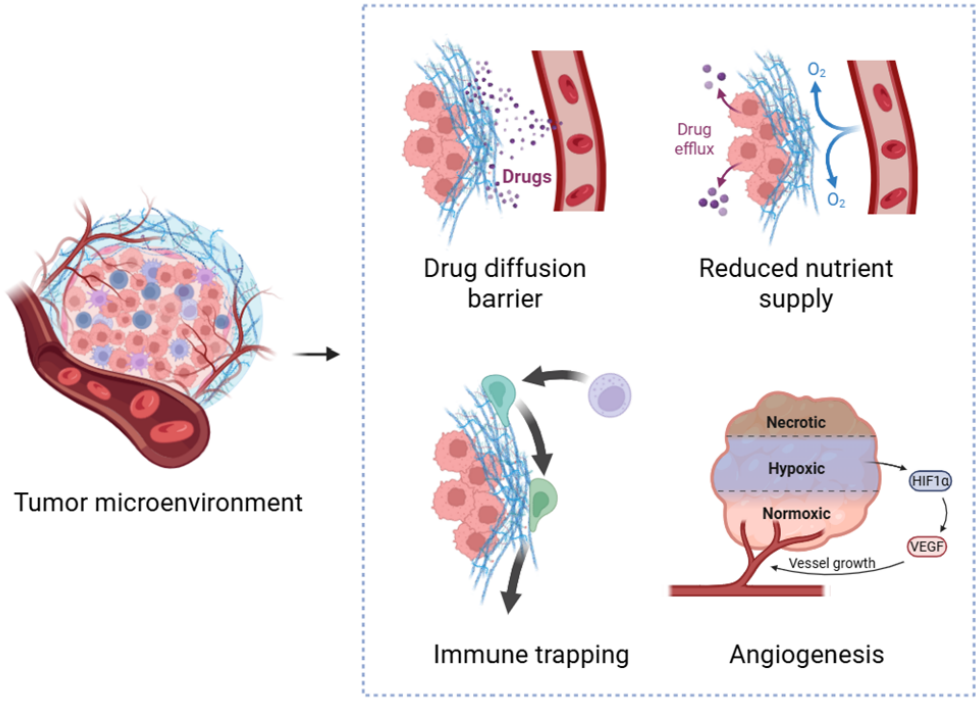

Figure 4: Challenges that reduce the therapeutic efficiency in solid tumors. Schematic illustration of key barriers imposed by the tumor TME. The dense ECM, composed of collagens, fibronectin, laminin, hyaluronic acid, and proteoglycans, provides mechanical stability but also forms a physical barrier that limits drug penetration into tumor tissue. In addition, the ECM restricts the diffusion of nutrients and oxygen, creating hypoxic conditions. Further, immune cells migrate along ECM structures, which can lead to immune trapping and thereby hinder effective immune-cell infiltration and effector function. Finally, hypoxia induces HIF-1α stabilization, which promotes VEGF-mediated angiogenesis. Collectively, these factors actively compromise therapeutic efficacy within the tumor site. Adapted from Wu *et al*., 2022 [80].

Tumor development is a highly heterogeneous process influenced by both intrinsic genetic alterations and extrinsic environmental factors [81]. The TME is a complex network composed of different cell types, molecules and structures that not only influence tumor growth and metastasis significantly but also play a crucial role in the response to therapeutic interventions. The TME consists of tumor cells, immune cells, epithelial cells and molecules. One subpopulation of tumor cells are the self-renewing cancer stem cells (CSCs). They have the potential to develop in different linages and extensively proliferation [82]. Thereby, CSCs can be capable to drive cancer growth, metastasis and to reconstruct tumor heterogeneity [83]. Also, CSCs often exhibit resistance to conventional cancer therapies, such as chemotherapy and radiation [84, 85]. Next, cancer associated fibroblasts (CAFs) are defined as a heterogenous

group of activated fibroblasts and a major component of stroma [86]. To maintain a continuously growth, tumor cells are recruiting CAFs, originated normal fibroblasts which undergoes genetic alteration [87]. Other potential origins are epithelial cells through epithelial-mesenchymal transition (EMT), mesenchymal cells and endothelial cells through endothelial to mesenchymal transition (EndMT) [87]. In pancreatic cancer two groups of CAFs were distinct inflammatory CAFs (iCAFs), which secrete pro-inflammatory cytokines such as Interleukin (IL)-6 and myofibroblastic CAFs (myCAFs), characterised by α-smooth muscle actin (α-SMA) expression and extracellular matrix support [88]. The stroma includes not only CAFs but also mesenchymal stem cells, adipocytes, and endothelial cells, the ECM and blood vessels, which are actively involved in the modulation of the tumor growth and progression, the metastasis and the immune modulation. Especially, Vimentin is expressed in mesenchymal cells during EMT to promote mobility and invasiveness, both of which are important for metastasis. When co-expressed with Cytokeratin 18, an epithelial marker of differentiated cells, metastasis is strongly promoted. Tumor cells will develop a hybrid EMT status supporting migration and invasion [89]. Studies have shown, that tumor patients with both markers co-expressed exhibit a poorer prognosis and higher likelihood of metastasis compared to patients with whose tumors express only one of the markers [90]. The ECM is known for its mechanic stability, tumor firmness and structural support. Furthermore, it enables the adhesion of tumor cells and influences their migration. The main components of the ECM include collagens, fibronectin, laminin, hyaluronic acid and proteoglycans. During tumor development, the ECM is constantly remodelled by enzymes released from tumor and stromal cells promoting tumor progression and invasion in surrounding tissues [91]. Additionally, the ECM acts as a physical barrier that impedes the diffusion of therapeutic drugs, limiting their ability to reach the tumor side [92]. Also, the dense of the ECM restricts the nutrient supply, promoting hypoxic conditions. The fast-proliferating tumor cells add to an increased energy demand, which are not able to be met in the TME [93]. Further, the ECM influences the immune defence by trapping immune cells resulting in reduced infiltration into the tumor side and promoting immune evasion [94]. Next, the angiogenesis is a crucial part of tumor progression. Growth factors like VEGF are released, resulting in the blood vessel formation [26]. These blood vessels are characterised trough their abnormal form and shape. In comparison to healthy tissue, blood vessels in the tumor side often leak and are badly structured, leading to an unbalanced nutrient and oxygen supply within the tumor tissue. This promotes hypoxic conditions and results in less effective therapies. Also, the unstructured vessel formation facilitates metastasis due to the easier access to the circulation for the tumor cells [95].

The tumor is defined by rapid and uncontrolled cell division, driven by genetic mutations and alterations in regulatory pathways, such as the cell cycle or tumor suppressors like p53 that normally control cell growth and replication [96]. To counteract, TILs migrate from the bloodstream into the TME and play a crucial role in the tumor response. TILs contain different immune cells among these are Macrophages (M1 and M2), natural killer cells (NK cells), natural killer T cells (NKT cells), T cells (Cluster of Differentiation (CD)4^+, $CD8^+$ and T_{reg}), B cells, dendritic cells (DCs), neutrophils and granulocytes [97].

2.6. Hypoxia in the Tumor microenvironment (TME)

The TME is generally immunosuppressive and contributes to immune dysfunction impairing anti-tumoral responses and T cell-based therapies. Specifically, tumor cells utilize aerobic glycolysis, thus limiting access to glucose and oxygen [98, 99] contributing to a dysregulated metabolic profile of effector T cells within the TME that might already be exhausted from chronic antigen stimulation. The increased glucose metabolism in tumor cells results in an increase of pyruvate and lactate production [99]. There exists a constant competition for glucose between the tumor and T cells, which can influence cancer progression [93]. Likewise, hypoxia can shape TME dynamics and immune cell infiltrates including T cells. Hypoxia gradients often develop within the TME due to the rapid proliferation of cancer cells outpacing the growth of new blood vessels resulting in inadequate oxygen supply to the tumor tissue [100]. Moreover, excessive or prolonged hypoxia can cause mitochondrial stress and mimic exposure to the tumor microenvironment driving T cells into an exhausted state [101]. Conversely, T cells conditioned by moderate hypoxia show increased effectivity against tumor cells [102] and HIF, whose expression is induced in response to hypoxia exposure, enhance effector T cell functions thereby limiting tumor growth in mice [103]. HIF-1α is regulated through post-translational modifications. Under normoxic conditions it is undergoing prolyl hydroxylation, forming a complex with von Hippel-Lindau (VHL) tumor suppressor protein, resulting in the ubiquitination and finally the proteasomal degradation [104, 105]. Under hypoxic conditions HIF-1α is stabilised in the cytosol following nuclear translocation and together with HIF-1β leads to transcription of hypoxic response elements (HRE) [106]. In a complimentary approach, pharmacological inhibition of HIF-1α can promote susceptibility towards checkpoint inhibition and reduce tumor growth suggesting that excessive HIF1α expression might curb T cell function [107]. Also, the transcriptional factor cAMP response element binding protein (CREB) together

with Nuclear Factor kappa-light-chain-enhancer of activated B cells (NF-κB) is triggered through hypoxia, the former through phosphorylation of Serine 133 by various kinases. CREB in turn regulated the matrix metalloproteinase 1 (MMP1), a collagenase which promotes the degradation of the ECM. High MMP1 levels can promote the migration, invasion and metastasis of tumor cells [108].

Furthermore, metabolic boosting of exhausted T cells through upregulation of OXPHOS can improve effector function against tumors [109]. Collectively, these data indicate that metabolic functions widely affect T cell fate and anti-cancer effector function potentially targetable by manipulation.

2.7. Reactive oxygen species (ROS)

ROS are oxygen containing molecules, which are highly reactive and occur as a by-product of mitochondrial aerobic metabolism and homeostasis. The dual role of ROS leads on the one hand to a beneficial cell signalling, by intentional generating ROS after cellular responses to cytokines or bacterial invasions. On the other hand it can cause irreversible damages due to oxidizing DNA or cellular components which results in function loss [110]. ROS are not clearly defined, they more represent a group of oxygen free radicals, such as superoxide anion radical ($O_2^{\cdot-}$), hydroxyl radical (·OH), and nonradical oxidants, such as hydrogen peroxide (H_2O_2) and singlet oxygen ($^1O_2$) [111]. Especially, the ·OH, which is mostly generated through Fenton reaction with H_2O_2, reacts irreversible with organic compounds [112]. High amount of ROS can lead to apoptosis, a programmed form of cellular death, through both intrinsic and extrinsic pathways. The intrinsic pathway is activated by the response of intracellular stressors, by phosphorylating proteins mostly belonging to the B-cell lymphoma (Bcl) 2 superfamily (Bcl-2-like protein 4 (BAX), Bcl-2 homologous antagonist/killer (BAK), Bcl-2-related Ovarian Killer (BOK) and Bcl-2 associated agonist of cell death (BAD)), which triggers the permeabilization of the mitochondrial outer membrane [113, 114]. Next, proapoptotic factors, like Cyt c are released from the mitochondrial intermembrane space into the cytoplasm where it interacts with apoptotic protease-activating factor-1 (Apaf-1), which further oligomerizes ATP-dependent building the apoptosome [115]. Subsequently, procaspase 9 is recruited through caspase recruitment domains (CARDs) [115]. The active caspase 9 processes caspase 3, which in turn cuts the Inhibitor of Caspase-Activated DNase (ICAD) whereby the Caspase-Activated DNase (CAD) is released, enters the nucleus and splits the chromosomal DNA, which

leads to cell death [116]. In the extrinsic pathway, the permeabilization of the mitochondrial outer membrane is triggered by a crosstalk of caspase-8 mediated cleavage of the Bcl-2 superfamily members. Therefore, ROS promote the upregulation of death receptors, like TNF-Related Apoptosis-Inducing Ligand Receptor 2 (TRAIL-R2) [117].

ROS also play a major role in the carcinogenesis. By oxidizing the DNA, mutations are introduced which leads to base exchange, single-strand breaks, DNA crosslinks or a mispair of DNA polymerase, lastly can happen when guanine is formed into 8-oxoguanine and pairs with adenine in the DNA replication [118]. Furthermore, it was shown that both exogenous and endogenous ROS are promoting tumor proliferation, which in turn promotes angiogenesis. High levels of ROS and the resulting oxidative stress in the TME initiates the secretion of angiogenic modulators, including VEGF [119]. In addition, the signalling cascade of Phosphoinositide-3 kinase (PI3K)/Protein kinase B (Akt)/ mechanistic Target of Rapamycin (mTOR) (see 2.9. T cell activation) is activated independent or dependent of hypoxia, in reference to the latter the production of HIF-1α is also stabilized [120]. This leads to an increased metabolomic demand, which in turn promotes high ROS levels [120]. Therefore, the targeting of ROS represents an interesting approach in the cancer therapy.

ROS were identified as triggers for the activation several signalling pathways for signal transduction or cellular defence. This way, ROS influence the activation or inhibition of NF-κB. Activation of NF-κB is usually dependent on IκB Kinase (IKK)-mediated phosphorylation of Inhibitor of κBα (IκBα) followed by its proteasomal degradation [121]. IκBα is known as an unstable protein that can be degraded upon stimulation by ROS, leading to the activation of NF-κB. Additionally, ROS can directly oxidize cysteine residues in the DNA binding domain of NF-κB, thereby inhibiting its DNA binding and signalling activity [122]. This dual role is also observed in the stimulation of proliferation with low ROS levels and the induction of apoptosis at high levels.

To protect the cell, ROS need to be transformed into less reactive products to reduce DNA damages through antioxidants. Therefore, $O_2^{\cdot-}$ can be transformed into H_2O_2 by the antioxidant superoxide dismutase (SOD) and further reduced to H_2O by catalase of glutathione peroxidase [123]. Studies have shown, that SOD overexpression in cells leads to reduced levels of mitochondrial ROS acting as a ROS scavenger [124]. Further, the NADPH oxidase (Nox), classified into multiple isoforms including Nox1, which catalyses the NADPH-dependent reduction of oxygen to superoxide [125]. This superoxide subsequently undergoes spontaneous

or enzyme-mediated dismutation to form H_2O_2. H_2O_2 can react with Glutathione (GSH), an antioxidant in mammal cells, in a reaction catalyzed by gluthatione peroxidase [126]. Thereby, its monomer form is oxidated in the dimer glutathione disulfide (GSSG) with the by-product H_2O [126]. Also, GSH has a free thiol group to add electrons on ROS to neutralize them. Glutathione-Reduktase reduces GSSG to GSH and the loss of NADPH to $NADP^+$ [127]. Another antioxidant to reduce H_2O_2 to H_2O under Class III peroxidase (Prx) is reduced Thioredoxin (Trx_{red}), which further transverts into oxidized Thioredoxin (Trx_{ox}) [128]. Thioredoxin reductase (TrxR) reduces Thioredoxin (Trx) under consumption of NADPH [128].

A crucial regulator is the transcriptional factor nuclear factor erythroid 2-related factor 2 (Nrf2), which is involved in the ROS homeostasis. Nrf2 regulates antioxidant enzymes and is involved in detoxification and elimination of oxidative stress [129]. Nrf2 is negatively regulated by Kelch-like ECH associated protein 1 (Keap1) as an antioxidant defence mechanism with ubiquiting sequences [129]. Under stress conditions the Ubiquitin sequences are degraded by the proteasome. Nrf2 is no longer bound by Keap1 and can enter the nucleus [130]. Here, target genes for ROS detoxification are transcribed.

2.8. Oxygen binding proteins (OBP)

OBP play a crucial role in the physiological processes of living organisms, serving as essential biomolecules for the transport, storage, and delivery of oxygen [131]. These molecules can be found in various organisms, ranging from bacteria to mammals, and play a critical role in respiration, providing the fundamental element for cellular metabolism [132]. One major superfamily of oxygen binding proteins are globins. They are characterized by a specific folding pattern and the ability to bind heme, an iron-containing molecule that binds oxygen and are spread over different organisms [133]. Examples here are Hemoglobin (Heme), found in the human blood circulation, Mb found in muscle tissue and Leghemoglobin (Leg) found in plants [132]. By determining the p50 value, or the thermodynamic and kinetic oxygen affinities Kd and KM, the oxygen-binding capacity of OBPs can be comprehensively assessed, in order to categorize them into six different sub-classes [134, 135]: Erythrocruorins (Ery), Hemocyanins (Hcy), Heme, Leg, Cytochromes (Cyt) and Mb [136]. These subclasses highlight the diversity of oxygen-binding proteins and their specialized roles in various organisms and biological processes. Ery are large, multi-subunit hemoproteins mostly found in in the blood of annelids and some arthropods facilitating the transport of oxygen throughout the organism [137]. They

are mostly characterised by forming a massive complex with a high molecular weight [137]. Hcy are copper-containing oxygen transport proteins of many arthropods and mollusks [138]. The large, multi-subunit proteins can bind oxygen reversibly, leading to a blue colour of blood if oxygenated [138]. Hemoglobin is an iron-containing oxygen-transport protein in the erythrocytes of vertebrates and some invertebrates. It carries oxygen from the respiratory organs to the tissue and returning CO_2 to the lungs. It is composed of four subunits, each containing an iron-bound heme group [139]. Leg, a heme protein found in nitrogen-fixing root nodules of leguminous plants shows a similar structure and function to hemoglobin, facilitating the transport of oxygen to the nitrogen-fixing bacteria, while keeping free radicals of oxygen low to avoid inhibiting the nitrogen fixation [132]. Cyt is involved in the ECT and energy production within cells, primarily in mitochondria. It plays a crucial role in the cellular respiration by transferring electrons in the ETC [72]. Changes in the affinity of oxygen-binding proteins for oxygen with regard to the concentration of CO_2 and acidity (pH) are known as the Bohr effect [140]. For example, in the case of hemoglobin A, as CO_2 and acidity increase, its affinity for oxygen decreases, facilitating oxygen release in tissues where cellular respiration produces both [141]. Conversely, in the lungs with lower CO_2 and higher pH, hemoglobin binds oxygen efficiently for transport. This adaptation ensures optimal oxygen delivery and utilization throughout the body.

2.8.1. Myoglobin (Mb):

The OBP Mb is a small, monomeric heme protein produced by myofibrills, that form the structural core and functional unit of muscle fibers of vertebrates [133]. Myofibrills consist of a series of sarcomeres, the contractile structure, which in turn are composed of myofilaments [142]. Myofilaments contain mainly actin, a structure protein forming the cytoskeleton, and myosin, a rod-shaped motor protein [143, 144]. Mb comprises 153AA and a molecular weight of 17kDa forming eight α-helix connected through turns with an oxygen binding site [133]. The active center of myoglobin is a heme which is composed of protoporphyrin IX with an iron (II) ion ligated via four internal nitrogens [145]. The heme is bound to the protein matrix via a proximal histidine axially coordinated to the central iron ion [145]. The second axial position is used to bind the oxygen molecule [145]. It serves as an oxygen storage protein, supporting oxygen transport and diffusion of oxygen [131]. The rate of oxymyoglobin (MbO_2) promotes mitochondrial oxygen uptake, indicating that myoglobin is a potent oxygen buffer capable of releasing oxygen for mitochondrial metabolism when required [146]. Mb has a six times higher

affinity for oxygen than hemoglobin, allowing it to effectively capture and release oxygen within muscle cells. Here, high concentrations of Mb are detectable up to 100µmol/l, with a p50-value of about 1-3 mmHg resulting in the red colour of the muscle tissue [131].

2.9. T cell activation

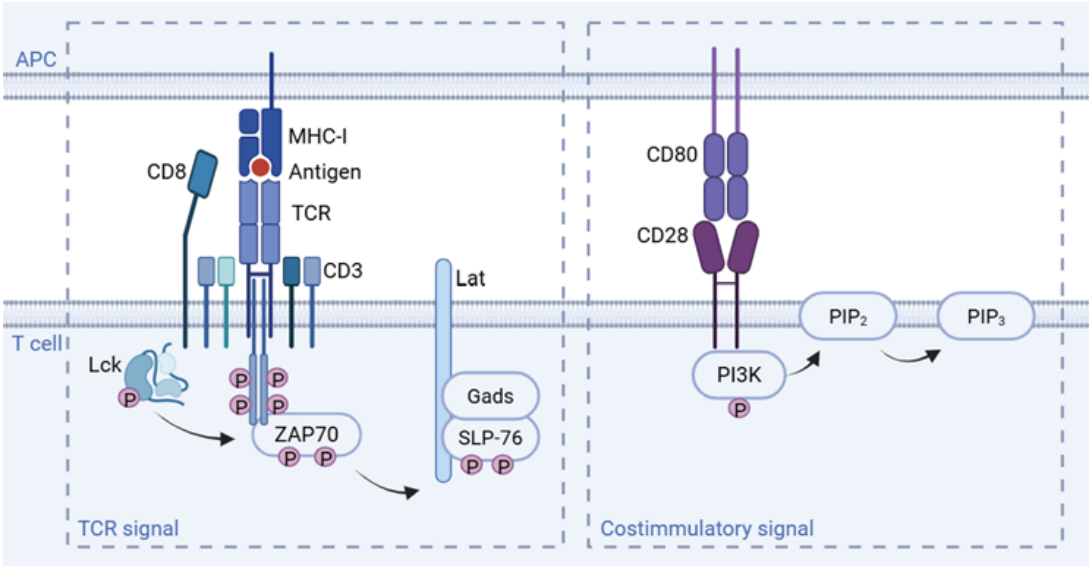

Figure 5: TCR and costimulatory signalling pathways following T-cell activation. Schematic illustration of the binding of the TCR to the MHC-I–peptide complex in conjunction with CD8, leading to Lck-mediated phosphorylation of the CD3 ITAMs and subsequent recruitment and activation of ZAP-70. Activated ZAP-70 phosphorylates LAT, which enables the recruitment of Gads and SLP-76 and their downstream phosphorylation events. In parallel, the costimulatory receptor CD28 is engaged by CD80, resulting in the activation of PI3K and the conversion of membrane-bound PIP_2 into PIP_3**.** Adapted by Brownlie *et al*., 2013 [147].

Naïve T cells circulate through the secondary lymphoid organs and are metabolically inactive in G_0 phase of the cell cycle, until they are encountered and activated by antigen presenting cells (APC), such as Monocytes, Macrophages, B cells or DCs [148]. APCs phagocytize extracellular particles, microorganism, liquid antigens, pathogen molecules or tumor fragments for the antigen uptake, which are further degraded in smaller fragments by lysosomal enzymes and processed for presentation over the MHC-complex [149]. Here, a distinction is made between MHC-I and MHC-II complexes for interaction with $CD8^+$ or $CD4^+$ T cells, respectively. The complex contains two polypeptide chains with one anchoring into the plasma membrane containing three α- and one β-microtubulin domains for MHC-I and two anchors containing two α- and two β- domains for MHC-II [150].

To be loaded endogenous antigens on MHC-I complex, such like viral proteins or tumor-derived peptides are degraded by the proteasome in the cytosol into small peptides [151]. These peptides are transported into the endoplasmic reticulum (ER) by transporter associated with Antigen Processing (TAP) to be loaded on the MHC-I complex with the assistance of the chaperone Tapasin, before being transported via the Golgi apparatus to the cell surface, where it can be recognized by $CD8^+$ T cells [152].

Contrastingly, MHC-II molecule is synthesized in the ER with an invariant chain (li) blocking the peptide-binding groove and transported to vesicles exchanging the invariant chain with class II-associated invariant chain peptide (CLIP), which is further removed in the endosomes [153, 154]. Here, exogenous antigens, which are previously degraded by phagolysosomes in the endosome and are loaded on the MHC-II complex, which is further transported to the cell surface [153]. Further, MHC-II can be recognized by $CD4^+$ T cells.

To interact with APCs, T cells bind membrane-bound intercellular adhesion molecule 1 (ICAM-1) via the integrin lymphocyte function-associated antigen 1 (LFA-1) [155]. This low affinity interaction is enhanced by a confirmation change in LFA-1 and stabilizes a prolonged interaction between both cells induced by the first of three essential signals for fully activation of T cells [156]. This first signal is transmitted by interaction of the TCR and the recognition molecules CD4 or CD8 binding the MHC-peptide complex and leads to activation of the T cells by shifting the cell cycle in G_1 phase [157, 158]. The second signal is transmitted by the binding of costimulatory receptors like CD28 on the T cell site binding CD80/CD86 and promotes survival of the T cell [159]. The third signal for the full activation and differentiation of T cells is provided by cytokines such as IL-6, IL-12, IL-23 and IL-4, which are secreted by APCs binding their specific receptors [160-163]. If the signal is insufficient or the cell does not receive all three essential signals, the T cell may become anergic, fail to proliferate or undergo apoptosis [164].

The TCR consists of an α and β chain which are spanning the plasma membrane of the T cell and is associated with CD3 to transduce the activation signal into the T cell and stabilizes the TCR for effective interaction with the MHC-antigen complex [165]. CD3 contains two ε domains, one δ and one γ extracellular domain [166, 167]. The signal is transmitted through immunoreceptor tyrosine-based activation motifs (ITAM) on the cytoplasmic tails of CD3-subunits and two intracellular CD3 ζ chains connected with the α and β chain of the TCR [168]. These ITAM motifs are phosphorylated by the Sarcoma (Src)-family kinase Lymphocyte-

specific protein tyrosine kinase (Lck), which are covalent bound to the coreceptor CD4/CD8 and are activated by the interaction of CD8/CD4 with MHC-I/MHC-II [169, 170]. The ζ chain-associated protein 70 (ZAP-70) is recruited and activated by engaging the tandem Src Homology 2 domains (SH2) with the doubly phosphorylated ITAMs of CD3 ζ [171]. Due to the proximity to the plasma membrane, ZAP-70 phosphorylates the linker for activation of T cells (LAT), a transmembrane protein with cytoplasmic domain and the adaptor protein SH2 domain-containing leukocyte protein of 76 kDa (SLP-76), which can be connected through the adaptor molecule GRB2-related adapter downstream of Shc (Gads) forming the LAT:Gads:SLP-76 complex [172]. The signal path splits at this point.

In addition, costimulatory signals are required for the full activation of T cells. Binding CD80/CD86 induces phosphorylation of CD28 and recruit with the ITAM-like motifs the p85/p110-subunit of PI3K [173]. PI3K can also be activated by Rat sarcoma virus (Ras) proteins, small GTPases that are activated by GTPase-activating proteins (GAP) through the interaction with the catalytic p110-subunit for the hydrolysis of GTP and also plays further roles in mediated cell survival and proliferation [174]. PI3K phosphorylates phosphatidylinositol 4,5-bisphosphate (PIP_2) to phosphatidylinositol-3,4-5-triphosphate (PIP_3) at the cellular membrane, a key protein for the different following signalling pathways [175]. Also, the costimulatory signal triggers the synthesis of the α chain of the Interleukin-2 receptor (IL-2R). Naïve T cells expressing already the γ- and β- chain of this receptor and are able to bind IL-2 with low affinity [176]. As soon as the missing chain is added to the receptor, IL-2 can be bound with high affinity [176]. This leads to activation of the Janus Kinase (JAK)- Signal Transducer and Activator of Transcription (STAT) signal pathway resulting in phosphorylation of STAT5 [177]. Furthermore, it can also stimulate the Ras/ Mitogen-Activated Protein Kinase (MAPK) and the PI3K/Protein Kinase B (Akt) signal pathway (see 2.9.2. Protein kinase B (Akt)-Signalling pathway). IL-2 promotes cell proliferation, differentiation and survival [178].

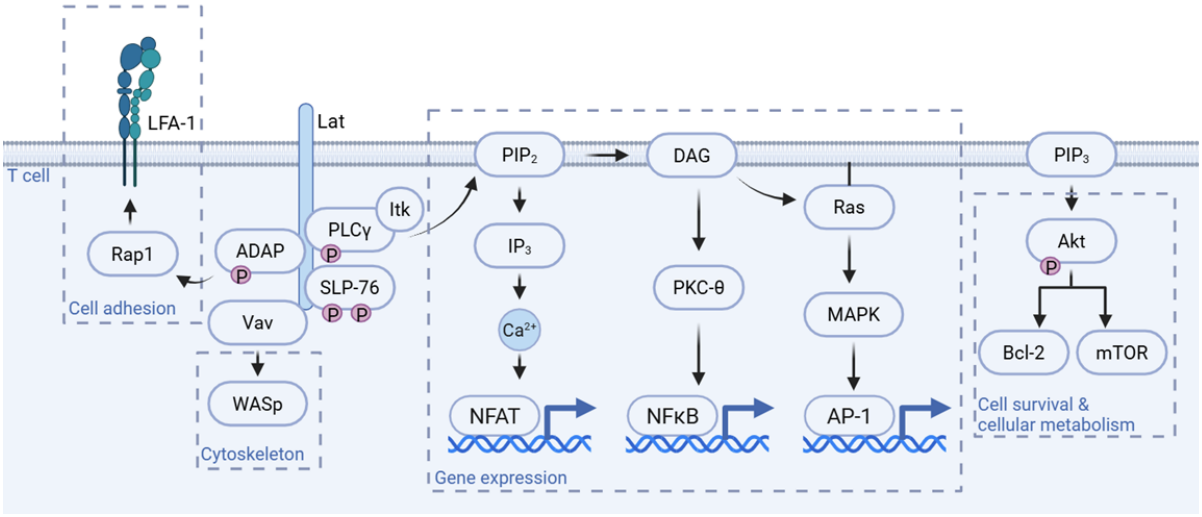

Figure 6: Key Downstream Signalling Modules in TCR Activation: PLC-γ, AKT, ADAP, and Vav1 Pathways. Schematic illustration of the downstream signalling after activation of T cells. Upon TCR engagement, LAT recruits multiple adaptor and signalling proteins, including ADAP, Vav1, and PLC-γ. These interactions activate Rap1, which promotes LFA-1 activation and T-cell adhesion, and engage WASp to regulate cytoskeletal remodelling. PLC-γ is recruited to membrane-bound PIP_2 and hydrolyses it into IP_3 and DAG. IP_3 induces calcium release, leading to NFAT activation, whereas DAG activates PKC-θ to drive NF-κB signalling and recruits Ras to activate the Ras–MAPK pathway, ultimately resulting in AP-1 expression. PIP_3 generated by PI3K signalling activates Akt, which in turn promotes Bcl-2-mediated survival and stimulates mTOR signalling to support cellular metabolism and growth. Adapted by Brownlie *et al*., 2013 [147].

2.9.1. Phospholipase C-γ (PLC-γ) signalling pathways

Next, Phospholipase C-γ (PLC-γ) plays a key role in triggering three distinct pathways, leading to activation of crucial transcriptional factors, like Nuclear Factor of Activated T cells (NFAT), Adaptor Protein 1 (AP-1) and NF-κB. PLC-γ is transported to the inner side of the plasma membrane by binding the Pleckstrin Homology (PH)-domain of PIP_3 and further binding the LAT:Gads:SLP-76 complex [179]. The Tyrosinkinase Itk is also recruited to the plasma membrane, triggered by interaction with the PH domain of PIP_3. SH2 and SH3 domains interact with SLP-76 for relocating Itk closely to PLC-γ for further activation [180]. PLC-γ now catalyses PIP_2, resulting in the products Diaglycerin (DAG) and Inositol-1,4,5-triphosphat (IP_3) [181]. DAG is a membrane lipid which further recruits signalling molecules. IP_3 is a soluble second messenger, which diffuses through the cytoplasm to the IP_3-receptors, also known as Ca^{2+} channels on the membrane of the ER [181]. The binding leads to the release of Calcium into the cytosol, resulting in a conformation change of the transmembrane protein Stromal Interaction Molecule 1 (STIM1), which in turn interacts with Calcium release-activated calcium

channel protein 1 (ORAI1), a Calcium channel of the plasma membrane and triggers Ca^{2+} influx [182]. The Ca^{2+}-ions binding Calmodulin causes a confirmation change, which in turn activates the protein phosphatase Calcineurin, which dephosphorylates NFAT [183]. NFAT is now recognized by the cell nucleus transport system and activates several target genes [183]. Simultaneously, the membrane protein DAG activates the GTPase Ras through the Guanine nucleotide exchange factor (GEF) RasGPR by facilitating the exchange of GDP to GTP [180]. Additionally, Ras can also be activated via the Growth factor receptor-bound protein 2 (Grb2)/ Son of Sevenless (Sos) complex, which is recruited to phosphorylated LAT [180]. Activated Ras then triggers a phosphorylation cascade involving three consecutive MAPK by phosphorylation. First, Rapidly Accelerated Fibrosarcoma kinase (Raf) is activated, which subsequently activates MAPK/ERK kinase 1 (MEK1) [184]. MEK1 then triggers the activation of extracellular signal-regulated kinase (Erk), which in following translocates into the cell nucleus [184]. This signalling cascade is supported by the scaffold protein kinase suppressor of Ras (KSR) [185]. In the cellular nucleus, Erk phosphorylates the transcription factor ETS-like protein 1 (Elk-1), which binds with the Serum-Response-Factor (SRF) at the Serum-Response-Element (SRE) of the promotor of the FOS gene [186]. This results in the transcription of the transcriptional factor c-Fos, which is crucially involved in the activation of AP-1 [186]. Full activation of AP-1 still requires the activated Jun kinase (JNK), which is induced by the recruitment of protein kinase C-θ (PKC-θ) by DAG. PKC-θ induces the phosphorylation of JNK, a MAP kinase, which then enters the nucleus and phosphorylates the transcription factor c-Jun. Phosphorylated c-Jun forms a dimer with c-Fos, which in turn forms the activated transcription factor AP-1, resulting in the transcription of target genes [187]. In addition to AP-1, PKC-θ is also involved in the activation of NF-κB by phosphorylating the membrane-bound protein Caspase Recruitment Domain-containing Membrane-Associated Guanylate Kinase Protein 1 (CARMA1). CARMA1 then oligomerizes and forms a complex with B-cell lymphoma/leukemia 10 (BCL10) and Mucosa-Associated Lymphoid Tissue Lymphoma Translocation Protein 1 (MALT1), which activates the E3 ubiquitin ligase TNF Receptor-Associated Factor (TRAF) 6 and induces the degradation of IKK [188, 189]. IKK phosphorylates IκB, which leads to its ubiquitination and subsequent degradation. IκB is an inhibitor bound to NF-κB located in the cytoplasm [188, 189]. The now active NF-κB enters the cell nucleus and initiates the further transcription of the target genes [188, 189].

2.9.2. Protein kinase B (Akt)-Signalling pathway

In addition, fully activated T cells must undergo a change in cellular metabolism, which is required by the rapidly proliferating cells. For this purpose, PIP_3 recruits Akt, which is phosphorylated and activated by phosphoinositol-dependent kinase 1 (PDK1), which in turn is recruited by PIP_3 [190]. Akt in turn phosphorylates the proapoptotic protein Bcl-2-associated death promoter (Bad), which as a result can no longer bind and block the anti-apoptotic protein Bcl-2 and is bound to the outer mitochondrial membrane [191]. Bad itself is captured by the protein 14-3-3 and the now unbound Bcl-2 promotes cell survival [191]. Furthermore, the activated kinase Akt phosphorylates the Tuberous Sclerosis Complex (TSC), a GAP of the small GTPase Ras homolog enriched in brain (Rheb) [192]. Rheb in turn activates mTOR, thereby affecting cellular metabolism [192]. Among other things, it ensures increased gene expression and lipid production.

2.9.3. Adhesion and Degranulation-promoting Adapter Protein (ADAP) signalling pathway

Next, an increased adhesion of integrins is induced by TCR stimulation. This strengthens the interaction of T cells and APCs. LFA-1 is present on naïve T cells in a state of low affinity. To achieve a stable immune synapse, it requires increased adhesiveness in the binding of LFA-1 with its target integrin ICAM-1 through a confirmatory change [155]. The increased subsequent adhesion between T cell and APC stabilizes the interaction of the cells. This is induced by the binding of the Adhesion and Degranulation-promoting Adapter Protein (ADAP) to the SH2 domain of SLP-76 of the LAT:Gads:SLP-76 complex [193]. Afterwards, Src kinase-associated phosphoprotein (SKAP) and Rap1-GTP-interacting adapter molecule (RIAM) are recruited, leading to the activation of the small GTPase Ras-proximate-1 or Ras-related protein 1 (Rap1) [194]. As a result, LFA-1 assembles and undergoes a conformational change [195].

2.9.4. Vav guanine nucleotide exchange factor 1 (Vav1) signalling pathway

The fourth TCR signalling module leads to the restructuring of the actin cytoskeleton, which is mediated by Vav guanine nucleotide exchange factor 1 (Vav1), a GEF of the rho family. Vav1 binds via its PH domain to PIP_3 as well as to the LAT:Gads:SLP-76 complex [196, 197]. The adaptor protein Non-catalytic region of tyrosine kinase adaptor protein (Nck) binds to a

phosphorylated tyrosine residue of SLP-76 and recruits Wiskott-Aldrich syndrome protein (WASp) [198]. Vav1 subsequently activates the GTPase Cell division control protein 42 homolog (Cdc42), which in turn binds and activates WASp [198]. The active WASp binds WASp-interacting protein (WIP), recruits Actin-related protein 2/3 complex (Arp2/3) and additionally induces actin polymerization [198]. This results in a change in the cytoskeleton.

2.10. T cell differentiation

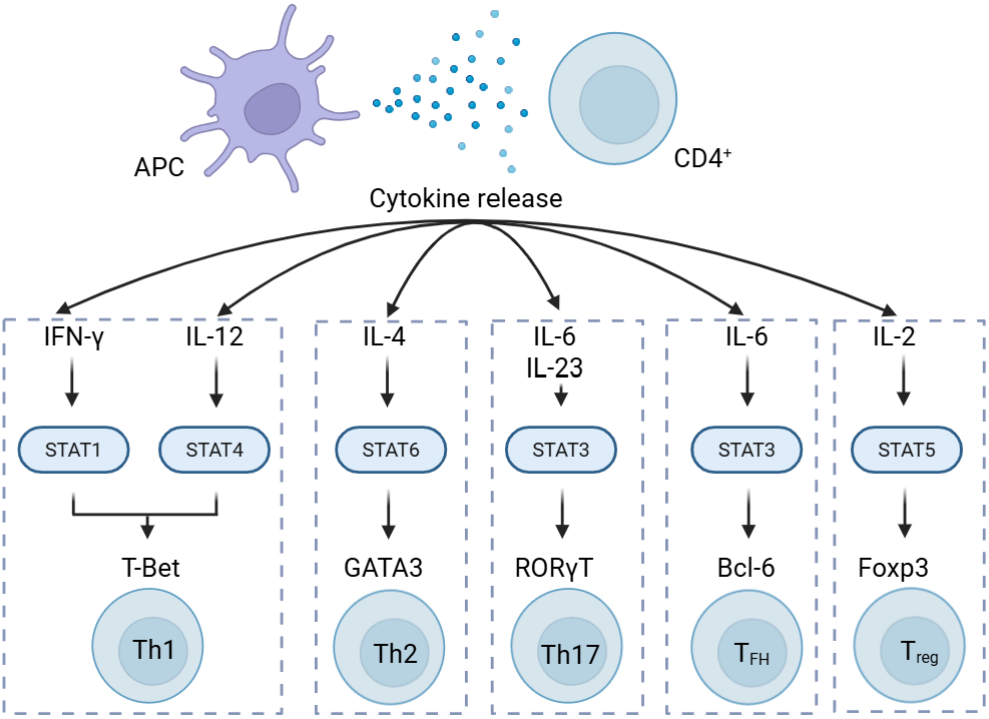

Figure 7: The differentiation of CD4$^+$ T cells in different subtypes through cytokine release. Illustration of the required cytokines and induced STAT signalling pathways for the differentiation of CD4+ T cells into Th1, Th2, Th17, T_{FH} and T_{reg} subpopulations. Adapted from Zhu *et al*., 2010 [199].

T cells are a type of lymphocyte that play a central role in the immune response by recognizing and combating foreign structures [200]. They differentiate into subgroups with distinct roles in regulation, coordination or execution of the immune response, which itself is classified into two main classes [200]. CD4$^+$ expressing T cells are described as T helper cells (Th), which, according to their name, help to activate cells of the acquired immune system [201]. They differentiate into several subclasses depending on the cytokine environment, with each subgroup performing specific functions [202]. Proliferating Th cells that develop into effector

T cells belong to the Th1 and Th2 subtypes. To reach stable Th1 phenotype, Interferon-γ (IFN-γ)- STAT1 and IL-12-STAT4 signalling pathways are induced resulting in expression of the transcriptional factor T-Bet triggering the secretion of the proinflammatory cytokines Tumor necrosis factor (TNF)-α and Ifn-γ [203]. TNF-α acts as a mediator of the innate immune response. By binding the receptors Tumor necrosis factor receptor (TNFR) 1 or TNFR2 it causes on the one hand an immunostimulatory effect with promoted survival, proliferation and activation of inflammatory signals, on the other hand the killing of the cell by apoptosis or necrosis, which often results in inflammation in the surrounding tissue [204]. The type II interferon IFN-γ is crucial for immunity against viral and protozoan infections [205]. It binds to the heterodimer receptor (Interferon-γ receptor 1 (IFNGR1) and IFNGR2) leading to upregulation of MHC-II-complexes and activation of macrophages, whose phagocytosis destroys pathogens [206, 207]. Th1 cells also promote the differentiation of $CD8^+$ T cells into cytotoxic T cells (CTL), which specifically kill direct target cells [208]. Th2 cells, on the other hand, are triggered by an IL-4 rich environment and play an important role in the humoral response, especially against parasites [202]. IL-4 activates STAT 6 which leads to expression of the transcriptional factor GATA-binding protein 3 (GATA3) and promotes the secretion of the cytokines IL-4, IL-5 and IL-13. The α chain of the heterodimer IL4R can bind IL-4 and IL-13 [209]. In both cases the JAK is activated resulting in phosphorylation of STAT6. IL-13 influences an Isotype change in B cell for producing IgE antibodies, which are mainly defending against parasites, but also triggers allergies [210]. Moreover, the goblet cells are stimulated for mucus production [211]. The growth and differentiation of basophiles are triggered by IL-5 binding to the heterodimer IL-5 receptor inducing JAK-STAT-pathway [212, 213]. Due to a Transforming Growth Factor Beta (TGF-β), IL-6 and IL-23 rich environment, $CD4^+$ T cells develop into Th17 [161, 214, 215]. This process is mediated by the activation of STAT3, which induces the expression of the transcriptional factor Retinoic acid-related orphan receptor gamma T (RORγT) [216, 217]. IL-17 production recruits neutrophils and macrophages, which are involved in the defence against fungi and bacteria [218, 219]. Moreover, it stimulates Fibroblasts and Epithelia cells for secretion of chemokines. IL-22 stimulates mucosal epithelium and skin to produce antimicrobial peptides [220]. Two key players are Granulocyte Colony-Stimulating Factor (G-CSF), a stimulation factor of granulocytes and IL-8 an inflammatory mediator which mobilizes basophil and neutrophil granulocytes through chemotactic stimuli and supports their degradation [221, 222]. While IL-6 is involved in differentiation into Th17 cells, it alone can also stimulate differentiation into follicular T helper cells (T_{FH} cells), which promote the transcription factor Bcl-6 by activating

STAT3 [223-225]. They are crucial for antibody production by promoting the differentiation of B cells into plasma cells and memory B cells through the binding of IL-21 secreted by T_{FH} cells bound to the IL21R [223, 226]. Furthermore, the differentiation into induced regulatory T cells (iTreg cells) is stimulated by TGF-β and IL-2 rich surrounding. IL-2 activates STAT5 which leads to expression of Forkhead-Box-Protein P3 (Foxp3) [227, 228]. Through the secretion of TGF-β and IL-10 they suppress the activation of several immune cell populations, such as T cells, B cells and macrophages [229-231]. They thus prevent the occurrence of autoimmune reactions. Another group consists of the self-reactive natural Treg cells (nTreg cells) that occur in the thymus and are identified by expressing the marker CD4, CD25, the α-chain of the IL-2 receptor and Cytotoxic T-Lymphocyte Antigen 4 (CTLA-4), which leads to a downregulation of the proliferation of activated T cells [232-234].

While $CD4^+$ cells differentiate in several subtypes supporting other immune cells, $CD8^+$ cells transform into CTLs after TCR activation, promoted by the cytokines IL-12, IFN-γ and IL-2 [235]. These cytokines are produced by $CD4^+$ cells and APCs. They further initiate several pathways which leads to killing of the target cell, after recognizing the specific MHC-I antigen complex. CTLs are expressing different surface marker, providing an indication of the activation status, effector function or the general T cell fate. The inhibitory receptor PD-1 of the CD28-superfamily leads to suppression of the effector function of the CTLs induced through binding to its ligand PD-L1 [236]. PD-1 exhibits immunoreceptor tyrosine-based inhibition motifs (ITIM) [237]. By phosphorylation of tyrosine in the ITIM motifs, the recruitment of SH2-containing phosphatase (SHP) or SH2-containing inositol phosphatase (SHIP) is inhibited [237]. This induces the dephosphorylation of different proteins, including PIP_3 to PIP_2, thereby inducing signal blocking. Studies have shown that its sustained activation of signalling pathways can lead to dysfunction in the CTLs, thereby failing to reduce viral loads in chronic infections [238]. PD-1 thus has an opposite mode of action. While on the one hand it indicates activated T cells and stabilizes effector function, on the other hand it can indicate exhaustion and downregulate effector function, which can also lead to T cell dysfunction [236, 238]. PD-1 is also an interesting candidate for immune checkpoint inhibition (ICI). Also, the inhibitory T cell immunoglobulin and mucin-domain containing-3 (Tim-3) prevents overreaction of the immune cells. Tim-3 has different binding sites binding the adhesion molecule carcinoembryonic antigen-related cell adhesion molecule 1 (CEACAM1) or the soluble lectin galectin 9 [239, 240]. These bindings can have several consequences. On the one hand, the TCR signalling pathway can be inhibited and, on the other hand, apoptosis can be

induced [239, 240]. The killer cell lectin-like receptor subfamily G member 1 (KLRG1) is characterised by the presence of an ITIM and binds to classical cadherins, such as E-cadherin, which are widely expressed on epithelial cells rather than predominantly on APCs [241]. The main function of KLRG1 is to suppress cytotoxicity and proliferation. In contrast, the interleukin-7 receptor (IL-7R), binds the cytokine IL-7, a crucial factor for T cell development and conveys survival and persistence both important factors for development and maintenance of memory T cells [242].

$CD4^+$ and $CD8^+$ T cells are able to develop in two main T cell subsets, effector and memory cells. Effector cells are highly active T cells which, in the case of $CD8^+$ T cells, are directly involved in the killing of target cells or, in the case of $CD4^+$ cells, activate or regulate other immune cells. Memory cells, on the other hand, are placed in a state of senescence, which are characterized by a long survival and reduced proliferation and can be activated in the event of a recurring disease, thereby stimulating proliferation in order to directly combat the target cells [243]. This results in an immunological memory that can combat recurring pathogens at an early stage. A distinction is made between Central memory T cells (T_{cm}), effector memory T cells (T_{em}) and tissue-resident memory T cells (T_{rm}). T_{cm} cells are circulating in the secondary lymphoid organs and characterised by overexpression of CD40 ligand (CD40L), which leads to an easier activation with DCs or B cells [243]. This activation leads to a rapid proliferation. Furthermore, they express C-C chemokine receptor type 7 (CCR7), a chemokine to guide immune cells to immune organs [243]. T_{em} on the other hand are easily activated by their specific antigen. They have lost the constitutive expression of CCR7, but instead are able to produce IFN-γ [243]. T_{rm} express two key markers, the αE integrin CD103 and the activation marker CD69, but in secondary lymphoid organs and the liver T_{RM} cells lack CD103 expression [244]. To distinguish between effector and memory cell population, CD44, an adhesion molecule important for cell-cell interactions and L-selectin (CD62L), which acts as a homing receptor enabling entry into secondary lymphoid organs, are used [245, 246]. Naïve T cells are characterized by $CD44^{low}$ and $CD62L^{high}$ expression. $CD44^{high}$ and $CD62L^{high}$ indicate T_{cm} cells, while $CD44^{high}$ and $CD62L^{low}$ indicates either Effector T cells (T_{eff}) or T_{em} cells [246].

Furthermore, to the expression of surface markers, intracellular transcription factors are crucial characteristics of the effector function of status of the lifespan of the T cell. Eomesodermin (EOMES), a conserved T-box protein plays an important role in the persistence and is crucial for memory cells [247]. Further, the nucleofector thymocyte selection-associated HMG box (TOX) acts as a regulator of tumor-specific T cell differentiation [248]. It is mostly expressed

in exhausted T cells and is necessary for epigenetic remodelling and survival [249, 250] Also, T cell factor-1 (TCF-1) is critical for survival of memory T cells with physiological conditions [251].

In addition to the differentiation of $CD4^+$ and $CD8^+$ T cells, a distinction is made between other T cell populations. γ-δ T cells usually belong to the innate immune system despite having the same precursor cells as $CD4^+$ and $CD8^+$ T cells, without the expression of the costimulatory molecules. γ-δ T cell ligands are induced by cellular stress or cell damage, whereby γ-δ T cells may also present antigens on non-classical MHC-class-Ib molecules (which include, among others: T22 and T10 (mouse) or MHC class I polypeptide–related gene (MIC)-A/MIC-B (human), the exact function is not known) [252, 253]. However, the γ-δ TCR can also bind surface proteins compared to the α-β TCR. It is assumed that γ-δ T cells control the activated lymphocytes through this binding the activating protein structure being indicators of stress factors or infections [254]. In addition to a TCR, NKT cells also express NK cell-specific genes, such as the lectin-like NK receptor NK1.1. NKT cells can kill virus-infected cells or tumor cells through the TCR, which binds specifically to lipids on CD1d molecules, or through the NK cell receptors, such as Natural Killer Group 2 member D (NKG2D) [255]. Furthermore, NKT cells produce stimulating or inhibiting cytokines that influence the immune response (IL-4, IL-13, TGF-β, IL-2, IFN-γ) [256].

2.11. Cytotoxicity in T cells

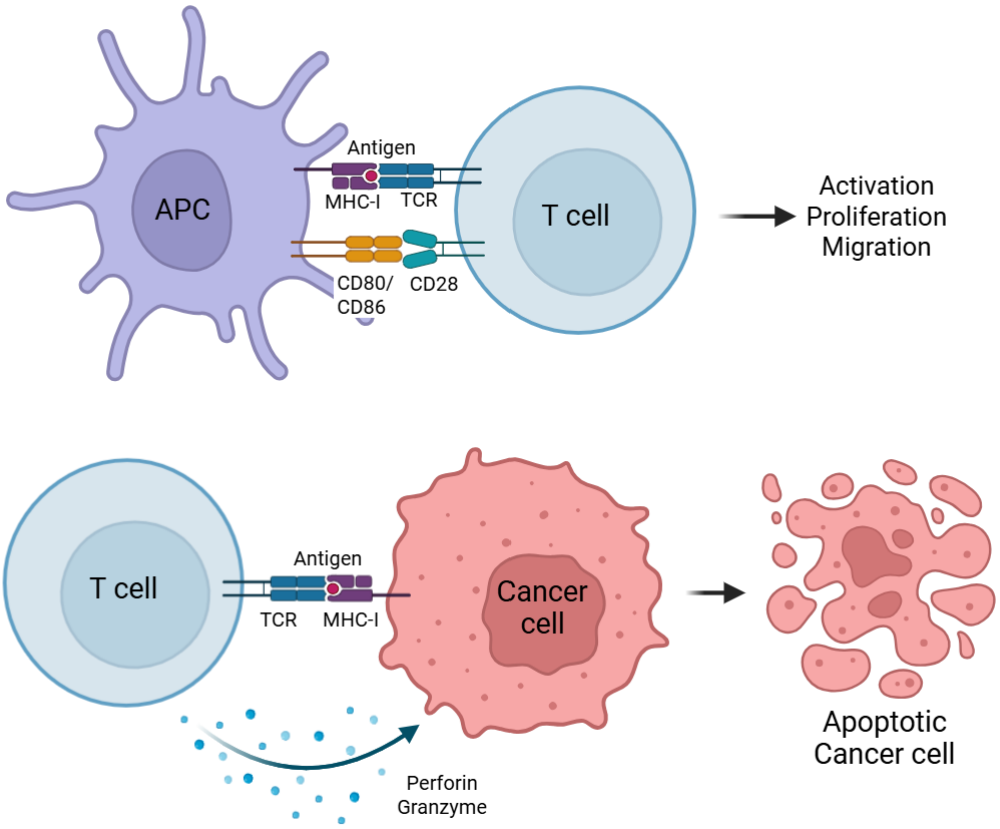

Figure 8: The cytotoxicity of CD8+ T cells against target cells. Schematic illustration of $CD8^+$ T-cell activation through recognition of the MHC-I–peptide complex by the TCR together with CD28 costimulation via CD80/CD86. These signals drive T-cell activation, proliferation, and migration. Activated $CD8^+$ T cells then traffic to the tumor site, where they recognize cancer cells presenting the cognate antigen on MHC-I. Upon target recognition, $CD8^+$ T cells release perforin and granzymes, which induce apoptosis in the target tumor cell. Adapted from Waldman *et al*., 2020 [257].

$CD8^+$ T cells can induce apoptosis in target cells, including those that are either mutated or infected by pathogens. After binding the MHC-I Peptide complex with the TCR, cytotoxic proteins, which were stored in lytic granules, are released by $CD8^+$ cytotoxic T cells [258]. Cytotoxic T cells can induce the apoptosis with either the extrinsic or intrinsic apoptosis (see 2.7. Reactive oxygen species (ROS)). Extrinsic apoptosis is induced by FasL and TNF- or Lymphotoxin alpha (LT-α) with the receptors Fas /CD95 and TNFR1, which are expressed by Immune and non-immune cells [259].

Cytotoxic T cells release cytotoxic granules in a calcium-dependent manner after recognizing the MHC class I–presented antigen via their TCR [258]. These granules contain Perforin, Granzyme (Gzm) and Granulysin [260]. Perforin interacts with the plasma membrane of the target cells to induce the formation of pores [258, 260]. Through these pores, further molecules enter the cytosol of the target cell. Gzm can activate apoptosis and Granulysin shows antimicrobial activity and can induce apoptosis at higher concentrations [258, 261]. Also, the proteoglycan Serglycin occurs in the granules, which acts as a scaffold molecule forming a complex with perforin and granzymes [262]. GzmA damages mitochondria and granzyme B activates caspase 3 by splitting aspartic acid residues and induces mitochondria to activate the intrinsic apoptosis pathway, by splitting BH3-interacting domain death agonist protein (BID) which leads to mitochondrial damage and in turn releases cytochrome c (see 2.7. Reactive oxygen species (ROS)) [263]. This signal is restricted to the target cell, whereby neighbouring cells are prevented from triggering apoptosis and specific killing is enabled [264]. After TCR binding, the synthesising of cytotoxic proteins is initiated.

Further, the release of the cytokines IFN-γ, TNF-α and LT-α also contribute to the immune defence (see 2.10. T cell differentiation). IFN-γ inhibits viral replication, stimulates MHC-I expression and activates macrophages and attracts them sites of infection, where they act as effector cells or APCs [205]. TNF-α and LT-α can also induce extrinsic apoptosis by binding to their target receptors [259, 265].

2.12. Metabolism in T cells

Metabolic pathways including glycolysis, fatty acid oxidation, fatty acid synthesis and amino acid metabolism are in constant flux in T cells in order to adjust to the increased energy demands required for expansion and effector differentiation in maintaining an antigen-specific response. This is usually accompanied by switching to aerobic glycolysis, a phenomenon termed `Warburg effect´ in order to support cell division [32]. When T cells are in quiescence, energy is primarily generated through glucose-derived pyruvate, which is transported for the TCA cycle to the mitochondria to support OXPHOS for ATP generation [266]. Hence, naive $CD8^+$ T cells use glucose metabolism and OXPHOS, but upon antigen recognition and differentiation into effector cells, they increase amino acid and glucose uptake while at the same time limiting the dependence on fatty acid oxidation [266]. Metabolic changes are not only observed in response to T cell activation, but can drive their function and regulate the progression to

exhaustion. While the switch towards aerobic glycolysis is important for T cell effector functions, it is, however, not strictly required for proliferation and survival, as T cells can adapt by utilizing other metabolic pathways, such as OXPHOS, when necessary [267]. Specifically, short lived effector cells (SLECs) require aerobic glycolysis to facilitate effector functions [267]. Mitochondrial dynamics play a critical role for modulation of memory and effector T cell fate [101, 268, 269]. Specifically, low mitochondrial function caused by PD-1 signalling in $CD8^+$ T cells is linked to T cell exhaustion and antigen persistence [269]. Moreover, limited mitochondrial OXPHOS and increased ROS production are associated with limited T cell proliferation, T cell dysfunction and exhaustion [101, 268, 269]. Likewise, increased production or defective elimination of ROS can result in T cell dysfunction and prolonged antigen persistence [270, 271]. Consistently, disturbed mitochondrial dynamics of anti-tumor T cells in cancer tissue can drive exhaustion [272]. Furthermore, impaired OXPHOS during antigen persistence can trigger T cell dysfunction, which can be restored following prevention of mitochondrial ROS [273]. Taken together, T cells at various stages of exhaustion and activation have complex and dynamic metabolic requirements that provide a window of manipulation due to their inherent plasticity.

2.13. Cancer Therapy

Conventional tumor therapies such as surgery, radiation and chemotherapy have historically been used for many different types of cancer, which, however are associated with numerous disadvantages and limitations. Local surgery is a very invasive method that appears promising in early stages or is used to obtain diagnostic biopsies to define further treatment options. Depending on the surrounding tissue or organ a local surgery cannot always be followed in case of risking organ damages. Further, the use of irradiation with a linear accelerator produces ionized particles that damage the DNA of healthy tissue as well as cancerous cells upon exposure. In contrast to healthy cells, tumor cells can hardly repair the damages and die. For deep-seated tumors higher radiation is needed [274]. Next, chemotherapy is a systemic drug treatment of either cytotoxin for induction of apoptosis or cytostatic agents to inhibit cell proliferation. Chemotherapy also shows many disadvantages like side effects with significant impact to the patients, developing drug resistance and immune suppression, resulting the patient to be more susceptible towards pathogens [275, 276]. Immunotherapies, on the other hand, offer promising approaches, addressing many limitations of conventional therapies. Boosting the

body's own immune system, mainly cytotoxic T cells, in order to achieve a highly specific pattern of action is the goal. Cytotoxic T cells induce apoptosis in the corresponding target cells by means of the TCR binding the corresponding peptide:MHC-I complex by releasing perforins and granzymes [277]. In 2014 the first bispecific T cell engager (BiTE) was approved by the United States (U.S.) Food and Drug Administration (FDA), so called Blinatumomab for the treatment of acute lymphoblastic leukaemia (ALL) [278]. This antibody is characterized by two different antigen binding sites binding on the one side CD19, a B cell marker and on the other side CD3, which is part of the TCR. Next, monoclonal antibodies (mAbs) can bind antigens of tumor cells or tumor promoting factors, like VEGF. The first FDA approved mAbs in 1997 are directed against CD20, a surface structure expressed on B cells for Non-Hodgkin-Lymphoma [279]. Therapeutic anti-drug conjugate (ADC) approach was first approved 2000 by the FDA, combining mAbs with a linker to a toxin or chemotherapeutical. Gemtuzumab ozogamicin is directed against CD33, which is expressed on myeloid cells, with a payload of Calicheamicin, an antitumor antibiotic derived from *Micromonospora echinospora [280]*. To boost long-term immunity against tumor antigens, cancer Vaccines were introduced into the clinic, which can be used as a preventive or treatment option. These cancer vaccines can be based on peptide, protein or mRNA, each of which serves as a platform to present tumor-associated antigens to the immune system and stimulate a targeted anti-tumor response. Next, oncolytic viruses are also used for the treatment of various cancers. Therefore, recombinant viruses are generated to infect selective tumor cells, resulting in its lysis and boosting of the immune response. In 2003 Gendicine, an oncolytic adenovirus, was approved in China, directed against head and neck squamous cell carcinoma to overexpress the p53 stimulating apoptotic pathway in tumor cells [281]. Last, T cell therapy are a crucial part in the treatment of tumor tissues. In this thesis we focus on the modification of $CD8^+$ T cells to overcome hypoxic conditions in melanoma and colon cancer. Therefore, Mb, a small oxygen binding protein is introduced in the cells to improve the oxygen absorption resulting in an enhanced T cell metabolism *in vitro* and *in vivo*. All these therapies can be combined with different treatment options to boost the host immunity or promote the elimination of tumor cells.

2.13.1. Checkpoint Therapy

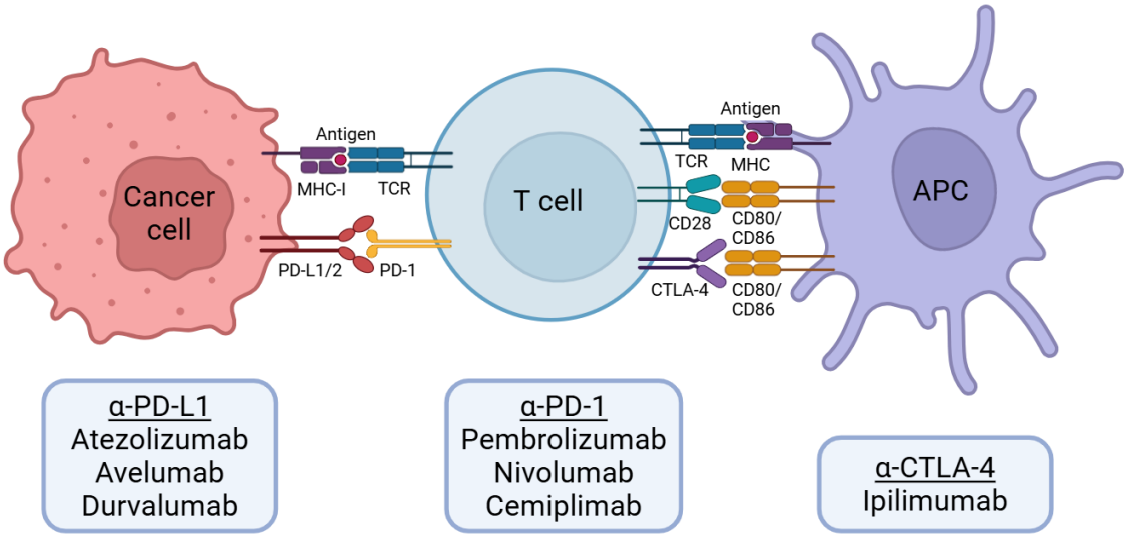

Figure 9: Checkpoint therapy to improve T cell function. Schematic illustration of T cells interacting with either cancer cells or APCs via the TCR–MHC-I–peptide complex. Cancer cells can inhibit T-cell activity through PD-L1/PD-L2 binding to PD-1 on T cells. FDA-approved α-PD-L1 inhibitors include Atezolizumab, Avelumab, and Durvalumab, while α-PD-1 inhibitors include Pembrolizumab, Nivolumab, and Cemiplimab. T cells also engage CD80/CD86 on APCs through either CD28, providing costimulatory signals, or CTLA-4, which suppresses T-cell activation. FDA-approved α-CTLA-4 therapy is Ipilimumab. Adapted from Sharma *et al*., 2015 [282].

A milestone in the cancer therapy was the introduction of ICI to maintain T cell function and promote anti-tumor immunity [283]. Tumor cells have developed strategies to evade immune surveillance by overexpressing ligands binding immune checkpoints on cytotoxic T cells. These checkpoints are important for the regulation of immune cells to prevent autoimmune reactions [232]. CTLA4 is homologous to the costimulatory protein CD28, binding B7-1 (CD80) and B7-2 (CD86) with a higher affinity on APCs [233, 284]. This competitive binding leads to a downregulation of T cell activation with reduction of proliferation and promotion of an anergic state [285]. The phosphorylation through Src-kinases of the intracellular YVKM-motif recruits Triphosphatases SHP-2 and PP2A, which in turn dephosphorylate key players in the TCR signal transduction like CD3zeta, ZAP70 and Lat [286-288] (see 2.9. T cell activation). Also, the Ras signal is disturbed by dephosphorylating p52SHC by not forming GRB2/SOS/Ras complexes [289]. This results in downregulation of NFAT and NF-κB. In 2011 the U.S. FDA approved the drug Ipilimumab, a monoclonal antibody directed against CTLA-4 for the treatment of metastatic malignant melanoma [35].

Furthermore, in 2014, Pembrolizumab and Nivolumab, and in 2025 Cemiplimab, monoclonal antibodies targeting PD-1, were approved. Subsequently, in 2016 and 2017, Atezolizumab, Avelumab and Durvalumab, monoclonal antibodies directed against Programmed Death Ligand 1 (PD-L1), received approval for the treatment of metastatic melanoma and bladder cancer, Merkel cell carcinoma, and non-small lung cancer, respectively. PD-1 is an inhibitory cell surface receptor of activated immune cells, mostly T cells, with intracellular ITIM and immunoreceptor tyrosine-based switch motif (ITSM) [290]. After the ligand binding of PD-L1, Src homology region 2 domain-containing phosphatase-2 (SHP-2) is recruited and further dephosphorylated proximal signalling protein of the TCR activation pathway, like PI3K and AKT [290, 291]. This results in a decrease of cell proliferation, cytokine production and survival. The overexpression of PD-L1 was observed in different solid tumors, including melanoma, pancreatic cancer and colon cancer [292-294]. It is known to play a key role in the cancer immune escape [295, 296]. Furthermore, it was reported that Melanoma patients with PD-L1 expressing cells are more sensitive to anti-PD-1 treatment [297]. Also, another study reported that high levels of PD-L1 expressed on tumor infiltrating immune cells correlates with anti-PD-L1 treatment [298]. In addition, by introducing ICT against PD-1 or PD-L1 a decreased tumor growth in solid tumors was observed, which can also be combined with different therapeutic approaches, like ACT [299].

However, ICT still show some risks and challenges to overcome, which has to be tackled in future researches. Not all patients respond to this form of therapy and may arise resistances [300]. In addition, the tumor heterogenicity exhibits various cell types that may respond differently to the therapeutic approach [301]. Further, no clear and reliable biomarkers could be detected to predict which patient respond well to the form of therapy [302]. Most known immune-related adverse events (irAEs) are dermatitis, colitis, hepatitis, pneumonitis and hypothyroidism [303]. Leading to the conclusion, that ICT still needs research to improve the positive effect and responders.

2.13.2. CART Therapy

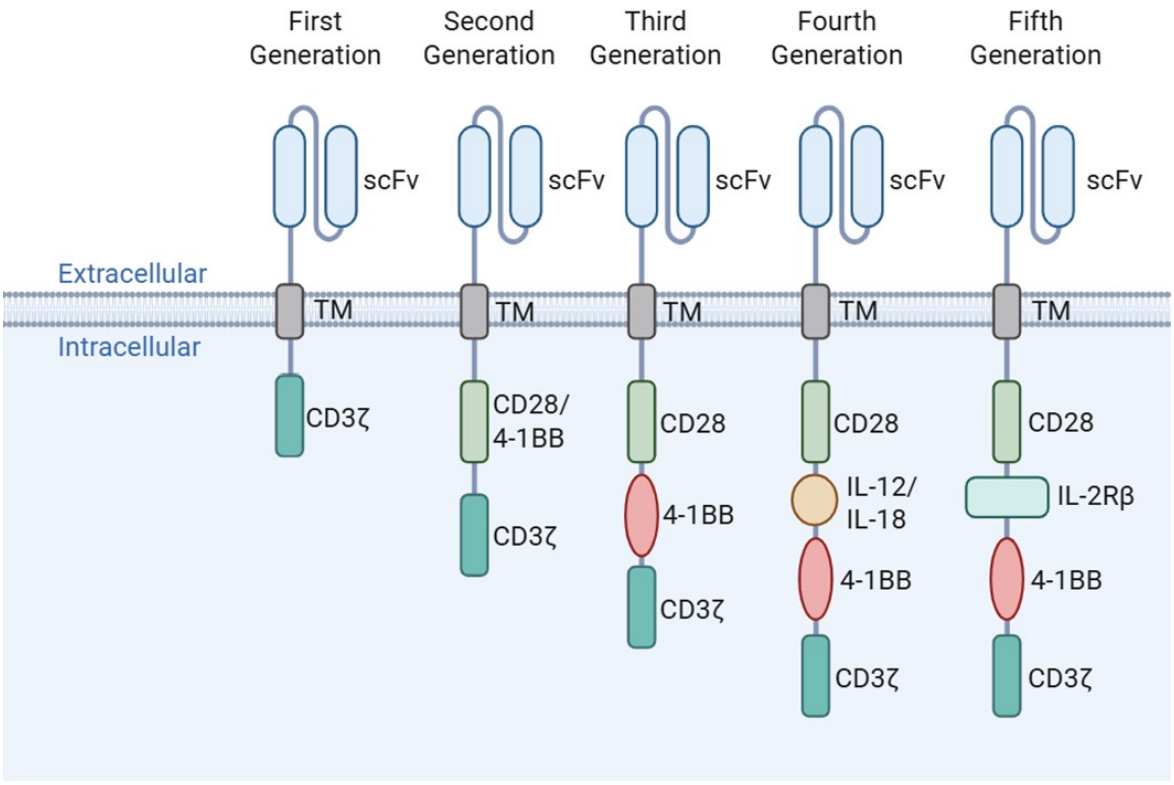

Figure 10: Five generations of CAR T cell therapy. Schematic illustration of the CAR T cell receptor. All generations contain the binding domain (scFv), the transmembrane (TM) domain, and the CD3ζ signalling domain. The first generation contains a single signalling domain, the second generation two, and the third to fifth generations three signalling domains, incorporating CD28 and 4-1BB co-stimulatory domains. Additionally, the fourth generation is designed to induce cytokine production, such as IL-12 or IL-18, while the fifth generation includes an IL-2 receptor β (IL-2Rβ) signalling domain. Adapted from Wang *et al*., 2025 [304].

A new method that has revolutionised cancer therapy is the use of synthetic receptors overexpressed on T cells. This chimeric antigen receptor (CAR) is directed against a tumour-associated antigen (TAA), which is located on the surface of the tumour cells to be targeted [305]. If possible, this TAA should be expressed on healthy tissue either in very small quantities or not at all in order to rule out an autoimmune reaction, by overcoming on-target off-target (OTOT) tumor toxicity [306]. By expressing the CAR, the cytotoxic T cells can be reprogrammed and directed against the tumour cells, which is expected to lead to successful therapy. The CAR is bound via a V_L and V_H chain of a monoclonal antibody directed against the respective TAA [37]. These chains are joined to form a scFv with the aid of a peptide linker [307]. A spacer sequence was added after the binding site, allowing the distance to the

membrane surface to be individually selected, which has a decisive influence on the effectiveness of the CAR construct [308]. A hinge region provides CAR stability [308]. CD28 or CD8 are commonly utilized in this context, which are also part of the TCR or are essential for signalling transduction of the costimulatory signal [309]. The transmembrane domain of the before mentioned structures is also used here. The signal transduction domain is listed intracellularly. CD3ζ is commonly used here, which carries ITAM motifs and is also responsible for signalling in a regular TCR (see 2.9. T cell activation) [309]. This construct is commonly called first generation CAR. The signal transduction domain can also be extended by the intracellular domain of CD28 (see 2.9. T cell activation) or 4-1BB (CD137) of the TNF-receptor superfamily [310]. In addition to CD28, 4-1BB is another costimulatory marker that triggers a signalling cascade by binding 4-1BBL expressed on APCs, including DCs, macrophages and B cells which positively regulated T cell immunity and survival of T cells [310, 311]. The Ligation of 4-1BB recruits TRAF1 and TRAF2, forming a 1:2 heterotrimer, which mobilizes cIAP1/2 [312]. This recruitment is essential for activation of TNF-α-induced NF-κB pathway [313]. TRAF2 initiates the signalling through K63-linked E3 ubiquitin ligase activity, catalysing the formation of K63-linked polyubiquitin chains [314]. This ubiquitination recruits TAK1, following the IKK-complex leading to the NF-κB translocation in the cellular nucleus, promoting survival [315]. Further it activates the MAPK/ERK signalling pathway promoting proliferation and differentiation and lastly it activates the PI3K-Akt-mTOR signalling pathway for cell growth and metabolic activation [316]. Depending on whether two or three signalling domains are maintained in the CAR construct, second or third generation CAR are designed. The fourth generation, so called T cells redirected for antigen-unrestricted cytokine-initiated killing (TRUCKs) of CARs are expanded by Cytokines under a NFAT promotor, mostly IL-12 or IL-18, to promote IIFN-γ secretion [317, 318]. Lastly, the fifth generation of CARs were designed to introduce IL2Rβ promoting survival effector genes and IL-2 itself [319]. Furthermore, to overcome antigen heterogenicity, Tandem CARs were designed to express two separate scFv, each targeting different antigens [320]. In 2017 the first CART cell therapy Tisagenlecleucel was approved by the FDA against ALL [321]. This CAR is directed against CD19 with an CD8α hinge and transmembrane domain and a 4-1BB and CD3ζ signalling domain [322]. CD19, a transmembrane glycoprotein a coreceptor of the B cell receptor (BCR) is involved in the activation process of the B cells and expressed from early pro-B cell state to mature B cells [323]. Targeting CD19 leads to B cell aplasia, resulting in a reduction of antibodies, a decreased immune memory and higher infection risk. Furthermore, CART can induce the Cytokine release Syndrome (CRS) by cytokine secretion, like the

proinflammatory IL-6 leasing to a strong immune response through various immune cells, which can lead to a shock in the patient [324]. In a study from 2022 Melenhorst *et al*. has shown that CART cells are still detectable in patients in remission 9 years after infusion [325]. Even if CART cells have shown strong effect especially against liquid leukaemia the key challenges to tackle in the future is to overcome also immune suppressive TME, which still compromises CART cell delivery and antitumor activity [326]. Also, CART cells exhaust faster due to one single antigen and potent signalling of the synthetic receptor [327]. Advantages of the CART cell therapy are the high specify targeting the TAA and the possibility to personalize the therapy. Further, long term effects are possible because of the persistence of CART cells forming an immunological memory [328]. Lastly, CART cells are MHC-independent, therefore no tumor escape through MHC downregulation is possible [38].

3. Aim of this study

Hypoxia in solid tumors has been shown to limit T cell effector functions and successful treatment options by promoting exhaustion. Therefore, we are aiming for overcoming hypoxic conditions by introducing Mb overexpression in primary murine cytotoxic T cells by retroviral transduction for solid tumor treatment. Mb is known for its oxygen storage capacity and ROS scavenging effects as an OBP predominantly expressed in muscle cells. This study examines the working hypothesis, whether Mb overexpression in T cells improves T cell metabolism and antitumor effector function *in vitro* and *in vivo*.

Therefore, we were aiming to determine the effect of Mb overexpression on T cell metabolism. Enhanced oxygen presence might boost the OXPHOS resulting in more ATP production, fulfilling the high energy demand needed in the TME. Also, this study was examining the potential formation of ROS, which are leading to cell damages, loss of function and apoptosis.

To determine the effector function of Mb-overexpression in T cells, transgenic TCR expressing T cells (P14), which are directed against the gp33 peptide of LCMV, were used. These T cells were cocultured with B16-F10-gp33 melanoma cells, which present the gp33 peptide via MHC-I. The readout focused mainly on the production of proinflammatory cytokines, GzmB and the killing potential of the target cells.

To date, the clinical approaches of solid tumor treatment are inadequate. Even newer approaches, like CART cell therapy are just approved for haematological malignancies. Therefore, B16-F10-gp33 tumor-bearing mice were treated with Mb-overexpressing $P14^+$ T cells and Control $P14^+$ T cells to determine the tumor effector function and tumor growth *in vivo*. Furthermore, we discovered with this approach that Mb-overexpressing T cells showed increased effector function and reduced tumor growth, however, this was accompanied by increased exhaustion. Thus, checkpoint inhibition against PD-1 was added to the experimental approach to further reduce tumor growth.

4. Material

4.1. Media and Buffer

Table 1: Composition of Buffer and Media used in this study

Buffer	**Composition**
Dulbecco's Modified Eagle's Medium (DMEM)	DMEM Medium, 10% FCS, Penicillin/ Streptavidin/ L-Glutamine
Iscove's Modified Dulbecco's Medium (IMDM)	DMEM Medium, 10% FCS, Penicillin/ Streptavidin/ L-Glutamine
Roswell Park Memorial Institue (RPMI) 1640 Medium	DMEM Medium, 10% FCS, Penicillin/ Streptavidin/ L-Glutamine, 50µM β-Mercaptoethanol
Seahorse XF RPMI Medium	10 mM glucose, 1 mM pyruvate, 2 mM L-glutamine
Magnetic-activated cell sorting (MACS) buffer	2 mM EDTA, 2.5g BSA in 500 ml PBS
Fluorescence-Activated cell Sorting (FACS) buffer	1% FCS, 5mM EDTA in PBS
Luria broth (LB) Medium	10g/l NaCl, 10g/l tryptone, 5g/l yeast extract in dH_2O
LB Agar	10g/l NaCl, 10g/l tryptone, 5g/l yeast extract, 15g/l agar, pH=7.0±0.2, in dH_2O
PBST	0.1% Triton X-100 in PBS
Histological blocking buffer (Methanol fixation)	3% donkey serum in 0.4% Triton X-100 in PBS
Histological blocking buffer (Acetone fixation)	10% FCS in PBS

4.2. Reagents

Table 2: Reagents and chemicals used in this study

Reagent	**Manufacturer**	**Catalog number**
Phosphate buffered saline (PBS)	Gibco™	14190-144
DMEM	PAN-Biotech	P04-03600
IMDM	Sigma-Aldrich	I3390

RPMI 1640 Medium	PAN-Biotech	P04-17525
Seahorse XF RPMI Medium	Agilent Technologies	103576-100
Ampicillin	AppliChem	A0839
2-Propanol/ Isopropanol	Merck	1.09634.2511
Super Optimal broth with Catabolite repression (S.O.C.) Medium	Invitrogen™	15544-034
jetPRIME® Transfection Reagent	Polyplus Reagents	101000046
Polybrene	Millipore-Sigma	TR-1003-G
hIL-2	Thermo Fisher Scientific	200-02
Gp33 – Peptide	Thermo Fisher Scientific	custom-made
SIINFEKL - Peptide	Thermo Fisher Scientific	custom-made
Poly I:C	Merck	27-4732-01
G418 sulfate (Geneticin)	Gibco	10131027
Brefeldin A (1000x)	Invitrogen™, eBioscience™	00-4506-51
Tissue-Tek® O.C.T.™ Compound	Sakura	4583
Methanol	Merck	1.06009.2511
Acetone	Sigma-Aldrich	320110
Triton™ X-100	Sigma-Aldrich	T9284
TRIzol® Reagent	Invitrogen™	15596018
Chloroform	Merck	1.02445.1000
Vectashield Vibrance Antifade Mounting Medium	Vector Laboratories	H-2000
Dihydroethidium (DHE)	Sigma-Aldrich	199303
Resazurin	Merck	R7017
Poly-L-lysine	Sigma-Aldrich	P4707
Annexin V Binding Buffer	BD Bioscience	51-66121E
AMP	Sigma-Aldrich	A1752
ADP	Sigma-Aldrich	A2754
ATP	Sigma-Aldrich	A7699
GMP	Sigma-Aldrich	G8377
cGMP	Sigma-Aldrich	G6129

Acetyl-CoA	Sigma-Aldrich	A2056
Succinyl-CoA	Sigma-Aldrich	S1129
IS Acetyl-CoA 13C2	Sigma-Aldrich	658650
IS ATP 15N5	Merck	3987
IS ADP 15N5	Cambridge Isotope Laboratories	741167
IS AMP 15N5	Sigma-Aldrich	3802
alpha-ketoglutarat	Sigma-Aldrich	K1128
succinic acid	Sigma-Aldrich	S3674
citric acid	Sigma-Aldrich	27109
Isocitrat	Sigma-Aldrich	I-1252
Pyruvat	Sigma-Aldrich	107360
cis-aconitic acid	Sigma-Aldrich	A3412
fumaric acid	Sigma-Aldrich	47910
malic acid	Sigma-Aldrich	94916
lactic acid	Sigma-Aldrich	L1750
oxalacetic acid	Sigma-Aldrich	4126
IS Pyruvat 13C3	Cambridge Isotope Laboratories	CLM 2440
IS Lactat d3	Cambridge Isotope Laboratories	DLM 9071
IS Fumaric acid 13C4	Cambridge Isotope Laboratories	CLM1529
IS Malic acid 13C4	Cambridge Isotope Laboratories	CLM 8065
IS Citric acid 13C3	Cambridge Isotope Laboratories	CLM 9876
IS alpha-glutaric acid 13C5	Cambridge Isotope Laboratories	CLM 2411
Phosphoenolpyruvat	Sigma-Aldrich	P0564
2-Phosphoglycerat	Sigma-Aldrich	19710
3-Phosphoglycerat	Sigma-Aldrich	P 8877
Fructose1,6biphosphat	Sigma-Aldrich	F6803

4.3. Antibodies and fluorescent dyes

4.3.1. T cell activation

Table 3: Antibodies used in this study for T cell activation

Antibody	Clone	Labelling	Manufactor	Catalog Number
CD3	145-2C11	unlabelled	Invitrogen, eBioscience™	16-0031-86
CD28	37.51	unlabelled	BD Biosciences, BD Pharmingen™	553294

4.3.2. Surface FACS staining

Table 4: Antibodies used in this study for surface staining

Antibody	Clone	Labelling	Manufactor	Catalog Number
CD8α	53-6.7	BV711	BD Biosciences, BD Horizon™	563046
CD8α	53-6.7	PerCP-Cyanine5.5	Invitrogen, eBioscience™	45-0081-82
Thy1.1	HIS51	FITC	Invitrogen, eBioscience™	11-0900-85
Thy1.1	HIS51	APC	Invitrogen, eBioscience™	17-0900-82
Vα2	B20.1	PE	Invitrogen, eBioscience™	12-5812-82
CD45.1	A20	PE-Cy7	Invitrogen, eBioscience™	25-0453-82
CD45.1	A20	FITC	Invitrogen, eBioscience™	11-0453-85
PD-1	J43	PE-CF594	BD Biosciences, BD Horizon™	562523

Tim-3	RMT3-23	PE	Invitrogen, eBioscience™	12-5870-82
CD62L	MEL-14	BV510	BD Biosciences, BD Horizon™	563117
CD44	IM7	BV786	BD Biosciences, BD Horizon™	563736
CD69	H1.2F3	Alexa Flour 700	BD Biosciences, BD Pharmingen™	561238
KLRG1	2F1	BV650	Invitrogen, eBioscience™	64-5893-82
IL-7R	A7R34	FITC	Invitrogen™	11-1271-82
IL-7R	A7R34	Alexa Fluor-700	Invitrogen™	56-1271-82
CD45.1	A20	PE-Cyanine 7	Invitrogen™	25-0453-82
TCR V α 2	B20.1	PE	Invitrogen™	12-5812-82
Cell Proliferation Dye		eFluor™ 450	Invitrogen, eBioscience™	65-0842-85
Annexin V	-	APC	ImmunoTools	31490016

4.3.3. Intracellular FACS staining

Table 5: Antibodies and fluorescent dyes used in this study for intracellular staining

Antibody	**Clone**	**Labelling**	**Manufactor**	**Catalog Number**
IFN-γ	XMG1.2	APC	Invitrogen, eBioscience™	17-7311-82
TNF-α	MP6-XT22	eFluor™ 450	Invitrogen, eBioscience™	48-7321-82
GzmB	NGZB	PE-CF594	Invitrogen, eBioscience™	61-8898-82
IL-2	JES6-5H4	PerCP-Cyanine5.5	Invitrogen, eBioscience™	45-7021-82

Eomes	Dan11mag	PE-CF594	Invitrogen, eBioscience™	61-4875-82
T-Bet	eBio4B10	PE-Cy7	Invitrogen, eBioscience™	25-5825-82
TOX	REA473 TXRX10	PE	Miltenyi	130-120-716
TCF1/TCF7	C63D9	APC	Cell Signaling	6709S
HIF-1α	Mgc3	PE	Invitrogen™	12-7528-82
DAPI	-	-	Invitrogen™	D1306
Fixable Viability Dye	-	eFluor™ 450	Invitrogen, eBioscience™	65-0863-14
7-AAD	-	-	Invitrogen™	00-6993-50
Peroxy Orange 1	-	-	APExBIO	B5775
MitoSOX™	-	-	Invitrogen™	M36008

4.3.4. Western Blot

Table 6: Antibodies used in this study for Western Blot

Antibody	**Clone**	**Manufactor**	**Catalog number**
Anti-α-Tubulin Mouse mAb	DM1A	Merck	CP06
Myoglobin	D2F5X	Cell Signaling	25919
Goat anti-mouse IgG	Polyclonal	Licor	IR800CW
Goat anti-rabbit IgG	Polyclonal	Licor	IR680RD

4.3.5. Histology staining

Table 7: Antibodies and fluorescent dyes used in this study for immunohistology staining

Antibody	**Clone**	**Labelling**	**Manufactor**	**Catalog number**
Anti-Cleaved Caspase-3	D175	unlabelled	Cell Signaling	9661S
Anti-CD8α	53-6.7	PerCP-Cyanine5.5	Invitrogen, eBioscience™	45-0081-82

Anti-HIF-1α	Polyclonal	unlabelled	Abcam	AB216842
Vimentin	V9	Alexa Fluor™ 488	Santa Cruz Biotechnology	B0625
Anti-Cytokeratin 18	C-04	Alexa Fluor™ 488	Santa Cruz Biotechnology	F2123
Donkey Anti-rabbit IgG	Polyclonal	Alexa Fluor™ 555	Invitrogen™	A31572
Donkey Anti-rabbit IgG	Polyclonal	Alexa Fluor™ 488	Invitrogen™	A21206
DAPI	-	-	Invitrogen™	D1306

4.3.6. Checkpoint Inhibition Antibodies

Table 8: Antibodies used in this study for ICT

Antibody	**Manufactor**	**Catalog number**
Anti-PD-1	Bio Cell	BE0089
Isotype Control	Bio Cell	BE0146

4.4. Primer

Table 9: Primers used in this study for RT-PCR

Gen	**Forward Primer**	**Reverse Primer**
HIF-1α	AGTGTACCCTAACTAGCCG	CACAAATCAGCACCAAGC
CREB	ACCATGGAATCTGGAGCCGAGAAC	CTGTAGGAAGGCCTCCTTGAAAGA
NOX1	CTCTCTCCTGGAATGGCATC	TGGAAAACATCCTCACTGGC
TBP	GTCCGGGCCCATGGAAGACAAAA	TGTTGCTCTTCAGAGGGACTGGG
mMyoglobin	CTGTTTAAGACTCACCCTGAGAC	GGTGCAACCATGCTTCTTCA
Thy1.1	TGCTCTCAGTCTTGCAGGTG	TGGATGGAGTTATCCTTGGTGTT

4.5. Kits

Table 10: Kits used in this study

Kit	Manufactor	Catalog number
OxyBlot™ Protein Oxidation Detection	Merck	S7150
Luminescent ATP Detection Assay Kit	abcam	ab113849
GSH-Glo™ Glutathione Assay	Promega	V6911
XF Cell Mito Stress Test	Agilent Technologies	103015-100
XF Glycolytic Rate Assay	Agilent Technologies	103344-100
$CD8^+$ T cell isolation Kit	Miltenyi Biotec	130-104-075
Anti-CD90.1 microbeads	Miltenyi Biotec	130-121-273
NucleoBond® Xtra Midi Kit	Macherey-Nagel	740410.100
NucleoBond® Xtra Maxi EF	Macherey-Nagel	740424.50
SYBR Green	Bio-Rad	1725151

4.6. Construct design

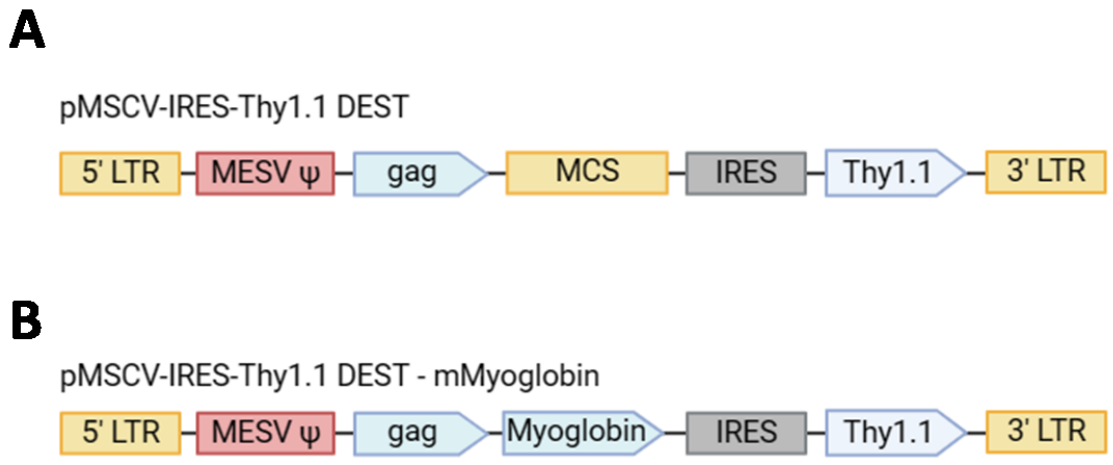

Figure 11: Used plasmids for the overexpression of Thy1.1 and mMyoglobin. Scheme of (A) pMSCV IRES-Thy1.1 DEST and (B) pMSCV-IRES-Thy1.1 DEST-mMyoglobin construct are illustrated.

The pMSCV-IRES-Thy1.1 DEST vector (Addgene #17442) was used as a control vector to overexpress Thy1.1 in target cells, functioning as a genetic marker (Figure 11A). For the

overexpression of Mb, the murine Mb gene was cloned in the multiple cloning side (MCS) of pMSCV-IRES-Thy1.1 DEST vector (Figure 11B). Both plasmids contain a 5´ Long Terminal Repeat (5´LTR), which includes promoter and transcriptional regulatory sequences. Further, the viral promotor of Moloney Murine Sarcoma Virus (MESV) and the packaging signal ψ are included to drive gene expression and enable viral RNA packaging, respectively. Next, gag is coding for viral structural proteins and the Internal Ribosome Entry Side (IRES). Last, 3´ Long Terminal Repeat (3´LTR) contains regulatory elements important for transcription termination and polyadenylation and provides together with 5´LTR the integration signals required for insertion of the viral genome into host DNA. The construct pMSCV-IRES-Thy1.1 DEST - mMyoglobin was generated by BioCat GmbH.

5. Methods

5.1. Mice

All mice were bred in house in the Central Institution for Animal Research and Scientific Animal Welfare (ZETT) at the Heinrich-Heine-University in Düsseldorf, Germany. The mice were maintained under specific pathogen-free conditions. Experiments were performed under the authorization of State Agency for Nature, Environment and Consumer Protection (LANUV) in accordance with the German law for animal protection. C57BL/6J mice were obtained and used in this experimental setup. For adoptive transfer experiments, $P14^+$ mice expressing a transgenic TCR recognizing LCMV glycoprotein gp33 presented by MHC class I-Db were used as previously described [329]. Additionally, $OT\text{-}1^+$ mice, which recognize SIINFEKL peptide of ovalbumin (ova) presented by MHC class I-Kb by transgenic TCR were included in the study [330]. Both mice lines are expressing CD45.1, a specific isoform of CD45, which is used as a marker molecule [331]. Tumor-bearing mice were sacrificed as indicated or when the tumor ulcerated or tumor volume reached a maximum of $1500mm^3$.

5.2. Cell lines

The B16F10-gp33 cancer cell line was used. It is derived from C57BL/6 murine B16F10 skin melanoma expressing the LCMV glycoprotein peptide gp33. B16F10-gp33 were provided by Dr. H.P. Pircher, Freiburg, Germany and cultured as described previously [332]. Also, MC38-ova, a murine colon cancer line derived from C57BL6, expressing the ova peptide was used. B16F10-gp33 and MC38-ova were maintained in Dulbecco's Modified Eagle Medium (DMEM) containing 10% fetal calf serum, 1% penicillin and streptomycin, 1% L-glutamine, and 0.4 mg/mL of G-418 selective antibiotic.

5.3. Purification and transduction of T cells

Following the manufacturer’s recommendations, single cell suspended splenocytes were enriched with the mouse CD8 purification kit (Miltenyi). They were activated overnight with 10 U/mL interleukin (IL)-2, 4 µg/mL anti-CD3 precoated in phosphate-buffered saline (PBS), and 1 µg/mL anti-CD28 overnight, before being transduced by spinoculation with Thy1.1 (Control) or Thy1.1-Myoglobin (Myoglobin) packaging retrovirus to induce overexpression in T cells with 100 U/mL IL-2 and 10 µg/mL Polybrene (Millipore-Sigma). These packaging retroviruses were obtained by transfection of 293T or Plat-E cells with jetPRIME Transfection

Reagent (Polyplus) containing pCL-Eco and pMSCV-IRES-Thy1.1 DEST or pMSCV-IRES-Thy1.1 DEST-mMyoglobin plasmids. T cells were sorted 1-day later for the $Thy1.1^+$ population using the CD90.1 purification kit (Miltenyi). T cells were cultured and expanded in Roswell Park Memorial Institute (RPMI) 1640 Medium containing 10% fetal calf serum, 1% penicillin and streptomycin, 1% L-glutamine, 50 µM β-mercaptoethanol and 10 U/mL IL-2.

5.4. Tumor-bearing mice and adoptive T cell transfer

5×10^5 B16F10-gp33 or 1×10^6 MC38-ova cells were subcutaneously injected in the left flank of C57BL/6J mice. For studying the influence of hypoxic and normoxic conditions on $CD8^+$ T cells, B16F10-gp33 injected mice were sacrificed on day 11 after tumor cell injection. Tumor and spleen tissue samples were collected and analysed. For adoptive T-cell transfer, splenocytes harvested from $P14^+$ mice were activated with 10 U/mL IL-2 and 0.1 µg/mL gp33 peptide overnight and splenocytes harvested from OT-I^+ mice were activated with 10 U/mL IL-2 and 0.1 µg/mL SIINFEKL peptide overnight. Afterwards, the cells were transduced with control or Mb packaged retrovirus. Splenocytes containing 5×10^5 or 2×10^6 $CD8^+$ $P14^+$ $CD45.1^+$ T cells were transferred at day 6–7 into B16F10-gp33 tumor-bearing C57BL/6J mice or 5×10^5 $CD8^+$ OT-1^+ $CD45.1^+$ T cells into MC38-ova tumor-bearing C57BL6J mice, which were matched and randomized according to tumor size. On the same day, 50 µg Poly I:C and 10 µg gp33 or SIINFEKL peptide were injected intravenously. The tumor was monitored every second day. For the use of checkpoint inhibition, every second day 200 µg anti-PD-1 or isotype control was injected intraperitoneally.

5.5. Plasmid expansion and transformation

Competent Stabl2 and Stbl3 Escherichia Coli (E. Coli) bacteria were used for the transformation and plasmid expansion. 2-5 µl of respective plasmid DNA (at least 50µg) were added to 10 µl competent bacterial cells and incubated on ice for 30 min. To create a thermal imbalance resulting in membrane destabilization and facilitate the uptake of extracellular plasmid DNA, the plasmid bacterial mixture was heat shocked at 42°C for 45 sec, followed by immediate cooling on ice for 2 min. 500 µl S.O.C. medium was added before the cells were shaken at 900 rpm for 1h at 37°C. The transformed bacteria were plated on an agar plate consisting LB Agar with respective antibiotics and incubated over night at 37°C. The formed single cell clones were picked and shaken in 500 µl blank LB Medium at 600-700 rpm for 3-4h at 37°C. 100 µl

(Plasmid DNA Midipreparation) or 300 µl (Plasmid DNA Maxipreparation) of bacterial cell suspension are transferred in 100 ml or 300 ml LB-Medium containing antibiotics in Erlenmeyer flask, respectively and shaken at 220 rpm overnight at 37°C. Following the manufacturer's recommendations of NucleoBond® Xtra Midi plasmid isolation kit or NucleoBond® Xtra Maxi plasmid isolation kit (Macherey-Nagel) for plasmid isolation. The plasmid is dissolved in a respective amount of DEPC-H_2O and the plasmid DNA concentration was determined using a NanoDrop spectrophotometer by measuring the absorbance at 230 nm, 260 nm and 280 nm.

5.6. RNA purification and RT-PCR

RNA was isolated from spleen and tumor tissues or primary T-cell cultures by homogenizing the samples in TRIzol (Invitrogen) as previously described [333]. Chloroform was added and the middle layer was collected and mixed with isopropanol for precipitation. After washing with ethanol and drying the sample the reverse transcription polymerase chain reaction (RT-PCR) was set up. SYBR Green was used to detect the double-stranded DNA. Primers were customized for the usage (see 4.4. Primer).

5.7. Western Blot

Proteins were loaded on 10% (w/v) sodium dodecyl sulfate (SDS)-polyacrylamide gel and transferred on nitrocellulose membrane. The membrane was blocked afterwards and probed with Myoglobin or α-Tubulin (Cell Signaling) primary antibodies. After washing, a secondary fluorescent-conjugated antibody (Li-COR) was added. The Odyssey Fc Imaging System (Li-COR) was used for signal detection.

5.8. Detection of carbonylated proteins

To quantify oxidative damage of proteins, the OxyBlot Protein Oxidation Detection Kit (Merck) was applied. Thiols in Thy1.1 (Control) or Thy1.1-Myoglobin (Myoglobin)-expressing $CD8^+$ T cells were blocked with 100 mM N-Ethylmaleimide (NEM). 5 µg of protein lysates were used to derivatize carbonyl groups to 2,4-dinitrophenylhydrazone (DNP-hydrazone) by reaction with 2,4-dinitrophenylhydrazine. Proteins were separated by SDS-polyacrylamide gel electrophoresis (PAGE) and blotted on nitrocellulose using stain-free gels (Bio-Rad) and the trans-blot turbo transfer system (Bio-Rad). Carbonylated proteins were

visualized by primary antibodies against DNP, secondary anti-rabbit antibodies coupled to StarBright Blue 700 (Bio-Rad), and the ChemiDoc imaging system (Bio-Rad). Band intensities were quantified by ImageJ.

5.9. Flow cytometric analysis

Experiments were performed using Fluorescence-Activated Cell Sorting (FACS) Fortessa and analysed using FlowJo software as previously described [334]. For T-cell staining, single cell suspensions were incubated with antibodies (anti-CD8a, anti-Thy1.1, anti-PD-1, anti-Tim-3, anti-CD44, anti-CD62L, anti-KLRG1, anti-IL-7R, Invitrogen) for 20 min at 4°C. Transcription factor and intracellular cytokine staining was performed as described previously [335]. For the staining of transcription factors, single cell suspensions were incubated with surface antibodies (anti-CD8, anti-Thy1.1, Invitrogen) for 20 min at 4°C, fixed and permeabilized with antibodies binding the respective transcription factor (HIF-1α, Eomes, TCF-1, TOX, Invitrogen, Nrf2, EnoGene). For intracellular cytokine re-stimulation, single cell suspensions were stimulated with LCMV-specific peptides gp33 for 1 hour. Brefeldin A (Invitrogen) was added for another 5 hours incubation at 37°C followed by staining (anti-CD8, anti-Thy1.1, anti-IFN-γ, anti-TNF-α, anti-GzmB, anti-IL-2, Invitrogen). Splenocytes from adoptively transferred $P14^+$ T cells were stained with anti-CD45.1, anti-CD8 and anti-Vα2 antibodies. For measurement of mitochondrial ROS or H_2O_2 signals in living cells, cells were incubated with surface antibodies (anti-CD8, anti-Thy1.1, Invitrogen) for 20 min at 4°C after adding MitoSox Red (Invitrogen) or Peroxy Orange 1 (PO1) (APExBIO) for 10 min or 30 min at 37°C. For the proliferation assay, the cells were stained beforehand with cell proliferation dye (Invitrogen) for 10 min at 37°C. After 24, 48 and 72 hours the cells were incubated with surface antibodies (anti-CD8, anti-Thy1.1, Invitrogen) for 20 min at 4°C. For viability assessment, cells were stained with Annexin V (ImmunoTools) and 7AAD (Invitrogen) in Annexin V binding Buffer (BD Bioscience) for 20 min at 4°C.

5.10. Detection of ATP, GSH, intracellular ROS and NAD^+/H_20 conversion

For the detection of ATP, cells were seeded into a 96-well white plate (5×10^4/well) and Luminescent ATP Detection Assay Kit (Abcam) was used following manufacturer's recommendations. For the detection of GSH, cells were seeded into a 96-well white plate

(2×10^5/well) and Luminescent GSH-Glo Glutathione Assay (Promega) was used following manufacturer's recommendations. For the detection of intracellular ROS generation, the technique using specific oxidation of dihydroethidium (DHE) by intracellular superoxide anion was used. Cells were seeded into 96-well black plates (50,000/well) and treated with 2.5 mM H_2O_2 for 1 hour. Following the incubation, cells were washed with PBS and resuspended in fresh medium containing DHE (2 µM) and a time kinetic measurement was performed at 518 nm excitation and 605 nm emission. For the detection of $NADH/H^+$ to NAD^+/H_2O conversion, cells were seeded in 96-well black plates (2×10^4/well) and resazurin (0.01 mg/mL, Merck) was added. After 30 min and 3 hours, measurements were performed at 530 nm excitation with 590 nm emission. Luminescence and kinetic fluorescence measurements were performed using Spark Multimode Microplate Reader (Tecan Group, Zürich, Switzerland).

5.11. Histology and immunofluorescence

Histological analysis of snap frozen tissue was performed as previously described [336]. For fixation, histology slides were put in pre-chilled methanol at - 20°C or in 100% acetone at room temperature (RT) for 30 min. For unconjugated antibodies, and overnight staining, the methanol fixation and staining protocol was followed, and for conjugated antibodies, the acetone fixation protocol for staining was followed.

In case of methanol fixation, the cryosections were washed three times for 5 min in phosphate-buffered saline with 0.1% Triton X-100 (PBST), blocked with 3% donkey serum in 0.4% Triton X-100 in PBS for 2 hours at RT, stained overnight with primary antibodies at 4°C followed by 3× washes in PBST and incubation with secondary antibody for 2 hours at RT. All antibodies were diluted in 0.4% Triton X-100/PBS solution containing 3% donkey serum. Sections were washed three times in PBST for 5 min, once in PBS for 5 min, followed by washing in ultrapure water for 5 min and mounted with Vectashield Vibrance Antifade Mounting Medium (Vector Labs, USA) with or without 4′,6-diamidino-2-phenylindole (DAPI), for counterstaining nuclei.

In case of acetone fixation, the cryosections were washed three times for 5 min in PBS (while shaking), blocked with 10% Fetal Calf Serum (FCS) in PBS (with FC-block) for 40 min at RT, stained with primary antibodies conjugated with fluorophores at RT for 1 hour followed by 3× washes in PBS. All antibodies were diluted in 1% FCS in PBS. Sections were mounted with Vectashield Vibrance Antifade Mounting Medium (Vector Labs, USA) with or without DAPI, for counterstaining nuclei.

Sections were stained with antibodies against cleaved caspase-3 (Cell Signaling), CD8a conjugated with PerCP-eFluor 710 (Invitrogen), HIF-1α (Abcam), Vimentin conjugated with Alexa 488 (Santa Cruz Biotech) and Cytokeratin 18 conjugated with Alexa 488 (Santa Cruz Biotech). Secondary antibodies such as donkey anti-rabbit IgG Alexa Fluor 555 or donkey anti-rabbit IgG Alexa Fluor 488 (Invitrogen) were used. Primary antibodies were used in 1:50 or 1:100 dilution and secondary antibodies were used in 1:500 dilution. Images were acquired with the ZEISS Axio Observer Z1 microscope and for quantifications, the images were analysed with ImageJ software, and for quantifications and statistical analysis GraphPad Prism was used. For HIF-1α and CD8a co-localization analysis, the JACoP plugin in ImageJ was used to determine colocalization correlation from the images by calculating Pearson's correlation coefficient. For each staining, four different mouse tumor/spleen sections were analysed. In each section, two to four ROIs (regions of interest) were analysed.

5.12. Electron microscopy

The cell samples were first fixed with a solution containing 4% paraformaldehyde and 2.5% glutaraldehyde in a buffer with 0.1% sodium cacodylate at pH 7.4. The pellets were enclosed in a small amount of 3% low melt agarose and stained for 1 hour in 1% osmium tetroxide. Subsequently, the samples were dehydrated using a series of ethanol washes (30%, 50%, 70%). Next, the samples underwent staining with a mixture of 1% uranyl acetate and 1% phosphotungstic acid in 70% ethanol for 1 hour. Subsequently, the samples were fully dehydrated using a graded ethanol series, embedded in Spurr's resin, and polymerized at 70°C for 8 hours. Thin sections (70 nm) were cut using an Ultracut EM UC7 (Leica, Wetzlar, Germany) and placed on 200 mesh copper grids. These sections were stained with 1.5% uranyl acetate for 25 min and lead citrate for 8 min. Images were captured using a Hitachi transmission electron microscope H7100 (Tokyo, Japan) operated at 100 kV with a Morada camera (EMSIS GmbH in Münster, Germany).

5.13. Focused ion beam scanning electron microscopy (FIB-SEM) and 3D-Modelling of mitochondria

The samples for transmission electron microscopy (TEM) images were also used for focused ion beam scanning electron microscopy (FIB-SEM) (Crossbeam 550, Carl Zeiss AG) measurements. The resin blocks were glued with conductive silver paste onto SEM aluminum

stubs and coated with a 25 nm gold layer (108 auto, Cressington Scientific Instruments, Watford, UK). Screening for cells was performed with the SmartSEM software package (Carl Zeiss AG, V.6.07) at an accelerating voltage of 15 kV (working distance 5 mm, SE2 detector). Image acquisition was done with Zeiss Atlas 5 (Carl Zeiss AG, software V.5.3.5.3).

Measurements of control T cells were done with gallium ion beam: 30 kV/3 nA, slice thickness: 25 nm, electron beam: 2 kV/2 nA, field of view: 32 µm, pixel size: 20 nm and dwell time: 0.7 µm with line average of 27. For Mb-expressing T cells, system parameters were: gallium ion beam: 30 kV/1.5 nA, slice thickness: 25 nm, electron beam: 2 kV/2 nA, field of view: 32 µm, pixel size: 20 nm and dwell time: 0.6 µm with line average of 21. For both sample types, SE2 and inLens detectors were used. The alignment and exportation of Image Stacks were carried out using the Zeiss Atlas 5 software suite.

Subsequently, these images were imported into the Thermo Fisher Amira 2021 software. The reconstruction of individual mitochondria was accomplished through manual segmentation of organelles in two dimensions (2D), culminating in the generation of a three-dimensional (3D) model. A minimum of 10 mitochondria per cell were subjected to the reconstruction process. Using the same software, the surface area and volume of each mitochondrion were computed.

5.14. Oxygen consumption rate and extracellular acidification

T cells were seeded into XF96 well plate pre-coated with poly-L-lysine at 2×10^5 cells per well. Prior to the measurement, cells were washed once and kept in Seahorse XF RPMI Medium containing 10 mM glucose, 1 mM pyruvate and 2 mM L-glutamine during the measurement. Mitochondrial respiration function was measured by Seahorse XF Cell Mito Stress Test Kit (Agilent) and glycolysis function was measured using Seahorse XF Glycolytic Rate Assay Kit (Agilent) according to the manufacturer's instructions.

5.15. Analysis of targeted metabolites by LC-MS/MS

Extraction of the targeted metabolites was performed by adding 300 µl Methanol/H_2O (80/20; v/v) to the 1 x 10^6 cells, which were homogenized by ceramic beads CK14 using Precellys lysing kit. The corresponding isotopically labelled internal standards were added to the extraction solution. The targeted compounds were analysed by UPLC-MS/MS. The system consists of a UPLC I-Class (Waters) coupled to a tandem mass spectrometer Xevo-TQ-XS (Waters). Electrospray ionization was performed in the negative ionization mode for the compounds fructose-1,6-bishphosphate, PEP and 2/3-phosphoglycerate [337]. The TCA,

energy metabolites (AMP, ADP and ATP) as well acetyl- and succinyl-CoA were measured in the positive ionization mode as referred in the literature [338-340]. Mass spectrometric quantitation of the compounds was carried out in the multiple reaction monitoring (MRM) mode. MassLynx software (v4.2; Waters, UK) was used for instrument's control and data acquisition. Quantitative analysis was performed by TagetLynx XS software (Waters, UK).

5.16. Statistical analysis and writing

GraphPad Prism (GraphPad Software, Inc.) was used for all statistical analyses. Data are expressed as mean ± SEM. For analysis of statistical significance between two groups, a Student´s t-test was used. For analysis of multiple time point experiments, two-way ANOVA was used. *$p<0.05$, **$p<0.01$, ***$p<0.001$ and ****$p<0.0001$ were considered as statistically significant. The programs GraphPad Prism, BioRender.com and Microsoft Power Point and were used for the creations of figures. The text was written using Microsoft Word, and the artificial intelligence tools ChatGPT (OpenAI), Perplexity.ai and DeepL were used to improve grammatical accuracy and enhance of the flow of the text.

6. Results

Due to the high demand for effective treatment strategies against solid tumors, we opt to develop a therapeutic approach to overcome hypoxic conditions within the TME. To achieve this, the OBP Mb is overexpressed in cytotoxic T cells, to compensate for the low oxygen levels typically occurring within the TME of solid tumors. Mb is known for its high oxygen affinity and its role in oxygen transport and storage [146]. Through its overexpression, T cells are expected to maintain their effector function even under hypoxic conditions. Improved T cell functionality under these otherwise immunosuppressive conditions may enhance anti-tumor immune responses and thereby contribute to reduced tumor growth.

6.1. Mb suppresses HIF-1α expression in activated T cells

The TME in solid tumors is immunosuppressive and characterized by hypoxic conditions, as indicated by the upregulation of HIF-1α, a key transcription factor in the cellular response to low oxygen levels. Furthermore, tumor cells shift their metabolism towards aerobic glycolysis, leading to increased glucose and oxygen consumption [99, 341]. We implanted B16F10-gp33 melanoma cells [342, 343], which present the LCMV GP (33-41) peptide over MHC-I complex, into the flank of C57BL/6J mice. Spleen and tumor tissue were harvested on day 14 after the tumor application. Increased CREB transcripts were detected in the tumor tissue in comparison to spleen tissue (Figure 12A). CREB regulates the MMP1, which in turn promotes the migration and invasion of tumor cells [108]. Further, increased transcripts of Nox1 were measured in the hypoxic tumor tissue in comparison to spleen tissue (Figure 12B), contributing to HIF-1α stabilization through ROS production and promoting cellular adaption and survival in the TME [341]. Next, HIF-1α transcript levels were significantly increased in tumor tissue compared to spleen tissue (Figure 12C). HIF-1α is associated as a key regulator of the hypoxic response in tumor tissue and drives the expression of genes involved in angiogenesis, metabolism, and cell survival [344]. Also, in snap frozen tissue sections following immunofluorescence labelling, HIF-1α was increased in tumor tissue when compared to spleen tissue (Figure 12D+E). These data indicate, that the TME is characterised by a hypoxic environment and upregulates specific hypoxic markers, including HIF-1α, Nox1 and CREB.

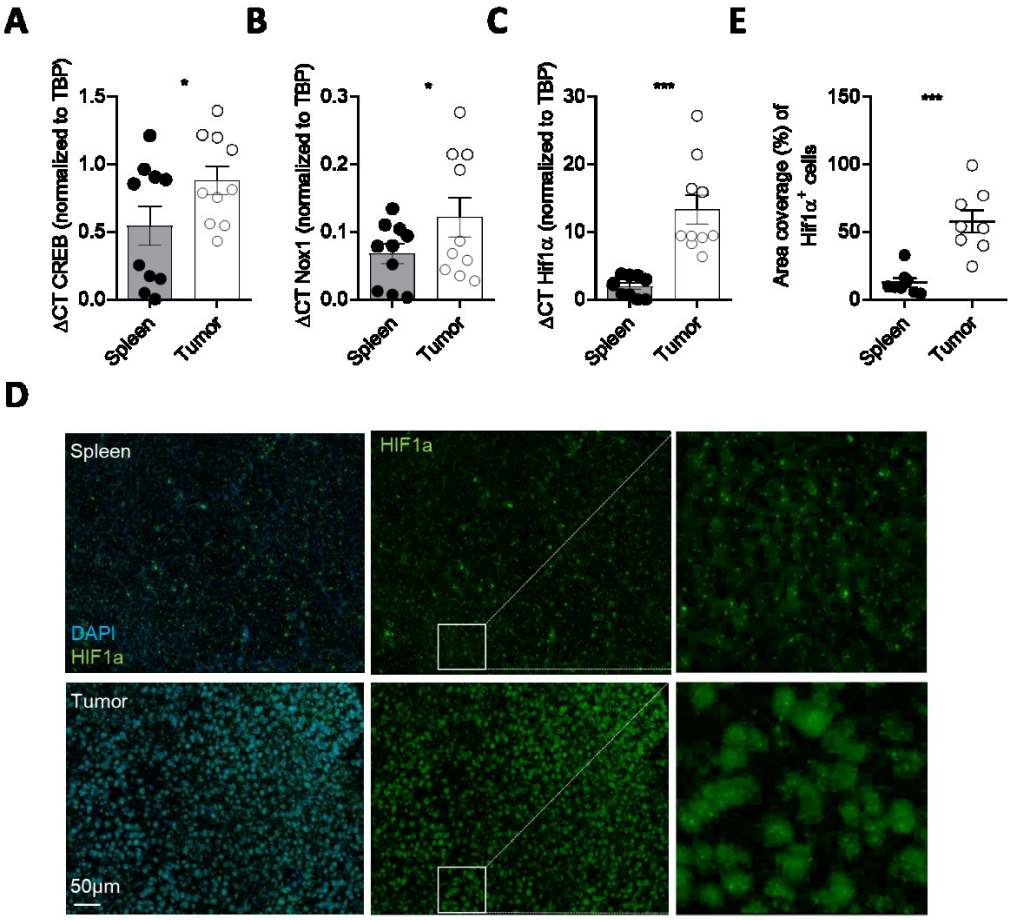

Figure 12: Solid tumor tissue exhibit increased hypoxia compared to spleen tissue. 5 x 10^5 B16F10-gp33 cells were injected into the left flank of C57BL/6J mice. After 14 days tumor and spleen were collected and analysed. (A-C) RNA was isolated from organ suspension and RT-PCR was performed. RNA levels of (A) CREB, (B) Nox1 and (C) HIF-1α were normalized to TBP (n=10). (D) Representative fluorescence images of spleen (top panel) and tumor (bottom panel) were taken. The scale bar is equivalent to 50 µm. (E) The frequency of area coverage of HIF-1α$^+$ cells of fluorescence images were determined (n=4). Error bars indicate SEM. Student´s t-test was performed and differences are classified as *P<0.05 and ***P<0.001 between the indicated groups.

Under hypoxic conditions, HIF-1α is stabilized in CD8$^+$ T cells and promotes their metabolic adaptation by inducing glycolysis, thereby supporting the maintenance of cytotoxic effector functions, including the expression of granzyme B, perforin, and IFN-γ [345]. Prolonged hypoxia and excessive HIF-1α signalling in CD8$^+$ T cells can impair mitochondrial function, reduce proliferative capacity, and contribute to T cell exhaustion, ultimately limiting their anti-tumor efficacy [346]. Snap frozen tissue section of implanted B16-gp33 tumor mice show a higher correlation of HIF-1α and CD8α immunofluorescence in tumor tissue, when compared to spleen tissue (Figure 13A-B). Consistently, CD44^{high} CD8$^+$ T cells infiltrating the tumor microenvironment showed high expression levels of HIF-1α when compared to T cells analysed

in spleen tissue (Figure 13C). Notably, these data suggest that TME infiltrating T cells express hypoxia markers in response to low oxygen exposures within the tumor.

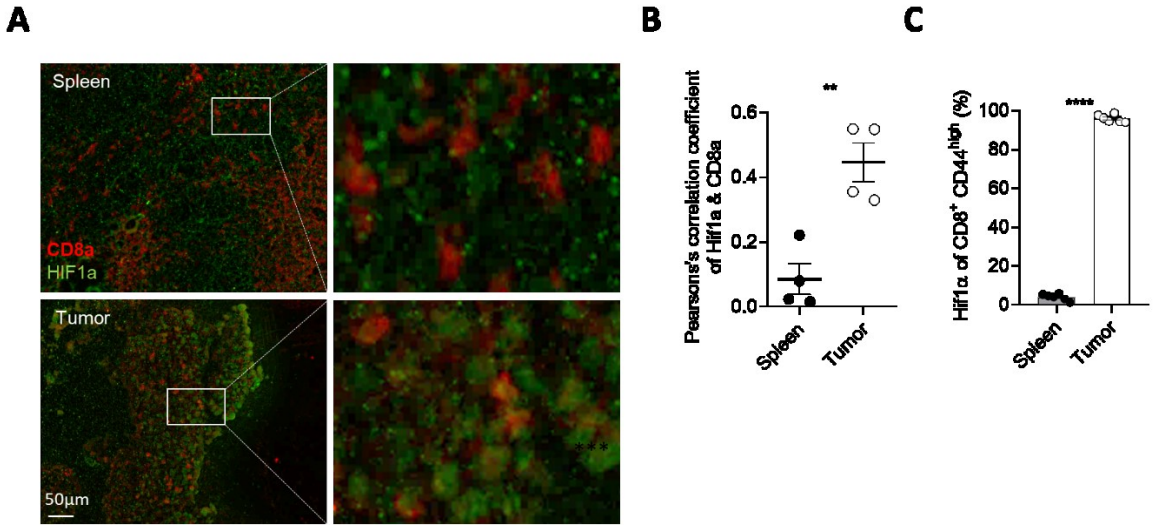

Figure 13: The influence of hypoxic and normoxic conditions on CD8$^+$ T cells. (A-B) 5 x 10^5 B16F10-gp33 cells were injected into the left flank of C57BL/6J mice. After 14 days tumor and spleen were collected and analysed. (A-B) Histology slides of spleen and tumor tissue were stained for CD8α and HIF-1α. (A) Representative fluorescence images of spleen (top panel) and tumor (bottom panel) were taken. The scale bar is equivalent to 50 µm. (B) The colocalization of HIF-1α in CD8 expression was determined (n=4). (C) 5 x 10^5 B16F10-gp33 cells were injected into the left flank of C57BL/6J mice. After 10 days, tumor and spleen were collected and MFI of HIF-1α on CD8$^+$ CD44^{high} T cells were determined using flow cytometry (n=6). Error bars indicate SEM. Student´s t-test was performed and differences are classified as **P<0.01 and ****P<0.0001 between the indicated groups.

Given the importance of oxygen availability for T cell metabolism and function, we aimed to enhance intracellular oxygen levels. To investigate whether increased oxygen supply in T cells can affect T cell immunity, we expressed the oxygen binding protein Mb. We hypothesized, that facilitating the intracellular oxygen storage and transport, especially under hypoxic conditions, enhances the oxygen availability within the T cells to sustain cellular function and metabolism promoting effector function [347]. Alongside with Mb, Thy1.1 was also expressed as a marker for the successful transduction of T cells. Following the retroviral expression of the constructs, Thy1.1 level were detected in transduced T cells but, slightly reduced expression levels of Thy1.1 were observed in T cells receiving the Mb constructs (Figure 14A). As expected, we did not observe Mb expression in control T cells, while transduced cells showed high expression of Mb, by analysing the transcript of Mb and control T cells (Figure 14B). Further, Western Blot analysis confirm these data by showing clear expression of Mb protein within the Mb-expressing T cells and no expression of in Control T cells (Figure 14C). By

normalizing the protein expression to the House-keeping Protein α-Tubulin, we could verify a significantly increased expression of Myoglobin in Mb-expressing T cells, when compared to control cells (Figure 14C-D). By measuring the expression of HIF-1α, we observed increased levels in activated T cells, which is consistent with the literature [348]. Interestingly, in the presence of Mb, expression levels of HIF-1α were highly reduced (Figure 14E). These data indicate that tumor infiltrating lymphocytes and activated T cells express HIF-1α and that the expression of HIF-1α can be reduced by following induction of the oxygen binding protein Mb in T cells leading us to further explore the metabolic consequences.

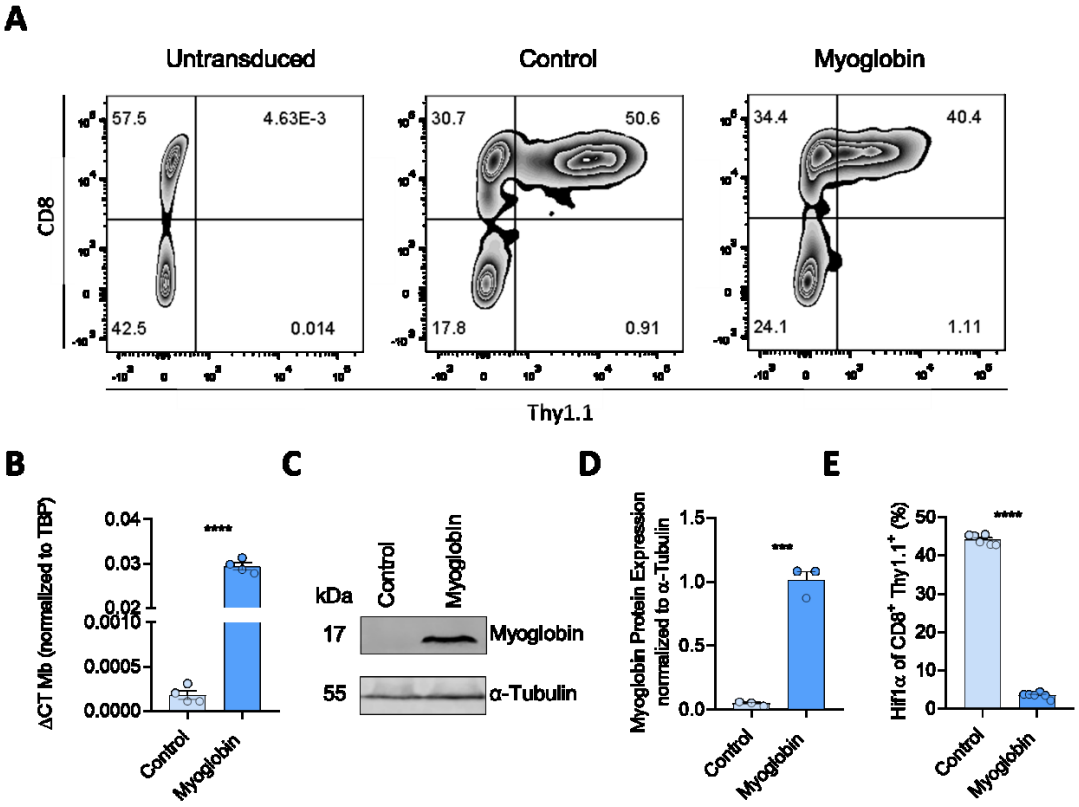

Figure 14: Myoglobin can be overexpressed in CD8⁺ T cells. (A) Splenocytes from C57BL/6J mice were transduced with Thy1.1 (Control) and Thy1.1-Myoglobin (Myoglobin). Representative FACS plots of untransduced and transduced Thy1.1 (Control) and Thy1.1-Myoglobin (Myoglobin) Splenocytes are illustrated. (B-E) CD8⁺ T cells isolated from C57BL/6J mice were transduced with Thy1.1 (Control) and Thy1.1-Myoglobin (Myoglobin). (B) After enrichment of Thy1.1 expression, RNA was isolated from T cell suspension and RT-PCR was performed. RNA levels of myoglobin normalized to TBP were detected (n=4). (C-D) Western Blot analysis for myoglobin and α-tubulin was performed. (C) Western Blot is shown (n=3) and (D) quantified relative to α-Tubulin (n=3). (E) Frequency of HIF-1α expression CD8⁺ Thy1.1⁺ T cells was determined with flow cytometry (n=6, from two independent experiments). Error bars indicate SEM. Student´s t-test was performed and differences are classified as ***P<0.001 and ****P<0.0001 between the indicated groups.

6.2. Mb expression increases T-cell metabolic function towards increased glycolysis and mitochondrial metabolism.

We hypothesized Mb plays an important role in facilitating the transport of oxygen to the mitochondria, where it is essential for the cellular respiration. Since mitochondria rely on a continuous oxygen supply to efficiently generate ATP through oxidative phosphorylation, any factor influencing oxygen delivery could directly impact energy production. Based on this reasoning, we hypothesized that the expression of Mb may significantly affect mitochondrial metabolism and thereby, alter overall cellular function [349]. We therefore performed transmission electron microscopy (TEM) on the control and Mb-expressing T cells (Figure 15A) and further analysed the shape of mitochondria. We observed an increased mitochondrial area in T cells expressing Mb compared to controls (Figure 15B+C). Furthermore, mitochondrial diameters were elevated in Mb-expressing T cells compared to controls (Figure 15B+D). Mitochondrial function depends on the organization of the inner mitochondrial membrane, which can be divided into the boundary membrane facing the outer mitochondrial membrane and invaginations of the inner mitochondrial membrane - the cristae membrane [350]. Tighter cristae with reduced width are associated with higher mitochondria function resulting from clustering of proteins and metabolites important for metabolic functions in close proximity [351, 352]. Following expression of Mb, the cristae were elongated with a reduced width, which suggests increased metabolic functions, as the supramolecular complexes facilitating OXPHOS-mediated ATP production is located at the cristae junction (Figure 15B+E+F) [352]. To sum up these results suggest, that Mb-expressing remodels T cell mitochondria to increase cellular metabolism.

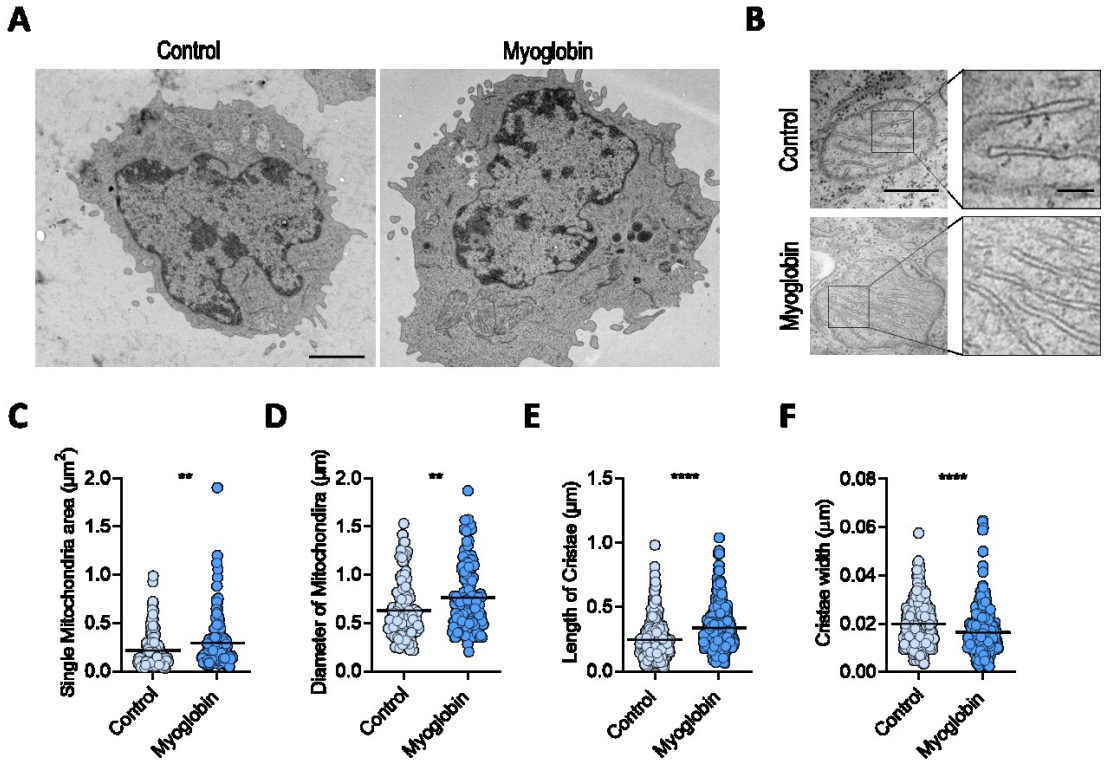

Figure 15: Myoglobin expressed CD8$^+$ T cells show a remodel of mitochondrial structure. CD8$^+$ T cells isolated from P14$^+$ mice were transduced with Thy1.1 (Control) and Thy1.1-Myoglobin (Myoglobin) following enrichment for Thy1.1 expression. (A) Representative TEM images of the cellular shape of Control and Myoglobin expressing T cells are shown as indicated (scale bar = 2 µm, n=3). (B) Representative TEM images of the mitochondrial shape of control and myoglobin T cells is shown as indicated (left panel: scale bar = 0.5 µm, right panel: scale bar = 0.1 µm, n=3). (C) Mitochondria area was calculated based on TEM images in µm^2 (n= 113-132). Measurement of the (D) mitochondria diameter (n=113-132), (E) the length of cristae (n=315-337) and (F) the width of cristae (n=297-338) based on TEM images in µm is shown. Error bars indicate SEM. Student´s t-test was performed and differences are classified as **P<0.01 and ****P<0.0001 between the indicated groups.

Further, we wanted to analyse the changes in fusion and fission of mitochondria of Mb-expressing T cells. Mitochondrial fusion and fission are dynamic processes that constantly reshape the mitochondrial network to cover the metabolic consumption [353]. Fusion enables the exchange of contents between mitochondria, such like proteins and DNA, promoting mitochondrial health and resilience [354]. Counteract, fission divides mitochondria in separate organelles to segregate damaged parts and before cell division [355]. However, excessive fission can lead to cellular dysfunction and promote cell death, whereas impaired fusion may result in the accumulation of mitochondrial defects and compromised energy production [356]. Using three-dimensional reconstruction of mitochondria from FIB-SEM images, no significant

difference was observed in control and Mb-expressing T cells, suggesting that mitochondrial fusion or fission was not highly influenced by Mb expression (Figure 16A-C).

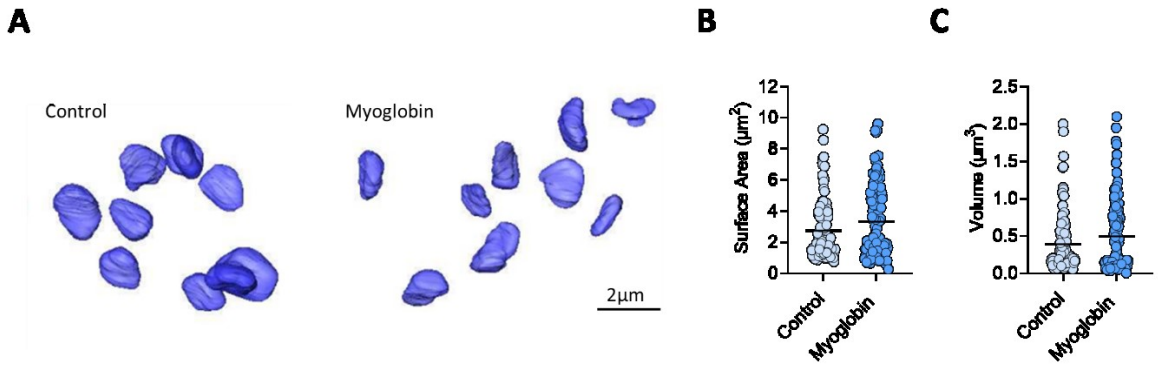

Figure 16: 3D-Structure of Myoglobin expressing CD8⁺ T cells do not show any fission or fusion in comparison to control T cells. CD8⁺ T cells isolated from P14⁺ mice were transduced with Thy1.1 (Control) and Thy1.1-Myoglobin (Myoglobin) following enrichment for Thy1.1 expression. (A) Mitochondrial three-dimensional structure reconstruction of FIB-SEM images of Thy1.1 (Control) and Thy1.1-Myoglobin (Myoglobin) expressing CD8⁺ T cells isolated from P14⁺ mice are shown (n=10). (B-C) Analysis of mitochondrial three-dimensional structure reconstruction of FIB-SEM images of Control and Myoglobin T cells. (B) Surface area and (C) volume of the mitochondria is shown (n=114-116). Error bars indicate SEM.

Although no significant changes were observed in mitochondrial morphology between Mb-expressing and control T cells, we next examined whether Mb impacts mitochondrial respiratory function. ATP production is based on a proton gradient across the inner mitochondrial membrane, which is generated by complex I-IV of the respiratory transport chain by consuming NADH and oxygen [266]. Complex I transfer electrons from NADH to ubiquinone and can be inhibit by Rotenone. Further, complex II passes' electrons from $FADH_2$ to ubiquinone, while complex III moves these to the cytochrome c and can be blocked by Antimycin A inhibition. Finally, complex IV accepts electrons from cytochrome c and reduces oxygen to H_2O, while the ATP synthase uses the proton gradient for ATP production. This process can be blocked by Oligomycin treatment [77]. Accordingly, the mitochondrial metabolic capacity was increased in Mb-expressing T cells when compared to controls (Figure 17A-G). Specifically, basal respiratory capacity was elevated in T cells expressing Mb compared to control cells (Figure 17A+B). Following treatment with FCCP and uncoupling of the proton gradient, we observed increased maximal respiratory capacity (Figure 17A+C). Furthermore, the spare respiratory capacity was also increased following Mb expression (Figure 17A+D). Non-mitochondrial respiration was also enhanced in Mb-expressing T cells (Figure

17A+E), as well as the Proton Leak (Figure 17A+F). Last, also ATP significantly increased following activation of Mb-expressing T cells (Supplementary Figure 17A+G). Summarized Mb-expressing T cells show an increased oxygen consumption in the OXPHOS resulting in more ATP production and reflecting a higher cellular energy capacity.

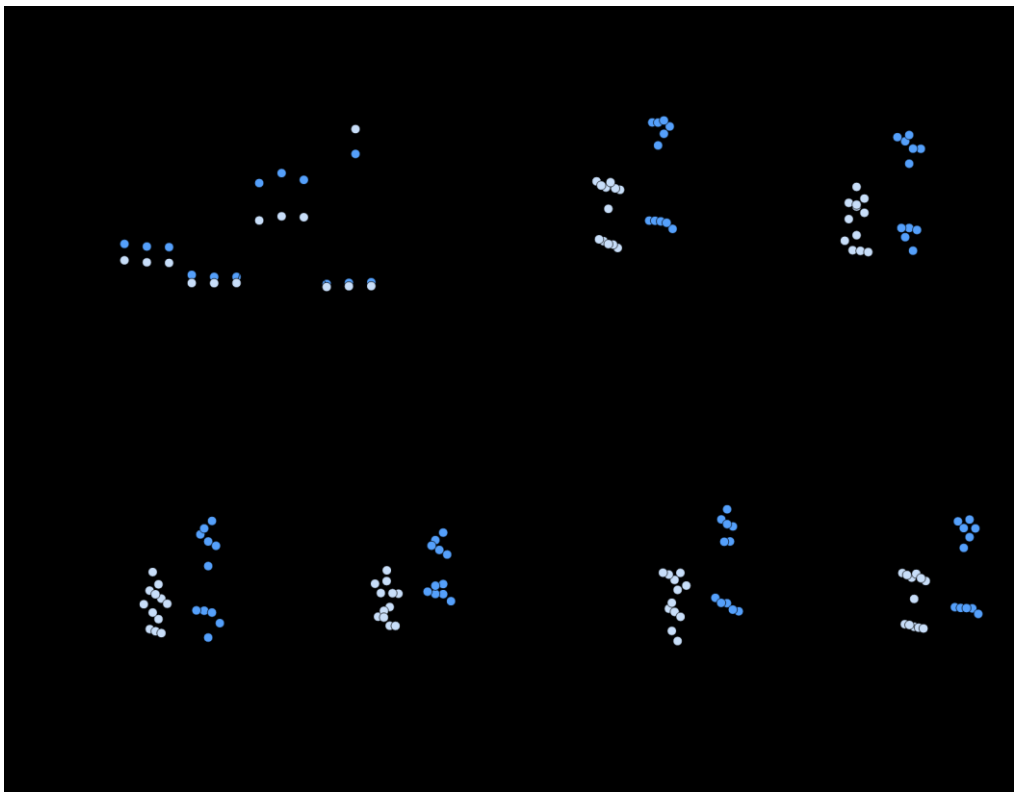

Figure 17: Myoglobin expressed CD8$^+$ T cells causes improved OXPHOS in comparison to control T cells. Seahorse analysis of Oxygen Consumption rate (OCR) of transduced CD8$^+$ T cells Thy1.1 (Control) and Thy1.1-Myoglobin (Myoglobin) isolated from C57BL/6J mice, following Thy1.1 enrichment by (A) time dependent drug treatment with Oligomycin, FCCP and Antimycin A (AA) + Rotenone (Rot) (n=11-14, from two independent experiments). (B) Basal respiration was determined by subtracting the basal level from the non-mitochondrial respiration (n=11-12, from two independent experiments). (C) The true maximal respiration was determined by subtracting the maximal respiration from the non-mitochondrial respiration (n=11-12, from two independent experiments). (D) Spare capacity was determined by subtracting the basal from the maximal respiration (n=11-12, from two independent experiments). (E) Non-mitochondrial respiration was measured after treating the T cells with oligomycin, FCCP and Antimycin A + rotenone (n=11-12, from two independent experiments). (F) Proton leak is calculated by oligomycin-treated cells subtracting the non-mitochondrial respiration (n=11-12, from two independent experiments). (F) ATP production is calculated by subtracting non-mitochondrial respiration from basal respiration (n=11-12, from two independent experiments). Error bars indicate SEM. Two-way ANOVA and Student´s t-test were performed and differences are classified as *P<0.05, **P<0.01, ***P<0.001 and ****P<0.0001 between the indicated groups.

The respiratory transport chain can induce the radical superoxide thus resulting in the production of mitochondrial ROS [357]. In T cells, this is important because increased mitochondrial ROS can trigger T cell dysfunction [101]. We therefore speculated, that ROS levels might be elevated following Mb expression. However, we observed highly reduced presence of mitochondrial superoxide in activated T cells following expression of Mb (Figure 18A). Mitochondrial superoxide can be scavenged by the superoxide dismutase 2 into H_2O_2, which can be further metabolized by glutathione peroxidase into H_2O and GSSG [357, 358]. Oxidized glutathione can be reduced by the glutathione reductase by consuming NADPH and H^+ [358]. Hence, we hypothesized that increased OXPHOS was associated with increased potential for ROS scavenging. Consistently, decreased intracellular levels of H_2O_2 could be detected in Mb-expressing T cells compared to control T cells (Figure 18B). In addition, we determined increased levels of GSH in Mb-expressing T cells when compared to control T cells (Figure 18C). Also, we detected enhanced metabolic activity with an increased conversion of $NADH/H^+$ to NAD^+/H_2O in Mb T cells in comparison to control T cells (Figure 18D+E). Notably, we observed slight but not significantly increased amounts of oxidized (carbonylated) proteins in Mb-expressing T cells after activation when compared to control T cells (Figure 18F+G) [270]. At the same time, ROS scavenging time after exposure towards H_2O_2 was increased in Mb-expressing T cells (Figure 18H+I). Taken together, these data indicate that Mb expression promotes oxygen consumption and mitochondrial metabolism, while consuming mitochondrial ROS. This reduction in mitochondrial ROS suggests an improved balance between oxidative metabolism and antioxidant defences.

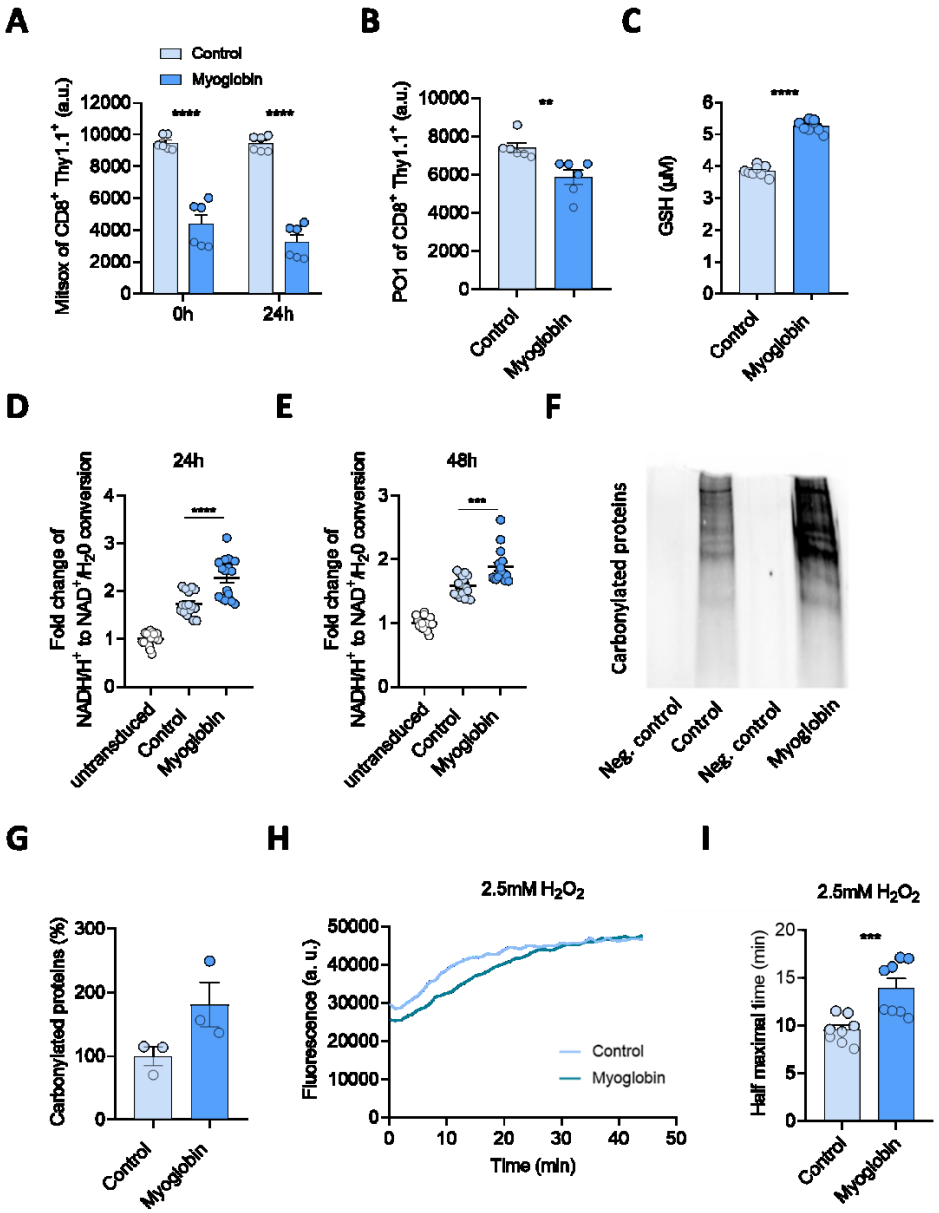

Figure 18: Myoglobin expressed CD8$^+$ T cells shows increased ROS scavenging in comparison to control T cells. (A-C) CD8$^+$ T cells isolated from C57BL/6J mice were transduced with Thy1.1 (Control) and Thy1.1-Myoglobin (Myoglobin) following enrichment for Thy1.1 expression. (A) MitoSox was determined after 0 and 24h via flow cytometry gated on CD8$^+$ Thy1.1$^+$ T cells to detect mitochondrial ROS (n=6, from two independent experiments). (B) Intracellular H_2O_2 levels were measured using Peroxy Orange 1 (PO1) via flow cytometry via flow cytometry gated on CD8$^+$ Thy1.1$^+$ T cells (n=6, from two independent experiments). (C) GSH concentration was measured via (n=8, from two independent experiments). (D-E) Untransduced, Thy1.1 (Control) and Thy1.1-Myoglobin (Myoglobin) expressing T cells isolated from C57BL/6J mice were cultured for (D) 24 h and (E) 48 h and treated with Resazurin. The fluorescence of metabolized Resorufin was measured after 30 min and 3 h. Fold change of NADH/H$^+$ to NAD$^+$/H_2O in comparison to untransduced cells is shown (n=16, from two independent experiments). (F) Western Blot of carbonylated proteins of transduced CD8$^+$ T cells Thy1.1 (Control) and Thy1.1-Myoglobin (Myoglobin) isolated from C57BL/6J mice and negative controls was performed (n=3). (G) Analysis

of carbonylated proteins of Control and Myoglobin expressing T cells from Western Blot normalized to the level of Control cells is shown (n=3). (I) DHE oxidation in Control and Myoglobin expressing T cells upon treatment with 2.5 mM H_2O_2 was determined over time (n=8, from two independent experiments). Error bars indicate SEM. ***P<0.001 and ****P<0.0001 between the indicated groups. (H-I) $CD8^+$ T cells isolated from C57BL/6J mice were transduced with Thy1.1 (Control) and Thy1.1-Myoglobin (Myoglobin) following enrichment for Thy1.1 expression. (H) DHE oxidation in Control and Myoglobin expressing T cells upon treatment with 2.5 mM H_2O_2 was (H) detected over time and the (I) Half maximal time of DHE oxidation was determined (n=8, from two independent experiments). Error bars indicate SEM. Two-way ANOVA, One-way ANOVA and Student´s t-test were performed and differences are classified as **P<0.01, ***P<0.001 and ****P<0.0001 between the indicated groups.

Given that metabolic reprogramming also influences glycolytic activity, we next assessed glycolytic function, as T cell fate is closely linked the metabolic function, with aerobic glycolysis being essential for effector T cell differentiation and function [266]. Therefore, we wondered whether increased mitochondrial metabolism and reduced expression of HIF-1α might impact the metabolic switch from OXPHOS to aerobic glycolysis following T cell activation. As expected, an increased proton efflux rate was determined in Mb-expressing T cells when compared to controls (Figure 19A+B). However, basal glycolysis was increased as subtraction of the proton efflux rate (PER) following inhibition of the hexokinase by addition of 2-DG from the basal PER, which still showed increased values (Figure 19A+C). Block of the respiratory chain with rotenone and antimycin A causes compensatory activation of glycolysis, which can be determined by increased PER (Figure 19A). Interestingly, an increased compensatory glycolytic capacity was detected following expression of Mb when compared to controls (Figure 19A+D).

Figure 19: Myoglobin expression in $CD8^+$ T cells increases glycolytic activity. (A-D) Seahorse analysis of Proton Efflux Rate (PER) of transduced $CD8^+$ T cells isolated from C57BL/6J mice with Thy1.1 (Control) and Thy1.1-Myoglobin (Myoglobin), following Thy1.1 enrichment by (A) time dependent drug treatment with

Antimycin A (AA) + Rotenone (Rot) and 2-Desoxy-D-glucose (2-DG) (n=5-6). (B) Basal Proton Efflux Rate is derived from A before drug treatment (n=5-6). (C) Basal glycolysis was determined by subtracting the untreated glycolysis rate from the mito acidification measured by OCR (n=5-6). (D) Compensatory glycolysis is derived from A after treating the cells with rotenone and antimycin A (n=5-6). Error bars indicate SEM. Two-way ANOVA and Student´s t-test were performed and differences are classified as ***P<0.001 and ****P<0.0001 between the indicated groups.

During glycolysis, glucose is metabolized to pyruvate, which can either be further processed in the mitochondria or into lactate, which causes acidification of the media. Accordingly, since we observed an increased acidification rate even in presence of mitochondrial respiratory chain inhibitors as well as an inhibitor of the hexokinase, we speculated that increased metabolic functions following expression of Mb facilitated increased lactate levels. Hence, we determined substrates and biogenic amines of the glycolysis and TCA cycle respectively. Consistent with the data from the seahorse studies, fructose-1,6-bisphosphate and lactate were significantly increased in T cells expressing Mb when compared to controls (Figure 20A). Moreover, organic acids of the TCA cycle exhibited increased concentrations following expression of Mb (Figure 20B). These data suggest enhanced metabolic activity in T cells following Mb expression. Consequently, increased ATP levels were observed in Mb-expressing cells when compared to controls (Figure 20C+D). Also, AMP and ADP levels were enhanced which stimulates energy-generating processes like glycolysis and OXPHOS and indicate together with increased ATP levels an active and dynamic energy state [359]. Taken together, these data indicate that Mb expression enhances glycolytic activity and mitochondrial metabolism supporting TCA cycle activity and ATP production.

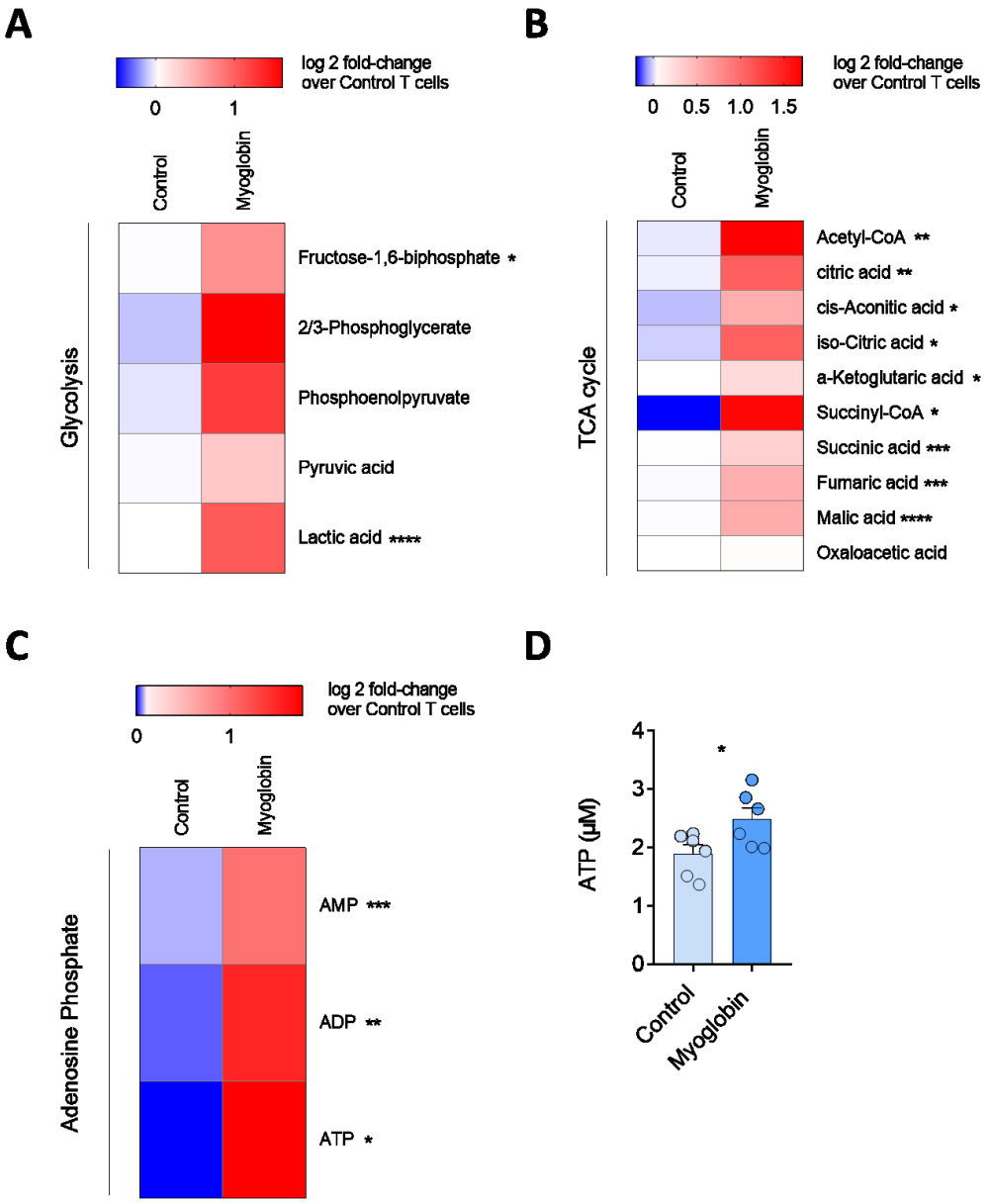

Figure 20: Myoglobin expressed in CD8$^+$ T cells causes an increased glycolysis activity and ATP expression. Metabolomic analysis of transduced CD8$^+$ T cells Thy1.1 (Control) and Thy1.1-Myoglobin (Myoglobin) isolated from C57BL/6J mice, following Thy1.1 enrichment, stimulated with 10mM glucose medium is illustrated. Shown are the products of (E) the glycolysis, (F) the TCA cycle and (G) the adenosine phosphates (n=5-6). (H) ATP concentration measured via luminescence of Thy1.1 (Control) and Thy1.1-Myoglobin (Myoglobin) CD8$^+$ T cells isolated from C57BL/6J mice, following Thy1.1 enrichment with 10mM glucose as sugar source (n=6, from two independent experiments). Error bars indicate SEM. Student´s t-test was performed and differences are classified as *P<0.05, **P<0.01, ***P<0.001 and ****P<0.0001 between the indicated groups.

6.3. Mb improves effector T cell differentiation.

Mb facilitates mitochondrial and glycolytic metabolism in T cells. Since metabolic dysfunction is associated with reduced effector function and exhaustion of T cells [101, 268, 269], we wondered whether Mb expression affects T cell viability. We did not find any difference in the viability of cells between the Mb-expressing or control T cells in our settings (Figure 21A). Further, we wondered whether T cell differentiation was affected by expression of Mb in an *in vitro* system. Although proliferation following expression of Mb was only slightly, but significantly increased compared to control T cells over time (Figure 21B), we observed increased differentiation into effector ($CD44^+$ $CD62L^-$) but not memory ($CD44^+$ $CD62L^+$) T cells following Mb expression (Figure 21C+D). Interestingly, Mb-expressing T cells express more IL-7R compared to control T cells (Figure 21E+F), which is associated with long-term survival and maintenance of naïve and memory T cells [242]. These data suggest that Mb expression triggered increased effector functions of anti-tumoral T cells.

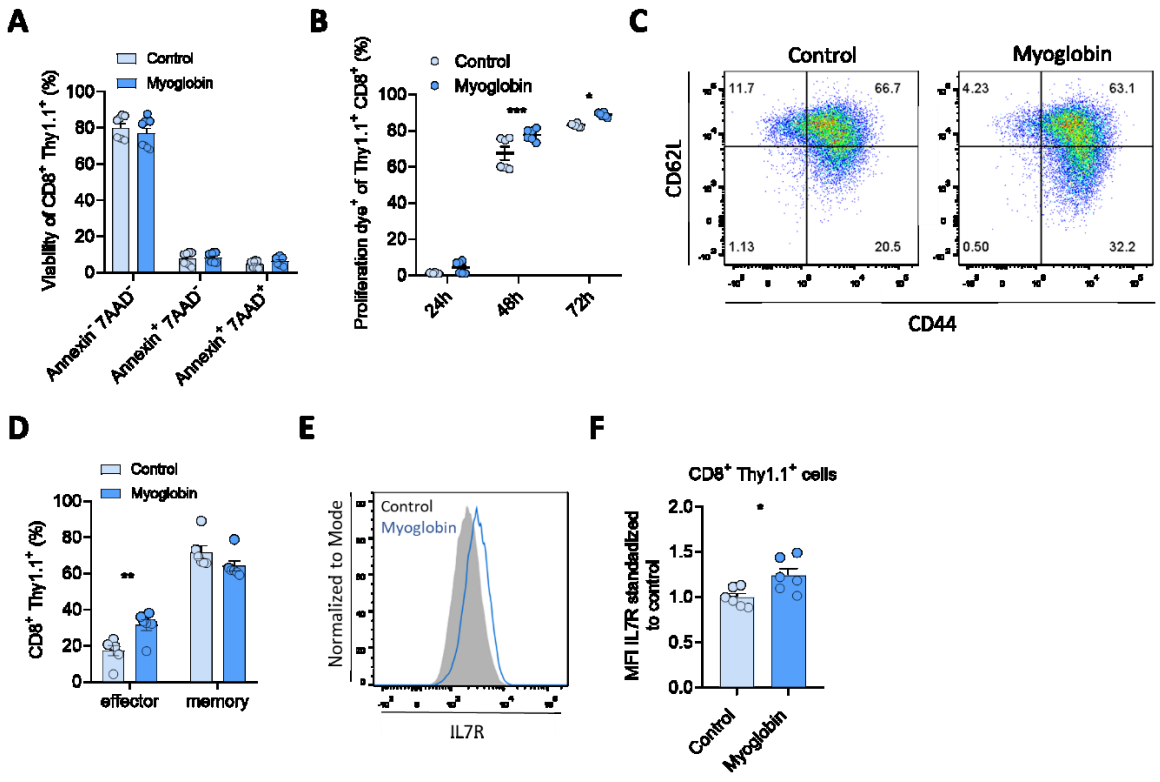

Figure 21: Myoglobin expressing $CD8^+$ T cells are viable and show increased differentiation in effector cells in comparison to control $CD8^+$ T cells. Transduced $CD8^+$ T cells with Thy1.1 (Control) and Thy1.1-Myoglobin (Myoglobin) isolated from C57BL/6J mice were analysed via flow cytometry. (A) viability gating on $Annexin^-$ $7AAD^-$ (living cells), $Annexin^+$ $7AAD^-$ (early apoptotic) and $Annexin^+$ $7AAD^+$ (late apoptotic) 24 h after transduction (n=8, from two individual experiments) and the (B) proliferation rate targeted by proliferation dye^+

of $CD8^+$ $Thy1.1^+$ T cells were detected (n=6, from two individual experiments). (C) Representative original FACS Blots of CD62L and CD44 gated on $Thy1.1^+$ $CD8^+$ T cells is shown. (D) The frequency of effector (with $CD44^+$ $CD62L^-$) and memory ($CD44^+$ $CD62L^+$) T cell subsets is shown (n=6, from two independent experiments). (E) Representative histogram of IL-7R gated on $Thy1.1^+$ $CD8^+$ T cells is illustrated. (F) The MFI of IL-7R normalized to Control gated on $Thy1.1^+$ $CD8^+$ T cells is shown (n=6, from two individual experiments). Error bars indicate SEM. Two-way ANOVA and Student´s t-test were performed and differences are classified as *P<0.05, **P<0.01 and ***P<0.001 between the indicated groups.

Next, we wondered about effects on exhaustion of T cells which can be triggered by the transcription factor TOX, often detected in tumor-infiltrating lymphocytes, showing an exhausted transcriptional program [248-250]. Accordingly, we observed reduced TOX^{high} Mb-expressing T cells when compared to control T cells (Figure 22A+B). Consistently, the proportion of TOX^{dim} T cells was increased following Mb expression (Figure 22A+B). Likewise, the MFI standardized to the control of the transcriptional factor EOMES of T cells was decreased (Figure 22C-D). Also, the percentage of T cells expressing TCF-1 was decreased in Mb-expressing T cells in comparison to control T cells (Figure 22E-F). Both factors are associated with exhaustion of antigen-specific T cells [360, 361]. As expected, the expression of exhaustion markers including PD-1 and Tim-3 were also reduced following Mb expression (Figure 22G-J). These data indicate that Mb expression shifts metabolic function to prevent an exhaustive state *in vitro*.

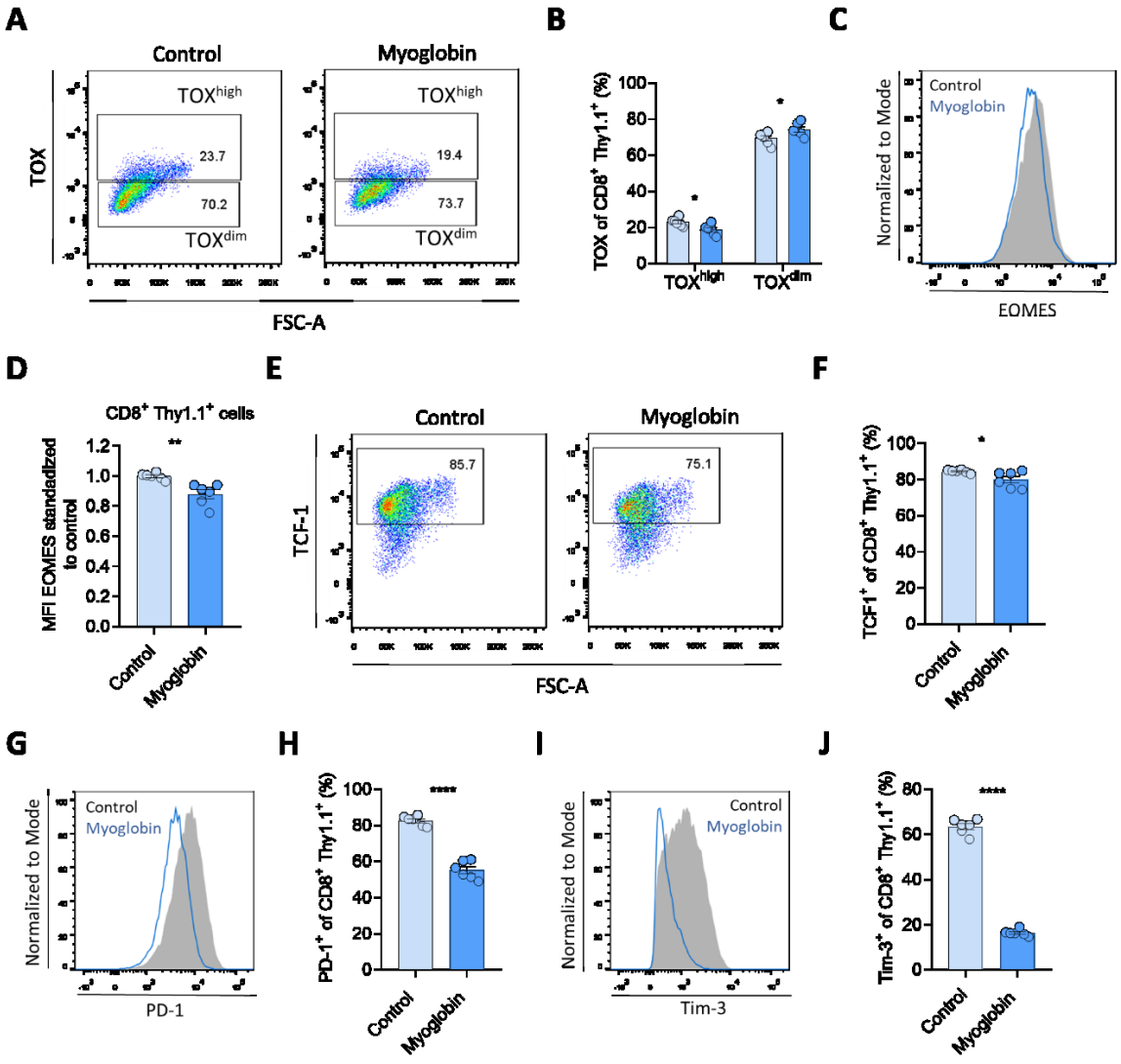

Figure 22: Myoglobin expressing CD8+ T cells show decreased exhaustion in comparison to control T cells. $CD8^+$ T cells isolated from C57BL/6J mice were transduced with Thy1.1 (Control) and Thy1.1-Myoglobin (Myoglobin) and analysed via flow cytometry. (A) Representative original FACS Blots of TOX and FSC-A gated on $Thy1.1^+$ $CD8^+$ T cells is shown. (B) The frequency of TOX^{high} and TOX^{dim} populations is shown (n=6, from two independent experiments). (C) Representative histogram of EOMES gated on $Thy1.1^+$ $CD8^+$ T cells is illustrated. (D) The MFI of EOMES normalized to Control gated on $Thy1.1^+$ $CD8^+$ T cells is shown (n=6, from two individual experiments). (E) Representative original FACS Blots of TCF-1 and FSC-A gated on $Thy1.1^+$ $CD8^+$ T cells are shown. (F) The frequency of TCF-1^+ gated on $CD8^+$ $Thy1.1^+$ T cells is illustrated (n=6, from two independent experiments). (G) Histogram and (H) frequency of PD-1 gated on and $CD8^+$ $Thy1.1^+$ T cells is shown (n=6, from two independent experiments). (I) Histogram and (J) frequency of Tim-3 gated on and $CD8^+$ $Thy1.1^+$ T cells is illustrated (n=6, from two independent experiments). Error bars indicate SEM. Two-way ANOVA and Student´s t-test were performed and differences are classified as *P<0.05, **P<0.01 and ****P<0.0001 between the indicated groups.

Next, we wondered how Mb expression would affect effector functions of tumor-specific T cells. Accordingly, we co-incubated B16F10-gp33 melanoma cells with the corresponding Mb or control T cells, expressing a TCR recognizing the H2-D^b presented gp33-41 epitope as a transgene [362]. IFN-γ and TNF-α production by Mb-expressing T cells was significantly increased in response to cancer cells, when compared to control T cells with indicated Target: Effector ratios (Figure 23A+B). Furthermore, granzyme B production was increased following Mb expression (Figure 23C). Hence, T cell-mediated killing of tumor cells was enhanced compared to controls (Figure 23D). Taken together, these data indicate that Mb can increase effector T cell differentiation and that T cells exhibit increased effector function against cancer cells.

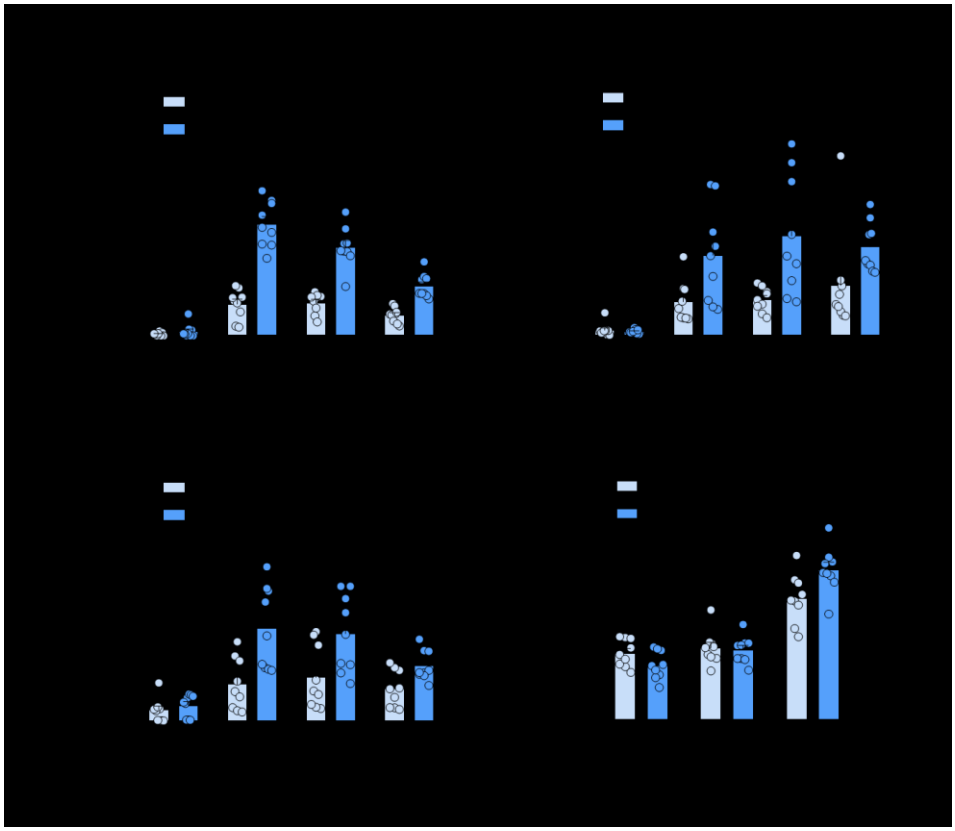

Figure 23: Myoglobin expressing $CD8^+$ T cells have increased cytokine production and killing in comparison to control T cells. Co-culture of Thy1.1 (Control) and Myoglobin-expressing Thy1.1 (Myoglobin) $CD8^+$ T cells isolated from $P14^+$ mice with B16F10-gp33 cells in indicated Target:Effector (T:E) ratios are analysed via flow cytometry. Frequency of (A) IFN-γ^+ (B) TNF-α^+ and (C) $GzmB^+$ of $Thy1.1^+$ $CD8^+$ T cells is shown (n=9, from three independent experiments). (D) Late apoptotic B16F10-gp33 cells are detected with 7AAD (n=9, from three independent experiments). Error bars indicate SEM. Two-way ANOVA was performed and differences are classified as ns: P>0.05, *P<0.05, **P<0.01, ***P<0.001 and ****P<0.0001 between the indicated groups.

6.4. Mb drives increased intratumoral T cell infiltration and delays tumor growth.

While the *in vitro* data demonstrate improved metabolic fitness and effector functions of Mb-expressing T cells, we next wondered whether Mb could improve anti-tumoral T cell immunity *in vivo*. We implanted 5 x 10^5 B16F10-gp33 melanoma cells into the flank of C57Bl/6J mice. Following 7 days of tumor growth, Mb-expressing and control T cells were adoptively transferred into tumor-bearing animals, followed by Poly I:C and gp33 peptide injection, with an early analysis 4 days after T cell transfer (Figure 24A). To increase the number of viable cells for adoptive transfers we used an established protocol to transduce activated T cells from splenocyte cultures (Figure 24B) [363]. When we analysed the infiltration of tumor specific T cells in the tumor tissue, we found an increased proportion of Mb-expressing T cells in the tumor tissue when compared to control T cells (Figure 24C). Interestingly, we detected a similar number of Mb and control T cells in spleen tissue (Figure 24D). However, in a hypoxic TME, Mb expression was able to promote T cell infiltration into the tumor tissue. Consistent with the *in vitro* findings, expression levels of HIF-1α were reduced in T cells expressing Mb compared to controls in both, tumor and spleen tissue (Figure 24E+F). These data suggest that Mb expression is leading to reduced hypoxia with better infiltration in hypoxic tissues. However, Mb did not affect the presence of T cells in normoxic tissues such as spleen.

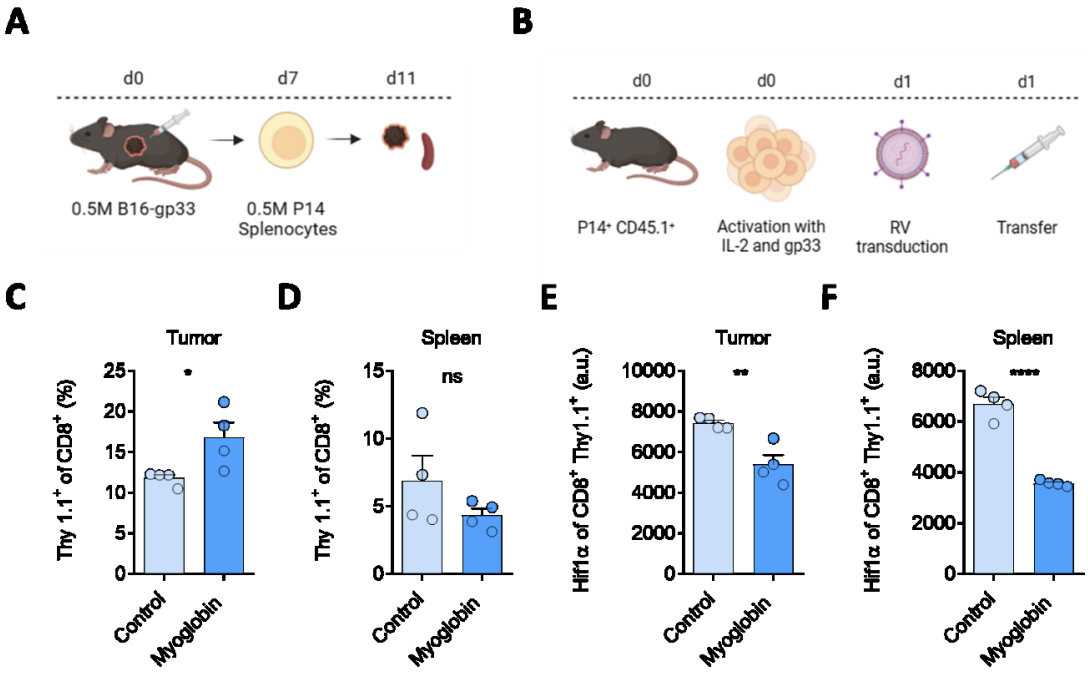

Figure 24: Myoglobin expressing CD8$^+$ T cells show decreased HIF-1α expression in bearing mice in comparison to control T cells. (A) A scheme of the preparation of splenocytes for i*n vivo* T cell transfer is shown. (B-F) B16F10-gp33 tumor-bearing C57BL/6J mice were treated at day 7 with 5 x 10^5 Thy1.1 (Control) and Thy1.1-Myoglobin (Myoglobin) expressing P14$^+$ CD8$^+$ T cells, Poly I:C and gp33 peptide. Spleen and tumor tissue were analysed at day 11 via flow cytometry. (B) A scheme of the experimental set up is shown. Frequency of Thy1.1$^+$ of CD8$^+$ T cells was determined in (C) tumor and (D) spleen tissue is illustrated (n=4). MFI of HIF-1α expression in (E) tumor and (F) spleen tissue of CD8$^+$ Thy1.1$^+$ T cells in spleen tissue is shown (n=4). Error bars indicate SEM. Student´s t-test was performed and differences are classified as ns: P>0.05, *P<0.05, **P<0.01 and ****P<0.0001 between the indicated groups.

Moreover, the proportion of effector (CD62L$^-$ CD44$^+$) T cells was increased following Mb expression, while (CD62L$^+$ CD44$^+$) memory T cells were comparable between both groups in spleen tissue (Figure 25A-B). Consistently, IFN-γ production was increased in Mb-expressing cells compared to control T cells in the spleen when cells were restimulated with the gp33 epitope (Figure 25C). We also identified increased expression of the exhaustion markers PD-1 and Tim-3 in Mb- expressing tumor infiltrating T cells suggesting that effector function might be even further improved following checkpoint inhibition (Figure 25D+E). Thus, these data indicate that Mb expression can increase T cell infiltration into tumor tissue with increased effector functions. Opposite to *in vitro* date, increased exhaustion was measured in Mb-expressing tumor infiltrating lymphocytes, through which the use of checkpoint inhibition could be considered.

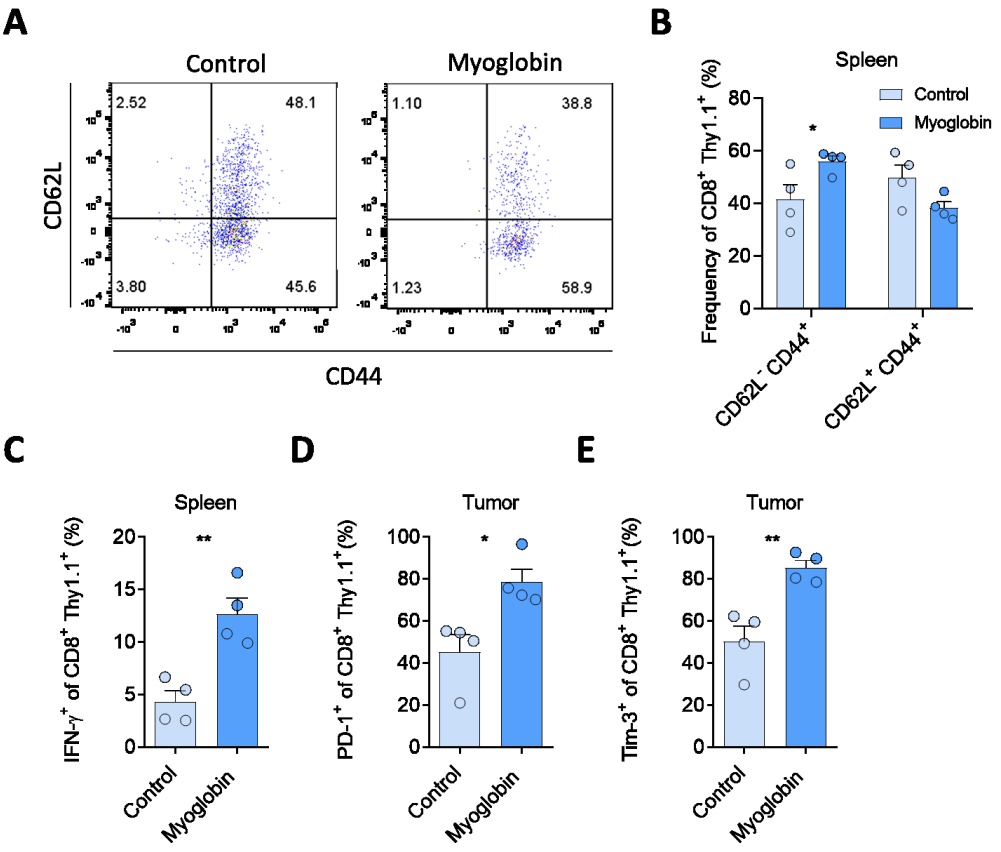

Figure 25: Myoglobin expressing CD8$^+$ T cells show enhanced effector function in tumor bearing mice in comparison to control T cells. B16F10-gp33 tumor-bearing C57BL/6J mice were treated at day 7 with 5 x 10^5 Thy1.1 (Control) and Thy1.1-Myoglobin (Myoglobin) expressing P14$^+$ CD8$^+$ T cells, Poly I:C and gp33 peptide. Spleen and tumor tissue were analysed at day 11 via flow cytometry. (A) Representative original FACS Blots of CD62L and CD44 gated on Thy1.1$^+$ CD8$^+$ T cells of spleen tissue are shown. Frequency of Thy1.1$^+$ of CD8$^+$ T cells was determined in (E) CD44$^+$ CD62L$^-$ (effector) and memory CD44$^+$ CD62L$^+$ (memory) T cell subsets of CD8$^+$ Thy1.1$^+$ in spleen tissue is shown (n=4). Frequency of (F) IFN-γ in spleen tissue and the expression of (G) PD-1 and (H) Tim-3 in tumor tissue of CD8$^+$ Thy1.1$^+$ is shown (n=4). Error bars indicate SEM. Two-way ANOVA and Student´s t-test were performed and differences are classified as *P<0.05 and **P<0.01 between the indicated groups.

Next, we queried whether adoptive transfer of Mb-expressing T cells can reduce tumor growth in the B16F10-gp33 model system (Figure 26A). When we monitored tumor growth over 27 days, we observed a significant reduction in tumor size in mice that received 2x10^6 Mb-expressing T cells on day 7 after tumor implanting when compared to mice that received the same amount of control T cells, following Poly I:C and gp33 peptide injection (Figure 26B). Consistently, frequency and absolute numbers of tumor-infiltrating T cells were increased at later time points following Mb-expression (Figure 26C+D). Moreover, increased numbers of

transferred T cells were observed in the tumor draining lymph nodes, while the frequency was not significantly changed (Figure 26E+F). Taken together, a high number of Mb-expressing T cell transfer can reduce the tumor volume and show an increased infiltration in hypoxic tumor tissue, but not in normoxic dLN tissue.

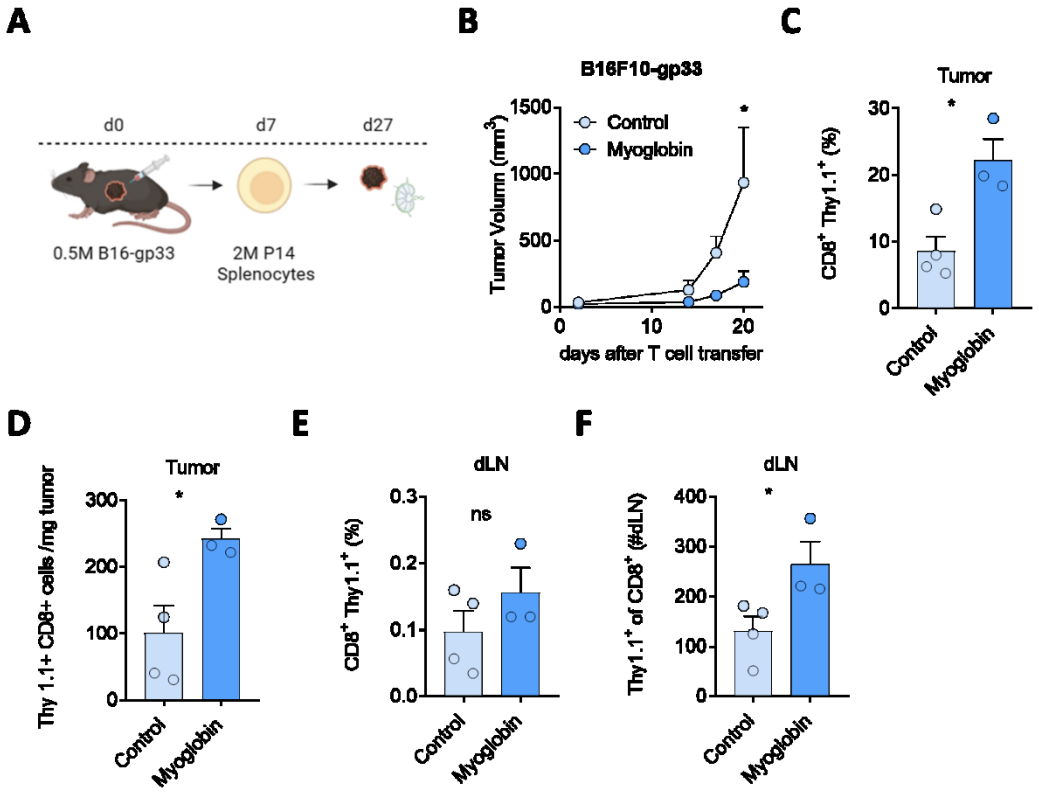

Figure 26: Melanoma-bearing mice show less tumor burden after treatment with Myoglobin-expressed CD8⁺ T cells in comparison to control CD8⁺ T cells. B16F10-gp33 tumor-bearing C57BL/6J mice were treated at day 7 with 2 x 10^6 Thy1.1 (Control) and Thy1.1-Myoglobin (Myoglobin) expressing P14⁺ CD8⁺ T cells, Poly I:C and gp33 peptide. dLN and tumor tissue were analysed at day 20 after T cell transfer. (A) A scheme of the experimental set up is shown. (B) Tumor growth curve after T cell transfer is shown (n=3-4). (C) Frequency of Thy1.1⁺ gated on CD8⁺ T cells was measured in the Tumor tissue via flow cytometry (n=3-4). (D) The absolute count of Thy1.1⁺ gated on CD8⁺ T cells per mg tumor was detected via flow cytometry (n=3-4). The (E) frequency and (F) absolute count of Thy1.1⁺ gated on CD8⁺ T cells in the dLN is measured via flow cytometry (n=3-4). Error bars indicate SEM. Two-way ANOVA and Student´s t-test were performed and differences are classified as ns: P>0.05 and *P<0.05 between the indicated groups.

Moreover, we looked whether transfer of a lower number (5x10^5) of Mb-expressing T cells was also beneficial during anti-tumor defence (Figure 27A). The more immunogenic MC38-Ova cells, which derived from colon cancer, were transplanted in mice and after 6 days Mb-

expressing T cells or control T cells, are expressing a TCR recognizing the H2-K^b presented SIINFEKL epitope as a transgene (OT-I) [364]. Afterwards, Poly I:C and SIINFEKL peptide were injected, following 9 days of monitoring the tumor growth (Figure 27A). A significant reduction of tumor growth was determined after transfer of Mb-expressing T cells when compared to controls (Figure 27B). These data suggest, that Mb can reduce the tumor growth with low number of transferred T cells in immunogenic tumor model.

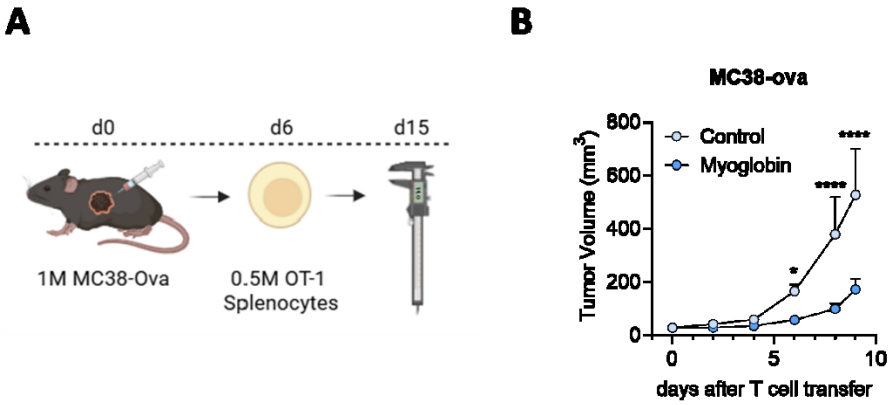

Figure 27: Colon-cancer-bearing mice show less tumor burden after treatment with Myoglobin-expressed $CD8^+$ T cells in comparison to control $CD8^+$ T cells. MC38-ova tumor-bearing C57BL/6J mice were treated at day 6 with 5 x 10^5 Thy1.1 (Control) and Thy1.1-Myoglobin (Myoglobin) expressing OT-1^+ $CD8^+$ T cells, Poly I:C and SIINFEKL peptide. (A) A scheme of the experimental set up is shown. (B) The tumor growth was monitored until day 9 after T cell transfer (n=5-11). Error bars indicate SEM. Two-way ANOVA was performed and differences are classified as *P<0.05 and ****P<0.0001 between the indicated groups.

Next, we planted 5x10^5 Mb-expressing T cells on day 7 in B16F10-gp33 tumor bearing mice, following Poly I:C and gp33 peptide injection (Figure 28A). We observed a significant reduction in tumor growth of B16F10-gp33 melanoma cells up to day 27 when Mb-expressing T cells were transferred, although as expected, the difference appeared more modest (Figure 28B). Consistently, the melanoma tumor weight was reduced in tissue harvested from animals receiving Mb-expressing T cells when compared to control T cells at day 27 (Figure 28C). Additionally, B16-gp33 tumor bearing mice treated with 5x10^5 Mb-expressing T cells, Poly I:C and gp33 peptide and monitored up to 39 days showed a significantly longer survival until animals needed to be sacrificed due to tumor size or ulceration when compared with control T cells (Figure 28D). Taken together, the injection of Mb-expressing T cells shows a significant reduction of the tumor growth and longer survival, even with low T cell numbers in the poorly immunogenic tumor model.

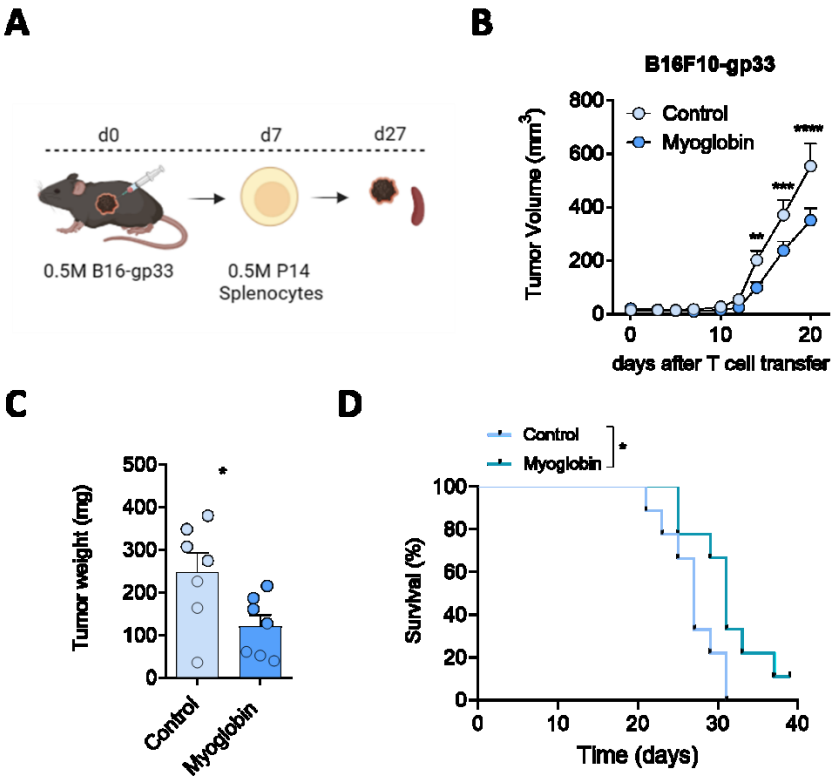

Figure 28: Melanoma-bearing mice show less tumor burden after treatment with low numbers of Myoglobin-expressed CD8⁺ T cells in comparison to control CD8⁺ T cells. (A-C) B16F10-gp33 tumor-bearing C57BL/6J mice treated at day 7 with 5 x 10^5 Thy1.1 (Control) and Thy1.1-Myoglobin (Myoglobin) expressing P14⁺ CD8⁺ T cells, Poly I:C and gp33 peptide. Spleen and tumor tissues were analysed at day 20 after T cell transfer. (A) A scheme of the experimental set up is shown. (B) The Tumor growth curve after T cell transfer is shown (n=7-8). (C) The final tumor weight is illustrated (n=7). (D) Survival of B16F10-gp33 tumor-bearing C57BL/6J mice treated at day 7 with 5 x 10^5 Thy1.1 (Control) and Thy1.1-Myoglobin (Myoglobin) expressing P14⁺ CD8⁺ T cells, Poly I:C and gp33 peptide up to 39 days. Mice were sacrificed due to tumor growth or ulceration (n=9). Error bars indicate SEM. Two-way ANOVA, survival curve and Student´s t-test were performed and differences are classified as *P<0.05, **P<0.01, ***P<0.001 and ****P<0.0001 between the indicated groups.

Subsequently, these findings were associated with increased anti-tumoral Mb T cells in the circulation at day 11 (Figure 29A). Further we verified these results by determining more Mb-expressing T cells in the tumor tissue when compared to controls (Figure 29B). Also, the proportion of Mb-expressing T cells in the tumor tissue in comparison to control T cells was increased at day 20 following T cell transfer (Figure 29C). Anti-CD8a staining of sections from snap frozen tumor tissue indicated increased infiltration of T cells in animals received Mb-expressing T cells when compared to controls (Figure 29D+E). These data suggest a better T cell infiltration in the tumor side, when treated with Mb-expressing T cells.

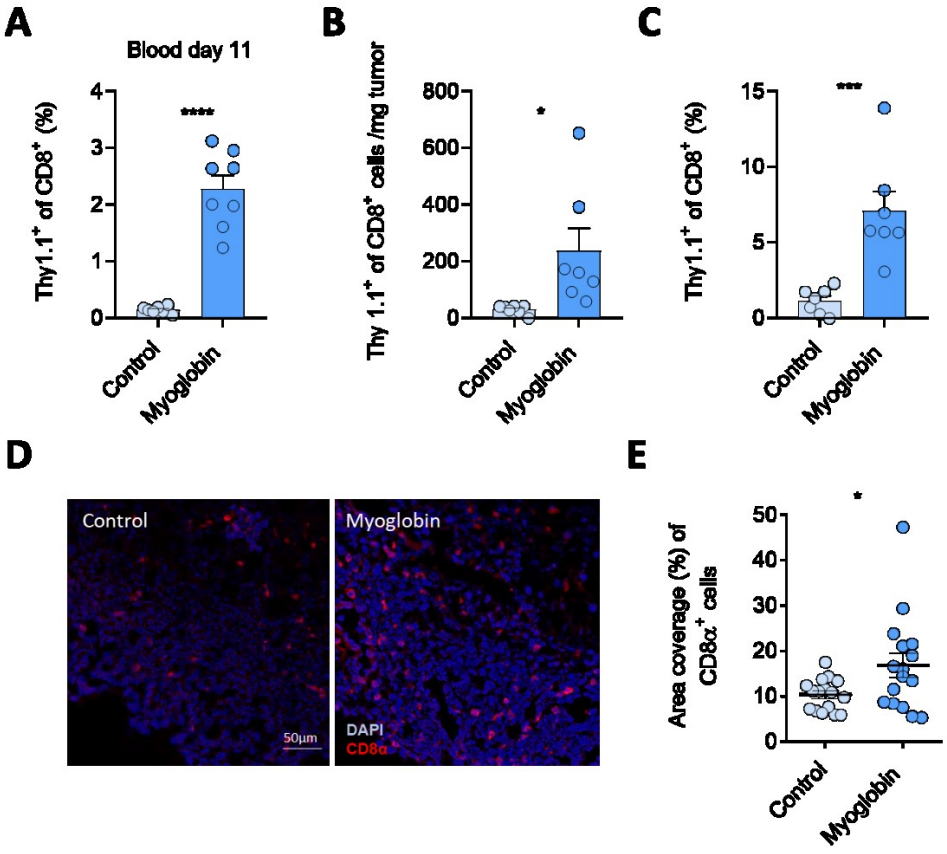

Figure 29: Melanoma-bearing mice show higher numbers of Myoglobin-expressed CD8$^+$ T cells in the tumor after treatment in comparison to control CD8$^+$ T cells. B16F10-gp33 tumor-bearing C57BL/6J mice treated at day 7 with 5 x 10^5 Thy1.1 (Control) and Thy1.1-Myoglobin (Myoglobin) expressing P14$^+$ CD8$^+$ T cells, Poly I:C and gp33 peptide. Spleen and tumor tissues were analysed at day 20 after T cell transfer. (A) The frequency of Thy1.1$^+$ gated on CD8$^+$ T cells was measured in the circulation taken at day 11 after tumor cell transfer via flow cytometry (n=7-8). (B) The absolute count of Thy1.1$^+$ gated on CD8$^+$ T cells per mg tumor was detected via flow cytometry (n=7). (C) Frequency of Thy1.1$^+$ gated on CD8$^+$ T cells were measured in the tumor tissue via flow cytometry (n=7). (D-E) Histology slides of tumor tissue sections were stained for DAPI and CD8α. (D) Representative images are shown (scale bar = 50 µm). (E) Analysis of the average coverage of CD8α is illustrated (n=16). Error bars indicate SEM. Student´s t-test was performed and differences are classified as *P<0.05, ***P<0.001 and ****P<0.0001 between the indicated groups.

Moreover, increased levels of the cytokine IFN-γ was measured in Mb T cells within the tumor tissue when compared to controls (Figure 30A). Similar, also GzmB expression was increased in the tumor tissue in Mb-expressing T cells in comparison to control T cells (Figure 30B). Also, enhanced expression of IL-2 was determined in Mb-expressing T cells when compared to control T cells (Figure 30C). Consequently, increased levels of cleaved caspase 3 was detected in tumor tissue harvested from hosts received Mb-expressing T cells compared to

controls (Figure 30D+E). Taken together, Mb-expressing T cells showing better effector function and more killing in the tumor tissue in comparison to control T cells.

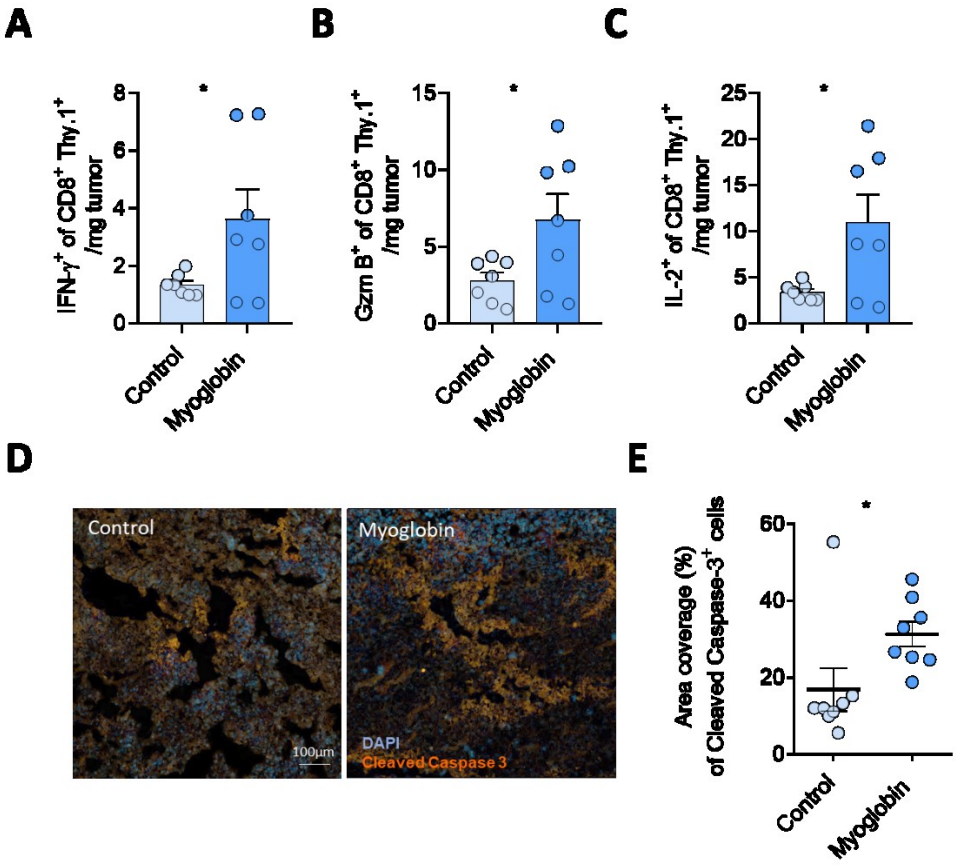

Figure 30: Melanoma-bearing mice show higher effector function of Myoglobin-expressed CD8$^+$ T cells in the tumor after treatment in comparison to control CD8$^+$ T cells. B16F10-gp33 tumor-bearing C57BL/6J mice treated at day 7 with 5 x 10^5 Thy1.1 (Control) and Thy1.1-Myoglobin (Myoglobin) expressing P14$^+$ CD8$^+$ T cells, Poly I:C and gp33 peptide. Spleen and tumor tissues were analysed at day 20 after T cell transfer. Absolute count per mg tumor of (A) IFN-γ$^+$, (B) GzmB$^+$ and (C) IL-2$^+$ gated on Thy1.1$^+$ CD8$^+$ T cells were detected with flow cytometry in the tumor tissue (n=7). (D-E) Histology slides of tumor tissue sections were stained for DAPI and cleaved caspase-3. (D) Representative images are shown (scale bar = 100 µm). (E) Analysis of the average coverage of cleaved caspase-3 is illustrated (n=8). Error bars indicate SEM. Student´s t-test was performed and differences are classified as *P<0.05 between the indicated groups.

We further wondered if Mb expressing T cells can reduce the risk of metastasis formation. Vimentin and cytokeratin 18 staining of snap frozen tumor tissue indicated no differences in the mesenchymal marker vimentin (Figure 31A+B). However, increased levels of cytokeratin 18 in sections of tumor tissues, harvested from animals treated with Mb-expressing T cells, in comparison to tumor tissue, harvested from animals treated with control T cells, were observed

(Figure 31C+D). This suggests the retention of epithelial-like features following transfer of Mb expressing T cells and may indicate a reduced propensity for metastasis [365].

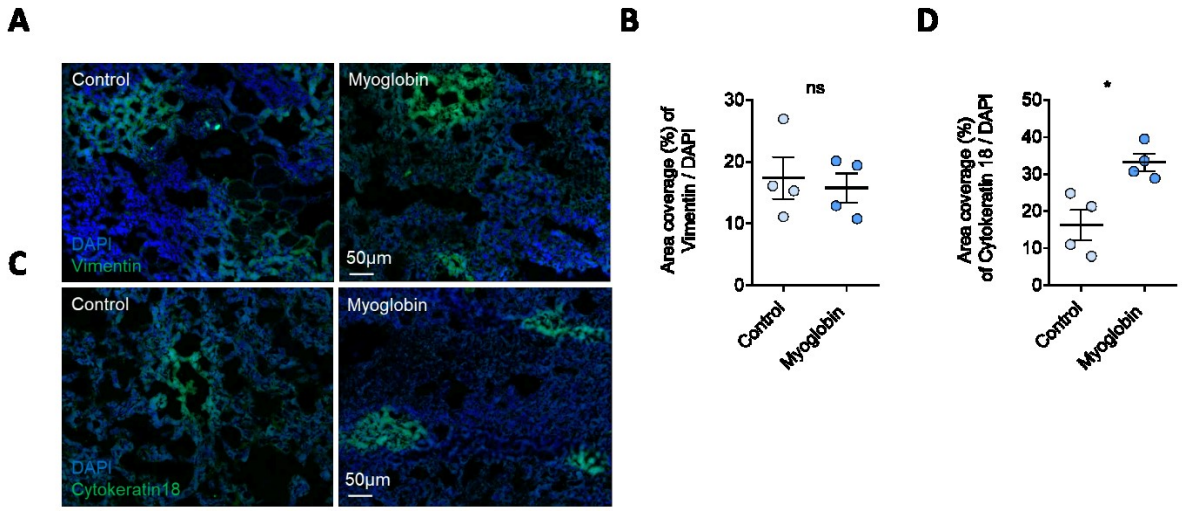

Figure 31: Melanoma-bearing mice does not show increased metastasis marker after treatment with low numbers of Myoglobin-expressed CD8$^+$ T cells in comparison to control CD8$^+$ T cells. B16F10-gp33 tumor-bearing C57BL/6J mice treated at day 7 with 5 x 10^5 Thy1.1 (Control) and Thy1.1-Myoglobin (Myoglobin) expressing P14$^+$ CD8$^+$ T cells, Poly I:C and gp33 peptide. Spleen and tumor tissues were analysed at day 20 after T cell transfer. (A-B) Histology slides of tumor tissue were stained for DAPI and Vimentin. (A) Representative fluorescence images are shown (scale bar = 50 µm). (B) Analysis of the frequency of area coverage of Vimentin / DAPI (n=4) is determined. (C-D) Histology slides of tumor tissue were stained for DAPI and Cytokeratin 18. (C) Representative fluorescence images are shown (scale bar = 50 µm). (D) Analysis of the frequency of area coverage of Cytokeratin 18 / DAPI (n=4) was determined. Error bars indicate SEM. Student´s t-test was performed and differences are classified as ns: P>0.05 and *P<0.05 between the indicated groups.

While at this time point, we observed reduced frequency of TOX^{high}-expressing T cells when Mb was expressed, PD-1 and TIM-3 could be still detected on adoptively-transferred T cells even in the presence of Mb (Figure 32A-C). Therefore, we hypothesized that a combination of Mb-expressing T cells with checkpoint inhibition might be beneficial for anti-cancer defence. We implanted 5x10^5 Mb expressing T cells or control T cells on day 7 into B16F10-gp33 tumor bearing mice, following Poly I:C, gp33 and every 2 days anti-PD-1 checkpoint inhibition or isotype control (Figure 32D). While in the isotype control treated animals, a modest difference was only observed early after transfer, anti-PD-1 treatment following transfer of Mb expressing T cells resulted in a further reduction in tumor growth (Figure 32E). Taken together, these data indicate that Mb expression improved infiltration of T cells into the tumor tissue and caused reduction of tumor growth in two cancer model systems.

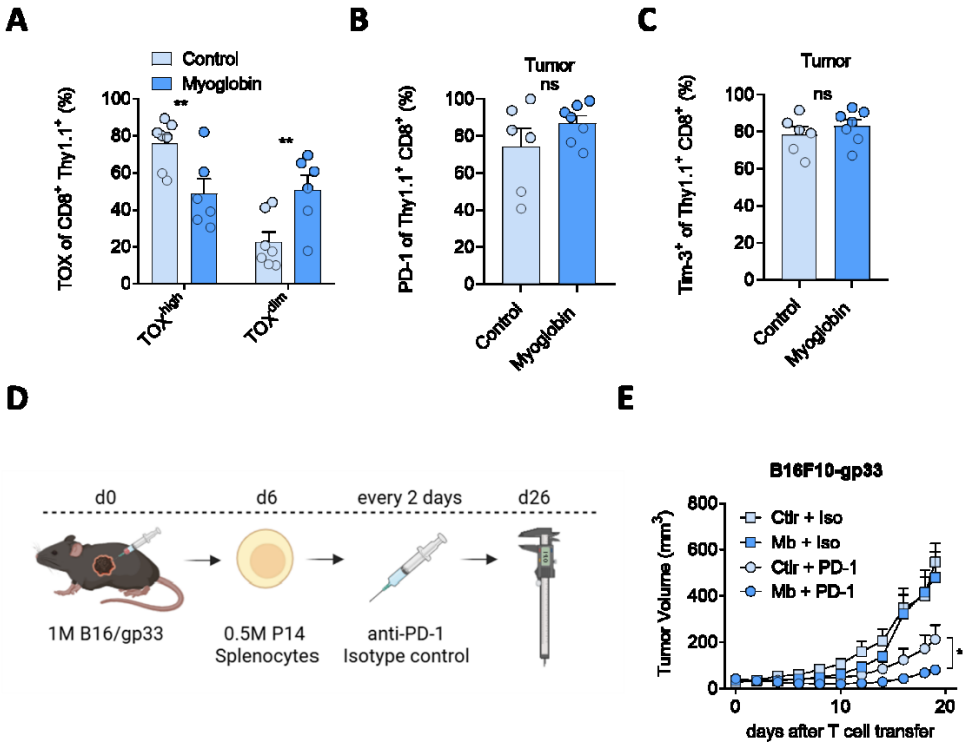

Figure 32: Melanoma-bearing mice show less tumor burden after treatment of checkpoint-inhibition in combination with low numbers of Myoglobin-expressed CD8$^+$ T cells in comparison to control CD8$^+$ T cells. (A-C) B16F10-gp33 tumor-bearing C57BL/6J mice treated at day 7 with 5 x 10^5 Thy1.1 (Control) and Thy1.1-Myoglobin (Myoglobin) expressing P14$^+$ CD8$^+$ T cells, Poly I:C and gp33 peptide. Spleen and tumor tissues were analysed at day 20 after T cell transfer. Flow cytometric analysis of (A) TOX^{high} and TOX^{dim} populations and the frequency of (B) PD-1 and (C) Tim-3 in tumor tissue were gated on CD8$^+$ Thy1.1$^+$ T cells (n=6-7). (D-E) B16F10-gp33 tumor-bearing C57BL/6J mice were treated at day 7 with 5 x 10^5 Thy1.1 (Ctlr) and Thy1.1-Myoglobin (Mb) expressing P14$^+$ T cells, Poly I:C and gp33 peptide. The mice were treated every second day with PD-1 blockade or Isotype control. (D) A scheme of the experimental set up is shown. (E) The tumor growth was monitored until day 20 after T cell transfer (n=6-9). Error bars indicate SEM. Two-way ANOVA and Student´s t-test were performed and differences are classified as ns: P>0.05, *P<0.05 and **P<0.01 between the indicated groups.

7. Discussion

In the present study we investigated whether increased oxygen metabolism in T cells can influence anti-tumor effector function and overcome hypoxic environments. We demonstrated that expression of Mb can increase mitochondrial and glycolytic metabolism resulting in increased level of specific metabolites and ATP. Accordingly, effector T cell differentiation was increased following expression of Mb *in vitro* and *in vivo*. Consistently, adoptive transfer of Mb-expressing T cells could reduce tumor growth and improve checkpoint therapy in a syngeneic model system.

Hypoxia represents a significant barrier to the efficacy of immunotherapies in solid tumors. Due to the high oxygen and nutrient demands of proliferating cancer cells, TILs are often metabolically deprived, compromising their effector function [366]. While CART cell therapy has shown considerable success in haematological malignancies such as ALL, its effectiveness in solid tumors remains limited [367]. This discrepancy reflects the broader challenge that T cells face in solid tumor environments, where hypoxia and metabolic restriction act synergistically to blunt antitumor immunity. Consequently, even highly activated T cells struggle to sustain their effector programs when exposed to persistent oxygen deprivation [368]. Under hypoxic conditions, the transcriptional factor HIF-1α is no longer targeted by VHL for degradation. As a result, HIF-1α accumulates, translocates to the nucleus and induces the expression of HRE [106]. Sustained expression of HIF-1α in $CD8^+$ T cells is associated with exhaustion, reduced proliferation and mitochondrial dysfunction [369]. In this study, we confirm the B16F10-gp33 tumor model exhibits a hypoxic milieu in the TME, making it suitable as an *in vivo* system for investigating hypoxia [370]. The spleen was verified as a normoxic reference tissue for distinguishing tumor-specific effects. Colocalization of HIF-1α with CD8α in tumor tissue indicates that T cells in the B16F10-gp33 model experience hypoxic stress. In addition, increased levels of HIF-1α were detected particularly in activated tumor-infiltrating effector T cells. This suggests that T cells undergo functional reprogramming in the hypoxic TME and may become chronically activated under hypoxic stress, contributing to tumor-mediated immune escape. This induced stress has a dual immunosuppressive effect by promoting tumor-adaptive processes and directly impairing the functionality of the immune cells.

Antigen specific T cells shift their metabolism upon activation from OXPHOS towards aerobic glycolysis to meet the increased nutritional demands associated with cell division [266]. This

function is triggered by expression of HIF-1α, which increases expression of genes involved in glycolysis [371, 372]. Increased glucose metabolism can promote T cell effector function [373]. Accordingly, we hypothesize that Mb-expression may enhance cellular metabolism and consequently, T cell effector function. The oxygen muscle protein Mb, known for its storage capacity and high oxygen affinity, was successfully overexpressed in $CD8^+$ T cells. Under normoxic conditions, we observed a significant downregulation of HIF-1α, suggesting that increased intracellular oxygen availability through Mb-expression may prevent its hypoxia-induced stabilization. This reduction of HIF-1α could in turn reduce hypoxia-induced metabolic stress, thereby preserving T cell proliferation and effector functions. Furthermore, we propose that Mb could serve as a tool to modulate intracellular oxygen availability in immune cells, potentially helping to maintain functionality under hypoxic conditions.

During anti-tumoral and anti-viral responses, metabolic functions of T cells are critical in preventing exhaustion [269]. Specifically, effector T cells exhibit punctate mitochondria, while memory T cells form networks, depending on the remodelling of the inner mitochondrial membrane through OPA-1, suggesting that mitochondrial metabolic function is critical for prolonged T cell effector function [268]. The rate of MbO_2 promotes mitochondrial oxygen uptake, indicating that Mb is a potent oxygen buffer capable of releasing oxygen for mitochondrial metabolism when required [349]. Accordingly, Mb can facilitate intracellular oxygen diffusion, increasing mitochondria access to oxygen and thereby promoting OXPHOS [374]. Consistently, we observed narrower and denser cristae, which are associated with increased functional efficiency, leading to enhanced ATP production via OXPHOS. Elongated cristae structures reflect a more metabolically active mitochondrial organisation. This suggests that Mb may support mitochondrial remodelling in favour of an increased metabolic capacity, potentially by improving oxygen availability directly at the cristae membrane. Such localized oxygen enrichment at the cristae could directly support T cell effector functions by optimizing ATP generation under metabolically demanding conditions. Together with the previously observed reduction of HIF-1α this restructure highlights the possibility of intracellular oxygen storage to support T cell fitness under hypoxic conditions. Interestingly, despite the prolonged structural changes of the cristae and the remodelling of the mitochondrial shape, no altered fusion or fission could be observed. Mitochondrial fusion and fission are dynamic processes regulated by GTPases that remodel mitochondrial membranes [353]. Fusion enables the exchange of mitochondrial DNA, proteins, and metabolites, thereby maintaining functional integrity [354]. Fission facilitates mitochondrial distribution during cell division and the

removal of damaged fragments via mitophagy [355]. A precise balance between fusion and fission is crucial for mitochondrial morphology, energy homeostasis, and overall, for the metabolic need of the cell [355]. This suggests, that Mb enhances mitochondrial function by remodelling of mitochondrial shapes rather than by triggering compensatory changes in organelle dynamics. This may reflect a balanced metabolic state, without inducing mitochondrial stress. Consistently, we observed enhanced OXPHOS underlining the functional relevance of mitochondrial structural remodelling. Enhanced basal respiration indicates a higher probability of oxygen supply through OXPHOS under normal conditions. Further, higher maximal respiration reflects increased mitochondrial potential and enhanced spare capacity is critical for T cell resilience. Collectively, these observations show that Mb expression not only remodels mitochondrial structures, but also increases OXPHOS under normal conditions and enhances the mitochondrial potential. This results in increased ATP production. Therefore, Mb is not only increasing respiration, but also the energetic supply of the T cell, which is essential for T cell effector function [359]. However, also the Proton Leak was enhanced. This observation might be interpreted as an indication of inefficient ATP synthases. However, this interpretation appears misleading, since reduced ATP synthase efficiency would also be expected to decrease overall ATP production. Interestingly, ATP production was found to be increased following Mb overexpression. This proton Leak might be a protection against forming of ROS particles through excess electrons, resulting in a mild uncoupling for metabolic protection. Taken together, the enhanced OXPHOS confirms a functional benefit of intracellular oxygen availability through Mb expression in T cells. Increased basal and maximal respiration, as well as elevated spare respiratory capacity, indicate a metabolically flexible phenotype capable of meeting the high energy demands associated with effector function in hypoxic environments [356]. Importantly, this metabolic advantage results in enhanced ATP production, supporting the concept that Mb enhances both oxygen availability its effective utilization in the mitochondrial respiratory chain.

Metabolic functions can increase the production of ROS, which might limit T cell function. Specifically, the superoxide radical $O_2^{\bullet-}$ can be produced by the ETC, which is transformed to H_2O_2 by the SOD2 in the mitochondria [357]. Next, H_2O_2 along with 2 GSH can be reduced to H_2O and GSSG by glutathione peroxidase [357, 358]. GSSG can be recycled by the glutathione reductase under the consumption of NADPH [358]. Notably, exposure of antigen-specific T cells to H_2O_2 curbs effector functions [271]. Furthermore, reduced levels of GSH by deletion of the glutamate cysteine ligase trigger T cell dysfunction and chronic antigen persistence [270].

Moreover, increased mitochondrial stress is associated with increased ROS levels and decreased T cell function [101]. Considering our data, we could expect increased mitochondrial ROS production, since OXPHOS was remarkably increased following Mb expression. However, we determined highly decreased presence of superoxide, which suggests increased ROS scavenging in presence of Mb. Consistently, H_2O_2 scavenging was increased in T cells expressing Mb along with increased presence of GSH. These findings indicate that Mb-expressing T cells achieve high ATP levels and oxygen utilization without a ROS-induced loss of function, highlighting a dual role of Mb in supporting both energy metabolism and redox balance and therefore, stabilizing mitochondrial dynamic and likely enhances T cell resistance in hypoxic TME. Also, an increased NAD^+/NADH conversion was detected in Mb-expressing T cells, which enhances the cellular reducing power by stimulating metabolic pathways such as the TCA cycle and nicotinamide nucleotide transhydrogenase (NNT) activity, resulting in the promotion of NADPH generation. NADPH availability drives glutathione reductase reaction, converting GSSG to GSH. Despite the enhanced ROS scavenging potential, we observed slightly increased protein carbonylation in Mb-expressing T cells. This occurs during high metabolic activity and enhanced OXPHOS generating transient ROS bursts that can overwhelm antioxidant defence mechanism. Consequently, even cells with strong antioxidant capacity remain vulnerable to irreversible oxidative modifications. Furthermore, we investigated whether enhanced ROS scavenging through Mb-expression only occurs in the mitochondria or can also be detected in the cytosol of the T cells. Our data confirm that Mb enhances the ROS scavenging time after H_2O_2 exposure. This confirms that ROS scavenging via Mb expression is not restricted to the mitochondria, providing enhanced protection of cytosolic proteins and lipids, which might result in improved effector function and increased cell survival.

The glycolytic activity in T cells provides crucial insights into their metabolic fitness and activation status [373]. After activation, T cells can undergo a metabolic switch towards aerobic glycolysis, which is descried as Warburg effect, to support rapid proliferation and effector function [32]. These metabolic adaptions are linked to T cell fate, because sustained glycolytic activity can promote effector differentiation but, in case of dysregulation, can also contribute to metabolic exhaustion and loss of function within the TME [375]. Our data suggest, that Mb enhances both basal and compensatory glycolysis activity. Increased compensatory glycolysis indicates improved metabolic flexibility, allowing cells to adapt in cases of mitochondrial dysfunction. Together with enhanced OXPHOS, Mb promotes an optimal balance of metabolic processes and therefore, potentially a higher metabolic flexibility. Also, increased levels of

Fructose-1,6-bisphosphat and lactic acid confirm the increased glycolysis flux. High Lactic acid levels correlate with reduced metabolism, limit effector function and reduced cytotoxic activity [33]. In Mb-expressing T cells, however, we observed increased metabolic activity, which indicates efficient lactic acid utilization and a maintained redox balance that supports energy production. This may result in enhanced effector function and reduced exhaustion. Also, TCA metabolites were significantly increased and therefore promoting the processing of pyruvic acid. The higher levels of TCA cycle intermediates also indicate enhanced mitochondrial activity and flexibility. An active anaplerotic and cataplerotic reaction supports both energy production and biosynthesis [376]. Also, metabolites such as α-ketoglutaric acid, succinic acid and citric acid may also act as signalling molecules, linking mitochondrial metabolism to the regulation of genes and effector function [377]. Consequently, a dynamic energy balance with increased ATP, ADP and AMP levels was measured in Mb-expressing T cells. High levels of AMP and ADP indicate a high energy demand in the T cell and activate energy-producing signalling pathways such as Adenosine Monophosphate-activated Kinase (AMPK) [378]. This indicates a high energy turnover rate and metabolic activity. The increased glycolysis, elevated TCA metabolites and enhanced OXPHOS indicate ideal conditions for adaption in the heterogeneous TME.

Given the metabolic adaptions, we assumed that Mb expression in T cells improve effector function. Enhanced metabolism often results in oxidative stress and therefore negatively influences the survival [111]. However, Mb does not influence the survival, supporting the metabolic stability of the engineered T cells. We measured slightly increased proliferation, which indicates improved cellular fitness and expansion. In addition, increased ATP levels might favour cell division. We detected more effector T cells, suggesting that Mb drives the differentiation into effector cells, without influencing the memory population *in vitro*. Consistent with these findings, IL-7R expression was increased after Mb-expression in T cells. IL-7R is essential for long-term survival and homeostasis and therefore might favour persistence in the TME [242]. Exhaustion in T cells negatively influences effector function. Terminal exhausted T cells are characterised by a loss of function [250]. Hypoxia and reduced nutrition supply promote the exhaustion of T cells in the TME, resulting in uncontrolled tumor growth. TOX is an important transcription factor for the initiation and maintenance of an exhausted transcription program in TILs [250]. Our observation shows reduced TOX levels in Mb-expressing T cells and, indicating a delayed or reduced exhaustion while maintaining functionality. EOMES and TCF-1 are transcription factors associated with distinct T cell

differentiation states, including progenitor-like and chronically stimulated phenotypes [247, 251]. The reduction of both factors indicates a shift away from a progenitor-like or memory-associated state towards a more differentiated effector phenotype. In particular, lower TCF-1 levels suggest enhanced effector differentiation, although this may come at the cost of reduced stem-like or long-term memory potential. Further, decreased levels of the exhaustion surface proteins PD-1 and Tim-3 were detected in Mb-expressing T cells. They are highly upregulated in T cells in the TME and reduce effector function. ICI, especially those targeting PD-1, enhance antitumor immunity by blocking inhibitory signalling pathways in T cells *in vivo* [297]. This underlines the importance of metabolic stability as a protective factor against the exhaustion phenotype and may prevent T cell dysfunction. Therefore, Mb expression might enhance T cell therapy by improving resilience to chronic antigen exposure in the TME, which is a major cause of exhaustion [30]. Proinflammatory cytokine production by activated T cells plays a crucial role in the antitumor defence. The type II class cytokine IFN-γ enhances antigen presentation and cytotoxic T cell activity by upregulation of MHC-I expression. In parallel, TNF-α induces apoptosis in malignant cells and shapes the TME to support T cell effector function [259]. Conversely, chronic cytokine signalling may also promote T cell exhaustion and tissue damage. Accordingly, Mb can increase IFN-γ and TNF-α expression when overexpressed in T cells with transgenic TCR directed against cocultivated malignant tumor cells. Also, GzmB expression was significant increased, a serine protease which is packed in cytotoxic granules and activates apoptosis by activating caspases, like caspase 3 [263]. This indicates enhanced cytotoxic activity and improved effector function of Mb-expressing T cells. This was confirmed by more efficient tumor cell lysis, indicating that metabolic reprogramming results in more effector function and effective tumor cell killing. In summary, our *in vitro* data analysis demonstrates that Mb expression in cytotoxic T cells drives metabolic reprogramming that enhances effector functionality. Importantly, Mb reduces hypoxia-associated marker while simultaneously boosting both glycolysis and OXPHOS, leading to an increased proportion of effector cells, reduced exhaustion and increased cytokine production.

Mb can improve T cell metabolism in a hostile tumor microenvironment. Like activated T cells, tumor cells utilize aerobic glycolysis to facilitate proliferation and growth [99]. Hence, the tumor microenvironment is associated with low glucose and oxygen along with expression of immunosuppressive molecules [98, 99]. Furthermore, mitochondrial reprogramming elevates antigen presentation leading to better melanoma tumor immunogenicity and response to immunotherapy [379, 380]. Accordingly, it is challenging for tumor-specific T cells in these

tumors to elicit an effective anti-cancer response. Specifically, T cells compete within the TME for nutrition including glucose to promote effector functions [93]. Interestingly, higher proportion of Mb-expressing T cells was detected in the tumor tissue, but not in the spleen, compared to control T cells four days after adoptive T cell transfer. This indicates improved migration and persistence specifically under hypoxic conditions in the TME in early stages. This is consistent with *in vitro* data on increased metabolic fitness and effector function, supporting the hypothesis that Mb offers advantages primarily under hypoxic conditions due to increased oxygen supply. Consistent with previous reports showing HIF-1α expression in T cells following hypoxia [103, 348], we also observed HIF-1α expression in tumor-infiltrating T cells. However, when we expressed Mb in antigen-specific T cells, we observed reduced expression levels of HIF-1α in the tumor and spleen tissue. This suggests an actual reduction in cellular hypoxia or HIF-1α stabilization, possibly through improved intracellular oxygen transport. Notably, while increased HIF-1α expression levels caused by deletion of the inhibitor von Hippel Lindau factor has been associated with enhanced T effector function and anti-tumor defence, Mb-expressing T cells showed reduced HIF-1α levels yet maintained improved effector function. [103, 381]. This indicates that increased glucose metabolism by increased OXPHOS may be sufficient to switch metabolic activity towards aerobic glycolysis despite reduced HIF-1α expression. Furthermore, since inhibition of HIF-1α can improve checkpoint therapy we speculate that this effect can also contribute to our observed reduction in tumor growth observed with anti-PD1 antibodies [107].

Simultaneously to increased effector function *in vitro*, we also observed an increased effector population with enhanced IFN-γ production. This indicates not only a shift in the metabolic profile, but also an enhanced antigenic response *in vivo* mediated by Mb. Interestingly, in the *in vivo* experimental setting, we observed PD-1 expression on tumor specific T cells, which was not affected by Mb expression. We speculate that the complex-immunosuppressive TME *in vivo* is regulated by metabolites, hypoxic-acidic conditions, cytokines, immune cells and stromal cells that could impair T cell functionality and upregulate PD-1 [382]. However, an active TME is also associated with upregulation of PD-1 on activated effector T cells [383], which respond to anti-PD1 therapies. It has also been demonstrated that during early activation, effector T cells can transiently downregulate the exhaustion markers, indicating that they are overcoming inhibitory signals and getting activated and capable of mounting immune response by initiating proliferation and cytokine production [384, 385]. Elevated exhaustion markers on T cells could also be attributed to the state of T cells that retain stem-like properties and can

differentiate into either effector T cells or terminally exhausted T cells depending on the local regulatory cues from the microenvironment [386, 387].

The adoptive transfer of $2x10^6$ Mb-expressing $CD8^+$ T cells resulted in a significant reduction in the tumor burden of the non-immunogenic B16-F10-gp33 tumor model in comparison to control T cells, underlining the functional relevance of the observed metabolic enhancements. Tumor regression was measured in connection with increased T cell infiltration in the hypoxic TME 20 days after adaptive T cell transfer. Increased T cell infiltration was observed in both early and late stages, suggesting a sustained immune involvement throughout the disease progression. This may indicate that the consistent presence of T cells contributes to increased immune surveillance and more effective tumor effector function, resulting in a limited disease progression.

The more immunogenic MC38-ova tumor model displays a TME with increased immune cell infiltration. Despite this, Mb maintains a tumor-suppressive effect, indicating that Mb has a universal metabolic benefit in T cells independently of the solid tumor model. Also, using a SIINFEKL-specific TCR confirms that the effect is not epitope specific. Therefore, Mb could be used as a universal strategy to overcome hypoxia in solid tumors. Decreasing the number of transferred T cells to $5x10^5$ is a relevant translational aspect, considering potential limitations in T cell availability in patients with low T cell output. Mb enhances the per-cell efficacy of adoptive T cell therapy, enabling smaller T cell populations to effectively control tumor growth through improved functionality, persistence, and proliferation. Even with decreased T cell numbers, Mb-expressing cells demonstrate potent anti-tumor activity in the non-immunogenic B16F10-gp33 model. The observed reductions in tumor growth and weight indicate a durable, long-term effect, further supported by extended survival and delayed tumor progression *in vivo*. Extending lifespan is an important preclinical goal in immunotherapy, as it reflects both tumor surveillance and the functional persistence of transferred T cells. Clinically, extended survival may translate into better quality of life, longer periods without disease progression, and increased opportunities for combination therapies.

The B16F10 tumor model is characterised by poor immune infiltration, hypoxia and low MHC-I expression. Despite the unfavourable conditions, Mb supports both infiltration and functional activity within the TME, even with decreased T cell numbers. Also, increased circulating T cell numbers were detected, indicating not only a local effect in the TME but also sustained systemic bioavailability, which may be related to the enhanced IL-7R levels observed *in vitro* and

associated with increased T cell survival *in vivo*. These findings support the hypothesis that Mb expression facilitates T cell persistence and accumulation in the hypoxic TME, thereby contributing to prolonged tumor control and improved survival. The enhanced oxygen handling and metabolic resilience of Mb-expressing T cells may underlie their superior expansion, infiltration, and retention within the tumor tissue.

Simultaneously, Mb-expressing T cells demonstrate enhanced effector function *in vivo*, as evidenced by increased production of IFN-γ, IL-2, and GzmB, reflecting stronger activation and cytotoxic capacity. These cytokines are essential for effective antitumor immune responses, supporting both direct tumor cell killing and the activation of additional immune effector cells [205, 388, 389]. Correspondingly, higher levels of cleaved Caspase-3 in the tumor tissue indicate increased tumor cell apoptosis, consistent with improved efficacy of Mb-expressing T cells against tumor targets. From a translational perspective, the combination of increased energy supply and heightened cytotoxic capacity highlights the potential of Mb expression as a strategy to optimize adoptive T cell therapies.

Another important therapeutic aspect is whether a particular treatment method can also reduce the formation of metastases. Metastases occur when cancer cells from a primary tumor spread to distant tissues and form secondary tumors there. This involves invasion, intravasation, transport, extravasation, and colonization [95]. Crucial biological processes include EMT to promote mobility and invasiveness, angiogenesis for vascular utilization, and immune evasion for survival in the circulation and establishment at the target site [89]. The occurrence and timing of metastases depend on tumor aggressiveness, genetic changes, and the patient's immune status. An increased expression of Cytokeratin 18 in tumors of mice treated with Mb-expressing T cells indicates enhanced maintenance of epithelial characteristics, suggesting a reduction of EMT. Unchanged Vimentin levels indicate that Mb-expressing T cells probably do not directly suppress the expression of mesenchymal markers but rather influence the balance between epithelial and mesenchymal properties. Considering the expression of both markers, Mb-expressing T cells are likely modulating the TME towards a less metastasis-promoting phenotype. This modulatory effect likely reflects enhanced T cell effector functions and heightened immune surveillance, which together prevent tumor cells from undergoing EMT and initiating metastatic progression.

Despite the expression of myoglobin reducing the frequency of TOX^{high} T cells, tumor-infiltrating T cells continue to express exhaustion markers such as PD-1 and TIM-3, indicating

that Mb alone is insufficient to fully reverse T cell exhaustion. This observation underscores the complexity of T cell exhaustion within the tumor microenvironment, which may require multifactorial interventions. Accordingly, the combination of Mb expression with ICI greatly enhanced the anti-tumor efficacy of anti-PD-1 treatment. Overexpressing Mb in T cells might offer therapeutic avenues for the treatment of solid tumors. This strategy enhances the effector functions of T cells by improving their survival and functionality in the hypoxic TME. This approach could be combined with existing immunotherapies, such as CAR T cell therapy together with checkpoint inhibition, to boost the overall immune response against solid tumors. However, enhanced metabolism of Mb-expressing T cells may contribute to adverse effects such as autoimmunity or hyperproliferation of T cells, which need to be further investigated to harness the full spectrum of benefits within an appropriate safety framework.

While enhanced T cell activity and persistence in CAR T cell therapy benefit antitumor efficacy, this may also increase the severity of side effects such as CRS, immune effector cell-associated neurotoxicity syndrome (ICANS) and long-term neutropenia [390]. These adverse events are closely linked to T cell activation. CRS results from excessive cytokine release causing fever, fatigue, and organ dysfunction, while ICANS manifests as confusion, seizures, and, in severe cases, cerebral edema. However, the frequency of these toxicities does not directly correlate with antitumor activity [391]. For example, CD28-based CD19-directed CAR T cells (e.g., axicabtagene ciloleucel, brexucabtagene autoleucel) show higher CRS rates than 4-1BB-based CAR T cells (e.g., lisocabtagene maraleucel) without loss of efficacy, emphasizing the need for rigorous *in vivo* evaluation. Moreover, increased metabolism in CAR T cells might contribute to TCR mediated autoimmunity [392]. Therefore, further studies, including long-term assessments and dose-finding studies are necessary to fully establish the safety profile and optimize potential therapeutic benefits. Taken together, in the present work we demonstrate that Mb expression can significantly increase metabolic functions of antigen-specific T cells, anti-tumor effector functions, and efficacy of checkpoint inhibition therapy.

8. Literature

1. Werner, J., et al., *Deep transfer learning approach for automatic recognition of drug toxicity and inhibition of SARS-CoV-2.* Viruses, 2021. **13**(4): p. 610.
2. Ettich, J., et al., *A hybrid soluble gp130/spike-nanobody fusion protein simultaneously blocks interleukin-6 trans-signaling and cellular infection with SARS-CoV-2.* Journal of virology, 2022. **96**(4): p. e01622-21.
3. Rafii, P., et al., *Constitutive activation of gp130 in T cells results in senescence and premature aging.* The Journal of Immunology, 2023. **210**(11): p. 1641-1652.
4. Gesiorowski, A., et al., *Bispecific soluble cytokine receptor-nanobody fusions inhibit Interleukin (IL-) 6 trans-signaling and IL-12/23 or tumor necrosis factor (TNF) signaling.* Journal of Biological Chemistry, 2023. **299**(11): p. 105343.
5. Longo, Y., et al., *The purinergic receptor P2X7 as a modulator of viral vector-mediated antigen cross-presentation.* Frontiers in Immunology, 2024. **15**: p. 1360140.
6. Werner, J., et al., *Myoglobin expression improves T-cell metabolism and antitumor effector function.* Journal for ImmunoTherapy of Cancer, 2025. **13**(6): p. e011503.
7. Katahira, I., et al., *Controlling mitochondrial membrane architecture via MIC60 determines viral replication to promote anti-viral immunity.* Cell Reports, 2025. **44**(7).
8. Lang, P.A., et al., *Optimized arenaviruses with tumor-tropic mutations promote safe anti-tumor efficacy via sustainable immune modulatory properties.* Cell Reports Medicine, 2025. **6**(10).
9. WHO, *Press Release No. 345*, in *Global cancer burden growing, amidst mounting need for services*. 2024, International Agency for Research on Cancer Geneva, Lyon.
10. WHO. *Cancer*. 2025 [cited 09.12.2025; Available from: https://www.who.int/news-room/fact-sheets/detail/cancer?utm_.
11. Li, C., et al., *Apoptosis regulation by Bcl-xL modulation of mammalian inositol 1, 4, 5-trisphosphate receptor channel isoform gating.* Proceedings of the National Academy of Sciences, 2007. **104**(30): p. 12565-12570.
12. Liu, X., J. Yan, and M.W. Kirschner, *Cell size homeostasis is tightly controlled throughout the cell cycle.* PLoS biology, 2024. **22**(1): p. e3002453.
13. Boon, N.J., et al., *DNA damage induces p53-independent apoptosis through ribosome stalling.* Science, 2024. **384**(6697): p. 785-792.
14. Flores-Romero, H., et al., *BCL-2-family protein tBID can act as a BAX-like effector of apoptosis.* The EMBO journal, 2022. **41**(2): p. e108690.
15. Varadhachary, A.S., et al., *Differential ability of T cell subsets to undergo activation-induced cell death.* Proceedings of the National Academy of Sciences, 1997. **94**(11): p. 5778-5783.
16. Innocente, S.A., et al., *p53 regulates a G2 checkpoint through cyclin B1.* Proceedings of the National Academy of Sciences, 1999. **96**(5): p. 2147-2152.
17. Zatulovskiy, E., et al., *Cell growth dilutes the cell cycle inhibitor Rb to trigger cell division.* Science, 2020. **369**(6502): p. 466-471.
18. Dahia, P., *PTEN, a unique tumor suppressor gene.* Endocrine-related cancer, 2000. **7**(2): p. 115-129.
19. Cooper, G.M., *Cellular transforming genes.* Science, 1982. **217**(4562): p. 801-806.
20. Spranger, S., R. Bao, and T.F. Gajewski, *Melanoma-intrinsic β-catenin signalling prevents anti-tumour immunity.* Nature, 2015. **523**(7559): p. 231-235.
21. Bernardez, B., et al., *Sex and gender differences in cancer pathogenesis and pharmacology.* Clinical and Translational Oncology, 2025: p. 1-12.
22. Jonklaas, J., H. Nsouli-Maktabi, and S.J. Soldin, *Endogenous thyrotropin and triiodothyronine concentrations in individuals with thyroid cancer.* Thyroid, 2008. **18**(9): p. 943-952.
23. LeClair, K., et al., *Evaluation of gender inequity in thyroid cancer diagnosis: differences by sex in US thyroid cancer incidence compared with a meta-analysis of subclinical thyroid cancer rates at autopsy.* JAMA internal medicine, 2021. **181**(10): p. 1351-1358.

24. Dürst, M., et al., *A papillomavirus DNA from a cervical carcinoma and its prevalence in cancer biopsy samples from different geographic regions.* Proceedings of the National Academy of Sciences, 1983. **80**(12): p. 3812-3815.
25. Kim, C.-M., et al., *HBx gene of hepatitis B virus induces liver cancer in transgenic mice.* Nature, 1991. **351**(6324): p. 317-320.
26. Ferrara, N. and W.J. Henzel, *Pituitary follicular cells secrete a novel heparin-binding growth factor specific for vascular endothelial cells.* Biochemical and biophysical research communications, 1989. **161**(2): p. 851-858.
27. Sullivan, M.R., et al., *Quantification of microenvironmental metabolites in murine cancers reveals determinants of tumor nutrient availability.* Elife, 2019. **8**: p. e44235.
28. Jiang, P., et al., *Signatures of T cell dysfunction and exclusion predict cancer immunotherapy response.* Nature medicine, 2018. **24**(10): p. 1550-1558.
29. Doedens, A.L., et al., *Hypoxia-inducible factors enhance the effector responses of CD8+ T cells to persistent antigen.* Nature immunology, 2013. **14**(11): p. 1173-1182.
30. Scharping, N.E., et al., *Mitochondrial stress induced by continuous stimulation under hypoxia rapidly drives T cell exhaustion.* Nature immunology, 2021. **22**(2): p. 205-215.
31. Millikan, G., *Muscle hemoglobin.* Physiological Reviews, 1939. **19**(4): p. 503-523.
32. Vander Heiden, M.G., L.C. Cantley, and C.B. Thompson, *Understanding the Warburg effect: the metabolic requirements of cell proliferation.* science, 2009. **324**(5930): p. 1029-1033.
33. Fischer, K., et al., *Inhibitory effect of tumor cell–derived lactic acid on human T cells.* Blood, 2007. **109**(9): p. 3812-3819.
34. Kägi, D., et al., *Cytotoxicity mediated by T cells and natural killer cells is greatly impaired in perforin-deficient mice.* Nature, 1994. **369**(6475): p. 31-37.
35. Hodi, F.S., et al., *Improved survival with ipilimumab in patients with metastatic melanoma.* New England Journal of Medicine, 2010. **363**(8): p. 711-723.
36. Rosenberg, S.A., et al., *Use of tumor-infiltrating lymphocytes and interleukin-2 in the immunotherapy of patients with metastatic melanoma.* New England Journal of Medicine, 1988. **319**(25): p. 1676-1680.
37. Carpenito, C., et al., *Control of large, established tumor xenografts with genetically retargeted human T cells containing CD28 and CD137 domains.* Proceedings of the National Academy of Sciences, 2009. **106**(9): p. 3360-3365.
38. Sterner, R.C. and R.M. Sterner, *CAR-T cell therapy: current limitations and potential strategies.* Blood cancer journal, 2021. **11**(4): p. 69.
39. Jin, L., et al., *CXCR1-or CXCR2-modified CAR T cells co-opt IL-8 for maximal antitumor efficacy in solid tumors.* Nature communications, 2019. **10**(1): p. 4016.
40. Hanahan, D. and R.A. Weinberg, *The hallmarks of cancer.* cell, 2000. **100**(1): p. 57-70.
41. Hanahan, D. and R.A. Weinberg, *Hallmarks of cancer: the next generation.* cell, 2011. **144**(5): p. 646-674.
42. Hanahan, D., *Hallmarks of cancer: new dimensions.* Cancer discovery, 2022. **12**(1): p. 31-46.
43. Schlange, T., et al., *Autocrine WNT signaling contributes to breast cancer cell proliferation via the canonical WNT pathway and EGFR transactivation.* Breast cancer research, 2007. **9**(5): p. R63.
44. Zetterberg, A., O. Larsson, and K.G. Wiman, *What is the restriction point?* Current opinion in cell biology, 1995. **7**(6): p. 835-842.
45. Liu, Q., et al., *Chk1 is an essential kinase that is regulated by Atr and required for the G2/M DNA damage checkpoint.* Genes & development, 2000. **14**(12): p. 1448-1459.
46. Molinari, M., *Cell cycle checkpoints and their inactivation in human cancer.* Cell proliferation, 2000. **33**(5): p. 261-274.
47. Yusupova, M., et al., *Apoptotic dysregulation mediates stem cell competition and tissue regeneration.* Nature communications, 2023. **14**(1): p. 7547.

48. Greider, C.W. and E.H. Blackburn, *Identification of a specific telomere terminal transferase activity in Tetrahymena extracts.* cell, 1985. **43**(2): p. 405-413.
49. Zhang, S.-s., et al., *CD133+ CXCR4+ colon cancer cells exhibit metastatic potential and predict poor prognosis of patients.* BMC medicine, 2012. **10**(1): p. 85.
50. Sade-Feldman, M., et al., *Resistance to checkpoint blockade therapy through inactivation of antigen presentation.* Nature communications, 2017. **8**(1): p. 1136.
51. Huang, H., et al., *Functional evaluation and clinical classification of BRCA2 variants.* Nature, 2025. **638**(8050): p. 528-537.
52. Albrengues, J., et al., *Neutrophil extracellular traps produced during inflammation awaken dormant cancer cells in mice.* Science, 2018. **361**(6409): p. eaao4227.
53. Na, F., et al., *KMT2C deficiency promotes small cell lung cancer metastasis through DNMT3A-mediated epigenetic reprogramming.* Nature cancer, 2022. **3**(6): p. 753-767.
54. Roje, B., et al., *Gut microbiota carcinogen metabolism causes distal tissue tumours.* Nature, 2024. **632**(8027): p. 1137-1144.
55. Dong, Z., et al., *Cellular senescence and SASP in tumor progression and therapeutic opportunities.* Molecular Cancer, 2024. **23**(1): p. 181.
56. Chandel, N.S., *Glycolysis.* Cold Spring Harbor Perspectives in Biology, 2021. **13**(5): p. a040535.
57. Wang, Y., et al., *Saturation of the mitochondrial NADH shuttles drives aerobic glycolysis in proliferating cells.* Molecular cell, 2022. **82**(17): p. 3270-3283. e9.
58. Pinna, S., et al., *A prebiotic basis for ATP as the universal energy currency.* PLoS biology, 2022. **20**(10): p. e3001437.
59. Dittrich, M., S. Hayashi, and K. Schulten, *On the mechanism of ATP hydrolysis in F1-ATPase.* Biophysical journal, 2003. **85**(4): p. 2253-2266.
60. Pajak, B., et al., *2-Deoxy-d-glucose and its analogs: from diagnostic to therapeutic agents.* International journal of molecular sciences, 2019. **21**(1): p. 234.
61. Arnold, P.K. and L.W. Finley, *Regulation and function of the mammalian tricarboxylic acid cycle.* Journal of Biological Chemistry, 2023. **299**(2).
62. Akiyama, S.K. and G.G. Hammes, *Elementary steps in the reaction mechanism of the pyruvate dehydrogenase multienzyme complex from Escherichia coli: kinetics of acetylation and deacetylation.* Biochemistry, 1980. **19**(18): p. 4208-4213.
63. Yankovskaya, V., et al., *Architecture of succinate dehydrogenase and reactive oxygen species generation.* Science, 2003. **299**(5607): p. 700-704.
64. Zhao, R.-Z., et al., *Mitochondrial electron transport chain, ROS generation and uncoupling.* International journal of molecular medicine, 2019. **44**(1): p. 3-15.
65. Mitchell, P., *Coupling of phosphorylation to electron and hydrogen transfer by a chemi-osmotic type of mechanism.* Nature, 1961. **191**(4784): p. 144-148.
66. Mitchell, P., *Chemiosmotic coupling in oxidative and photosynthetic phosphorylation.* Biological Reviews, 1966. **41**(3): p. 445-501.
67. Sazanov, L.A. and P. Hinchliffe, *Structure of the hydrophilic domain of respiratory complex I from Thermus thermophilus.* science, 2006. **311**(5766): p. 1430-1436.
68. Jones, A.J., et al., *Respiratory complex I in Bos taurus and Paracoccus denitrificans pumps four protons across the membrane for every NADH oxidized.* Journal of Biological Chemistry, 2017. **292**(12): p. 4987-4995.
69. Singer, T.P., *[57] Mitochondrial electron-transport inhibitors*, in *Methods in enzymology*. 1979, Elsevier. p. 454-462.
70. Goetzman, E., et al., *Complex II biology in aging, health, and disease.* Antioxidants, 2023. **12**(7): p. 1477.
71. Ackrell, B.A., E.B. Kearney, and M. Mayr, *Role of oxalacetate in the regulation of mammalian succinate dehydrogenase.* Journal of Biological Chemistry, 1974. **249**(7): p. 2021-2027.
72. Mitchell, P., *Possible molecular mechanisms of the protonmotive function of cytochrome systems.* Journal of theoretical biology, 1976. **62**(2): p. 327-367.

73. Turrens, J.F. and A. Boveris, *Generation of superoxide anion by the NADH dehydrogenase of bovine heart mitochondria.* Biochemical journal, 1980. **191**(2): p. 421-427.
74. Boveris, A. and B. Chance, *The mitochondrial generation of hydrogen peroxide. General properties and effect of hyperbaric oxygen.* Biochemical Journal, 1973. **134**(3): p. 707-716.
75. Kolbe, F., et al., *Cryo-EM structures of intermediates suggest an alternative catalytic reaction cycle for cytochrome c oxidase.* Nature communications, 2021. **12**(1): p. 6903.
76. Abrahams, J.P., et al., *Structure at 2.8 A resolution of F1-ATPase from bovine heart mitochondria.* Nature, 1994. **370**(6491): p. 621-628.
77. Lardy, H.A., D. Johnson, and W. McMurray, *Antibiotics as tools for metabolic studies. I. A survey of toxic antibiotics in respiratory, phosphorylative and glycolytic systems.* Archives of biochemistry and biophysics, 1958. **78**(2): p. 587-597.
78. Heytler, P., *Uncoupling of oxidative phosphorylation by carbonyl cyanide phenylhydrazones. I. Some characteristics of m-CI-CCP action on mitochondria and chloroplasts.* Biochemistry, 1963. **2**(2): p. 357-361.
79. Salabei, J.K., A.A. Gibb, and B.G. Hill, *Comprehensive measurement of respiratory activity in permeabilized cells using extracellular flux analysis.* Nature protocols, 2014. **9**(2): p. 421-438.
80. Wu, P., et al., *Nanoparticle-based drug delivery systems targeting tumor microenvironment for cancer immunotherapy resistance: current advances and applications.* Pharmaceutics, 2022. **14**(10): p. 1990.
81. Mo, C.-K., et al., *Tumour evolution and microenvironment interactions in 2D and 3D space.* Nature, 2024. **634**(8036): p. 1178-1186.
82. Bonnet, D. and J.E. Dick, *Human acute myeloid leukemia is organized as a hierarchy that originates from a primitive hematopoietic cell.* Nature medicine, 1997. **3**(7): p. 730-737.
83. Batlle, E. and H. Clevers, *Cancer stem cells revisited.* Nature medicine, 2017. **23**(10): p. 1124-1134.
84. Hermann, P.C., et al., *Distinct populations of cancer stem cells determine tumor growth and metastatic activity in human pancreatic cancer.* Cell stem cell, 2007. **1**(3): p. 313-323.
85. Bao, S., et al., *Glioma stem cells promote radioresistance by preferential activation of the DNA damage response.* nature, 2006. **444**(7120): p. 756-760.
86. Xiao, Q., et al., *Cancer-associated fibroblasts in pancreatic cancer are reprogrammed by tumor-induced alterations in genomic DNA methylation.* Cancer research, 2016. **76**(18): p. 5395-5404.
87. Zeisberg, E.M., et al., *Discovery of endothelial to mesenchymal transition as a source for carcinoma-associated fibroblasts.* Cancer research, 2007. **67**(21): p. 10123-10128.
88. Öhlund, D., et al., *Distinct populations of inflammatory fibroblasts and myofibroblasts in pancreatic cancer.* Journal of Experimental Medicine, 2017. **214**(3): p. 579-596.
89. Kröger, C., et al., *Acquisition of a hybrid E/M state is essential for tumorigenicity of basal breast cancer cells.* Proceedings of the National Academy of Sciences, 2019. **116**(15): p. 7353-7362.
90. Vora, H.H., et al., *Cytokeratin and vimentin expression in breast cancer.* The International journal of biological markers, 2009. **24**(1): p. 38-46.
91. Fullár, A., et al., *Remodeling of extracellular matrix by normal and tumor-associated fibroblasts promotes cervical cancer progression.* BMC cancer, 2015. **15**(1): p. 256.
92. Stylianopoulos, T., L.L. Munn, and R.K. Jain, *Reengineering the physical microenvironment of tumors to improve drug delivery and efficacy: from mathematical modeling to bench to bedside.* Trends in cancer, 2018. **4**(4): p. 292-319.
93. Chang, C.H., et al., *Metabolic Competition in the Tumor Microenvironment Is a Driver of Cancer Progression.* Cell, 2015. **162**(6): p. 1229-41.
94. Nicolas-Boluda, A., et al., *Tumor stiffening reversion through collagen crosslinking inhibition improves T cell migration and anti-PD-1 treatment.* Elife, 2021. **10**: p. e58688.
95. Carmeliet, P. and R.K. Jain, *Angiogenesis in cancer and other diseases.* nature, 2000. **407**(6801): p. 249-257.

96. Baker, S.J., et al., *Suppression of human colorectal carcinoma cell growth by wild-type p53.* Science, 1990. **249**(4971): p. 912-915.
97. Paijens, S.T., et al., *Tumor-infiltrating lymphocytes in the immunotherapy era.* Cellular & molecular immunology, 2021. **18**(4): p. 842-859.
98. Kao, K.C., et al., *Metabolic communication in the tumour-immune microenvironment.* Nat Cell Biol, 2022. **24**(11): p. 1574-1583.
99. Vander Heiden, M.G., L.C. Cantley, and C.B. Thompson, *Understanding the Warburg effect: the metabolic requirements of cell proliferation.* Science, 2009. **324**(5930): p. 1029-33.
100. Pandkar, M.R., S.G. Dhamdhere, and S. Shukla, *Oxygen gradient and tumor heterogeneity: The chronicle of a toxic relationship.* Biochimica et Biophysica Acta (BBA)-Reviews on Cancer, 2021. **1876**(1): p. 188553.
101. Scharping, N.E., et al., *Mitochondrial stress induced by continuous stimulation under hypoxia rapidly drives T cell exhaustion.* Nat Immunol, 2021. **22**(2): p. 205-215.
102. Gropper, Y., et al., *Culturing CTLs under Hypoxic Conditions Enhances Their Cytolysis and Improves Their Anti-tumor Function.* Cell Rep, 2017. **20**(11): p. 2547-2555.
103. Doedens, A.L., et al., *Hypoxia-inducible factors enhance the effector responses of CD8(+) T cells to persistent antigen.* Nat Immunol, 2013. **14**(11): p. 1173-82.
104. Tanimoto, K., et al., *Mechanism of regulation of the hypoxia-inducible factor-1α by the von Hippel-Lindau tumor suppressor protein.* The EMBO journal, 2000.
105. Pagé, E.L., et al., *Hypoxia-inducible factor-1α stabilization in nonhypoxic conditions: role of oxidation and intracellular ascorbate depletion.* Molecular biology of the cell, 2008. **19**(1): p. 86-94.
106. Jiang, B.-H., et al., *Dimerization, DNA binding, and transactivation properties of hypoxia-inducible factor 1.* Journal of Biological Chemistry, 1996. **271**(30): p. 17771-17778.
107. Ma, S., et al., *Hypoxia induces HIF1alpha-dependent epigenetic vulnerability in triple negative breast cancer to confer immune effector dysfunction and resistance to anti-PD-1 immunotherapy.* Nat Commun, 2022. **13**(1): p. 4118.
108. Nakayama, K., *cAMP-response element-binding protein (CREB) and NF-κB transcription factors are activated during prolonged hypoxia and cooperatively regulate the induction of matrix metalloproteinase MMP1.* Journal of Biological Chemistry, 2013. **288**(31): p. 22584-22595.
109. Guo, Y., et al., *Metabolic reprogramming of terminally exhausted CD8(+) T cells by IL-10 enhances anti-tumor immunity.* Nat Immunol, 2021. **22**(6): p. 746-756.
110. Balasubramanian, B., W.K. Pogozelski, and T.D. Tullius, *DNA strand breaking by the hydroxyl radical is governed by the accessible surface areas of the hydrogen atoms of the DNA backbone.* Proceedings of the National Academy of Sciences, 1998. **95**(17): p. 9738-9743.
111. Zorov, D.B., M. Juhaszova, and S.J. Sollott, *Mitochondrial reactive oxygen species (ROS) and ROS-induced ROS release.* Physiological reviews, 2014. **94**(3): p. 909-950.
112. Imlay, J.A., S.M. Chin, and S. Linn, *Toxic DNA damage by hydrogen peroxide through the Fenton reaction in vivo and in vitro.* Science, 1988. **240**(4852): p. 640-642.
113. Ke, F.F., et al., *Embryogenesis and adult life in the absence of intrinsic apoptosis effectors BAX, BAK, and BOK.* Cell, 2018. **173**(5): p. 1217-1230. e17.
114. Yang, E., et al., *Bad, a heterodimeric partner for Bcl-XL and Bcl-2, displaces Bax and promotes cell death.* Cell, 1995. **80**(2): p. 285-291.
115. Zou, H., et al., *An APAF-1· cytochrome c multimeric complex is a functional apoptosome that activates procaspase-9.* Journal of Biological Chemistry, 1999. **274**(17): p. 11549-11556.
116. Enari, M., et al., *A caspase-activated DNase that degrades DNA during apoptosis, and its inhibitor ICAD.* Nature, 1998. **391**(6662): p. 43-50.
117. Walczak, H., et al., *TRAIL-R2: a novel apoptosis-mediating receptor for TRAIL.* The EMBO journal, 1997.
118. Shibutani, S., M. Takeshita, and A.P. Grollman, *Insertion of specific bases during DNA synthesis past the oxidation-damaged base 8-oxodG.* Nature, 1991. **349**(6308): p. 431-434.

119. Xia, C., et al., *Reactive oxygen species regulate angiogenesis and tumor growth through vascular endothelial growth factor.* Cancer research, 2007. **67**(22): p. 10823-10830.
120. Dong, S., et al., *ROS/PI3K/Akt and Wnt/β-catenin signalings activate HIF-1α-induced metabolic reprogramming to impart 5-fluorouracil resistance in colorectal cancer.* Journal of Experimental & Clinical Cancer Research, 2022. **41**(1): p. 15.
121. Chen, Z.J., L. Parent, and T. Maniatis, *Site-specific phosphorylation of IκBα by a novel ubiquitination-dependent protein kinase activity.* Cell, 1996. **84**(6): p. 853-862.
122. Matthews, J.R., et al., *Inhibition of NF-κB DNA binding by nitric oxide.* Nucleic acids research, 1996. **24**(12): p. 2236-2242.
123. McCord, J.M. and I. Fridovich, *Superoxide dismutase: an enzymic function for erythrocuprein (hemocuprein).* Journal of Biological chemistry, 1969. **244**(22): p. 6049-6055.
124. Li, Y., et al., *Dilated cardiomyopathy and neonatal lethality in mutant mice lacking manganese superoxide dismutase.* Nature genetics, 1995. **11**(4): p. 376-381.
125. Suh, Y.-A., et al., *Cell transformation by the superoxide-generating oxidase Mox1.* Nature, 1999. **401**(6748): p. 79-82.
126. Mills, G.C., *Hemoglobin catabolism: I. Glutathione peroxidase, an erythrocyte enzyme which protects hemoglobin from oxidative breakdown.* Journal of Biological Chemistry, 1957. **229**(1): p. 189-197.
127. Worthington, D.J. and M.A. Rosemeyer, *Glutathione reductase from human erythrocytes: catalytic properties and aggregation.* European Journal of Biochemistry, 1976. **67**(1): p. 231-238.
128. Chae, H.Z., S.J. Chung, and S.G. Rhee, *Thioredoxin-dependent peroxide reductase from yeast.* Journal of Biological Chemistry, 1994. **269**(44): p. 27670-27678.
129. Kobayashi, A., et al., *Oxidative stress sensor Keap1 functions as an adaptor for Cul3-based E3 ligase to regulate proteasomal degradation of Nrf2.* Molecular and cellular biology, 2004. **24**(16): p. 7130-7139.
130. Tong, K.I., et al., *Two-site substrate recognition model for the Keap1-Nrf2 system: a hinge and latch mechanism.* 2006.
131. Wittenberg, J.B., *Myoglobin-facilitated oxygen diffusion: role of myoglobin in oxygen entry into muscle.* Physiological Reviews, 1970. **50**(4): p. 559-636.
132. Hardison, R.C., *A brief history of hemoglobins: plant, animal, protist, and bacteria.* Proceedings of the National Academy of Sciences, 1996. **93**(12): p. 5675-5679.
133. Kendrew, J.C., et al., *A three-dimensional model of the myoglobin molecule obtained by x-ray analysis.* Nature, 1958. **181**(4610): p. 662-666.
134. Patel, M.P., et al., *Development and validation of an oxygen dissociation assay, a screening platform for discovering, and characterizing hemoglobin–oxygen affinity modifiers.* Drug design, development and therapy, 2018: p. 1599-1607.
135. Sanyal, R. and A. Bhagi-Damodaran, *An enzymatic method for precise oxygen affinity measurements over nanomolar-to-millimolar concentration regime.* JBIC Journal of Biological Inorganic Chemistry, 2020. **25**: p. 181-186.
136. Muthukrishnan, S. and M. Puri, *Harnessing the evolutionary information on oxygen binding proteins through Support Vector Machines based modules.* BMC Research Notes, 2018. **11**(1): p. 1-8.
137. Waxman, L., *The structure of annelid and mollusc hemoglobins.* Journal of Biological Chemistry, 1975. **250**(10): p. 3790-3795.
138. Volbeda, A. and W.G. Hol, *Crystal structure of hexameric haemocyanin from Panulirus interruptus refined at 3.2 Å resolution.* Journal of molecular biology, 1989. **209**(2): p. 249-279.
139. Perutz, M.F., et al., *Structure of hæmoglobin: a three-dimensional Fourier synthesis at 5.5-Å. resolution, obtained by X-ray analysis.* Nature, 1960. **185**(4711): p. 416-422.

140. Bohr, C., K. Hasselbalch, and A. Krogh, *Ueber einen in biologischer Beziehung wichtigen Einfluss, den die Kohlensäurespannung des Blutes auf dessen Sauerstoffbindung übt 1.* Skandinavisches Archiv Für Physiologie, 1904. **16**(2): p. 402-412.
141. Tyuma, I., *The Bohr effect and the Haldane effect in human hemoglobin.* The Japanese journal of physiology, 1984. **34**(2): p. 205-216.
142. Huxley, H., *The double array of filaments in cross-striated muscle.* The Journal of Cell Biology, 1957. **3**(5): p. 631-648.
143. Hanson, J. and H.E. Huxley, *Structural basis of the cross-striations in muscle.* Nature, 1953. **172**(4377): p. 530-532.
144. Oda, T., et al., *The nature of the globular-to fibrous-actin transition.* Nature, 2009. **457**(7228): p. 441-445.
145. Springer, B.A., et al., *Mechanisms of ligand recognition in myoglobin.* Chemical Reviews, 1994. **94**(3): p. 699-714.
146. Wittenberg, J.B. and B.A. Wittenberg, *Myoglobin function reassessed.* Journal of experimental biology, 2003. **206**(12): p. 2011-2020.
147. Brownlie, R.J. and R. Zamoyska, *T cell receptor signalling networks: branched, diversified and bounded.* Nature Reviews Immunology, 2013. **13**(4): p. 257-269.
148. Sprent, J. and D.F. Tough, *Lymphocyte life-span and memory.* Science, 1994. **265**(5177): p. 1395-1400.
149. Ackerman, A.L., et al., *Early phagosomes in dendritic cells form a cellular compartment sufficient for cross presentation of exogenous antigens.* Proceedings of the National Academy of Sciences, 2003. **100**(22): p. 12889-12894.
150. Collins, E.J., et al., *The three-dimensional structure of a class I major histocompatibility complex molecule missing the alpha 3 domain of the heavy chain.* Proceedings of the National Academy of Sciences, 1995. **92**(4): p. 1218-1221.
151. Rock, K.L., et al., *Inhibitors of the proteasome block the degradation of most cell proteins and the generation of peptides presented on MHC class I molecules.* Cell, 1994. **78**(5): p. 761-771.
152. Lauvau, G., et al., *Human transporters associated with antigen processing (TAPs) select epitope precursor peptides for processing in the endoplasmic reticulum and presentation to T cells.* The Journal of experimental medicine, 1999. **190**(9): p. 1227-1240.
153. Lotteau, V., et al., *Intracellular transport of class II MHC molecules directed by invariant chain.* nature, 1990. **348**(6302): p. 600-605.
154. Romagnoli, P. and R.N. Germain, *The CLIP region of invariant chain plays a critical role in regulating major histocompatibility complex class II folding, transport, and peptide occupancy.* The Journal of experimental medicine, 1994. **180**(3): p. 1107-1113.
155. Van Seventer, G.A., et al., *The LFA-1 ligand ICAM-1 provides an important costimulatory signal for T cell receptor-mediated activation of resting T cells.* The Journal of Immunology, 1990. **144**(12): p. 4579-4586.
156. Dransfield, I., et al., *Divalent cation regulation of the function of the leukocyte integrin LFA-1.* The Journal of cell biology, 1992. **116**(1): p. 219-226.
157. Bird, J.J., et al., *Helper T cell differentiation is controlled by the cell cycle.* Immunity, 1998. **9**(2): p. 229-237.
158. van Stipdonk, M.J., E.E. Lemmens, and S.P. Schoenberger, *Naive CTLs require a single brief period of antigenic stimulation for clonal expansion and differentiation.* Nature immunology, 2001. **2**(5): p. 423-429.
159. Harding, F.A., et al., *CD28-mediated signalling co-stimulates murine T cells and prevents induction of anergy in T-cell clones.* Nature, 1992. **356**(6370): p. 607-609.
160. Oppmann, B., et al., *Novel p19 protein engages IL-12p40 to form a cytokine, IL-23, with biological activities similar as well as distinct from IL-12.* Immunity, 2000. **13**(5): p. 715-725.
161. Bettelli, E., et al., *Reciprocal developmental pathways for the generation of pathogenic effector TH17 and regulatory T cells.* Nature, 2006. **441**(7090): p. 235-238.

162. Hu-Li, J., et al., *B cell stimulatory factor 1 (interleukin 4) is a potent costimulant for normal resting T lymphocytes.* The Journal of experimental medicine, 1987. **165**(1): p. 157-172.
163. Valenzuela, J., C. Schmidt, and M. Mescher, *The roles of IL-12 in providing a third signal for clonal expansion of naive CD8 T cells.* The Journal of Immunology, 2002. **169**(12): p. 6842-6849.
164. DeSilva, D.R., K. Urdahl, and M. Jenkins, *Clonal anergy is induced in vitro by T cell receptor occupancy in the absence of proliferation.* The Journal of Immunology, 1991. **147**(10): p. 3261-3267.
165. Kuhns, M.S., et al., *Evidence for a functional sidedness to the αβTCR.* Proceedings of the National Academy of Sciences, 2010. **107**(11): p. 5094-5099.
166. de la Hera, A., et al., *Structure of the T cell antigen receptor (TCR): two CD3 epsilon subunits in a functional TCR/CD3 complex.* The Journal of experimental medicine, 1991. **173**(1): p. 7-17.
167. Alarcon, B., et al., *The CD3-gamma and CD3-delta subunits of the T cell antigen receptor can be expressed within distinct functional TCR/CD3 complexes.* The EMBO Journal, 1991. **10**(4): p. 903-912.
168. Irving, B.A. and A. Weiss, *The cytoplasmic domain of the T cell receptor ζ chain is sufficient to couple to receptor-associated signal transduction pathways.* Cell, 1991. **64**(5): p. 891-901.
169. Veillette, A., et al., *The CD4 and CD8 T cell surface antigens are associated with the internal membrane tyrosine-protein kinase p56lck.* Cell, 1988. **55**(2): p. 301-308.
170. Glaichenhaus, N., et al., *Requirement for association of p56lck with CD4 in antigen-specific signal transduction in T cells.* Cell, 1991. **64**(3): p. 511-520.
171. Chan, A.C., et al., *ZAP-70: a 70 kd protein-tyrosine kinase that associates with the TCR ζ chain.* Cell, 1992. **71**(4): p. 649-662.
172. Zhang, W., et al., *LAT: the ZAP-70 tyrosine kinase substrate that links T cell receptor to cellular activation.* Cell, 1998. **92**(1): p. 83-92.
173. Pages, F., et al., *Binding of phosphatidyl-inositol-3-OH kinase to CD28 is required for T-cell signalling.* Nature, 1994. **369**(6478): p. 327-329.
174. Yang, H.W., et al., *Cooperative activation of PI3K by Ras and Rho family small GTPases.* Molecular cell, 2012. **47**(2): p. 281-290.
175. Harriague, J. and G. Bismuth, *Imaging antigen-induced PI3K activation in T cells.* Nature immunology, 2002. **3**(11): p. 1090-1096.
176. Leonard, W.J., et al., *Interleukin 2 receptor gene expression in normal human T lymphocytes.* Proceedings of the National Academy of Sciences, 1985. **82**(18): p. 6281-6285.
177. Johnston, J.A., et al., *Tyrosine phosphorylation and activation of STAT5, STAT3, and Janus kinases by interleukins 2 and 15.* Proceedings of the National Academy of Sciences, 1995. **92**(19): p. 8705-8709.
178. Smith, K.A., *Interleukin-2: inception, impact, and implications.* Science, 1988. **240**(4856): p. 1169-1176.
179. Braiman, A., et al., *Recruitment and activation of PLCγ1 in T cells: a new insight into old domains.* The EMBO journal, 2006. **25**(4): p. 774-784.
180. Gallagher, M.P., et al., *Hierarchy of signaling thresholds downstream of the T cell receptor and the Tec kinase ITK.* Proceedings of the National Academy of Sciences, 2021. **118**(35): p. e2025825118.
181. Rhee, S.G., et al., *Studies of inositol phospholipid-specific phospholipase C.* Science, 1989. **244**(4904): p. 546-550.
182. Liou, J., et al., *STIM is a Ca2+ sensor essential for Ca2+-store-depletion-triggered Ca2+ influx.* Current biology, 2005. **15**(13): p. 1235-1241.
183. Clipstone, N.A. and G.R. Crabtree, *Identification of calcineurin as a key signalling enzyme in T-lymphocyte activation.* Nature, 1992. **357**(6380): p. 695-697.
184. Robinson, M.J. and M.H. Cobb, *Mitogen-activated protein kinase pathways.* Current opinion in cell biology, 1997. **9**(2): p. 180-186.

185. Roy, F., et al., *KSR is a scaffold required for activation of the ERK/MAPK module.* Genes & development, 2002. **16**(4): p. 427-438.
186. Cavigelli, M., et al., *Induction of c-fos expression through JNK-mediated TCF/Elk-1 phosphorylation.* The EMBO journal, 1995. **14**(23): p. 5957-5964.
187. Baier-Bitterlich, G., et al., *Protein kinase C-ϑ isoenzyme selective stimulation of the transcription factor complex AP-1 in T lymphocytes.* Molecular and cellular biology, 1996. **16**(4): p. 1842-1850.
188. Sun, L., et al., *The TRAF6 ubiquitin ligase and TAK1 kinase mediate IKK activation by BCL10 and MALT1 in T lymphocytes.* Molecular cell, 2004. **14**(3): p. 289-301.
189. Wegener, E., et al., *Essential role for IκB kinase β in remodeling Carma1-Bcl10-Malt1 complexes upon T cell activation.* Molecular cell, 2006. **23**(1): p. 13-23.
190. Levina, A., et al., *Activation of the essential kinase PDK1 by phosphoinositide-driven trans-autophosphorylation.* Nature communications, 2022. **13**(1): p. 1874.
191. Datta, S.R., et al., *Akt phosphorylation of BAD couples survival signals to the cell-intrinsic death machinery.* Cell, 1997. **91**(2): p. 231-241.
192. Inoki, K., et al., *TSC2 is phosphorylated and inhibited by Akt and suppresses mTOR signalling.* Nature cell biology, 2002. **4**(9): p. 648-657.
193. Houtman, J.C., et al., *Early phosphorylation kinetics of proteins involved in proximal TCR-mediated signaling pathways.* The Journal of Immunology, 2005. **175**(4): p. 2449-2458.
194. Ménasché, G., et al., *RIAM links the ADAP/SKAP-55 signaling module to Rap1, facilitating T-cell-receptor-mediated integrin activation.* Molecular and cellular biology, 2007. **27**(11): p. 4070-4081.
195. Katagiri, K., et al., *Rap1 functions as a key regulator of T-cell and antigen-presenting cell interactions and modulates T-cell responses.* Molecular and cellular biology, 2002. **22**(4): p. 1001-1015.
196. Han, J., et al., *Role of substrates and products of PI 3-kinase in regulating activation of Rac-related guanosine triphosphatases by Vav.* Science, 1998. **279**(5350): p. 558-560.
197. Reynolds, L.F., et al., *Vav1 transduces T cell receptor signals to the activation of phospholipase C-γ1 via phosphoinositide 3-kinase-dependent and-independent pathways.* The Journal of experimental medicine, 2002. **195**(9): p. 1103-1114.
198. Zeng, R., et al., *SLP-76 coordinates Nck-dependent Wiskott-Aldrich syndrome protein recruitment with Vav-1/Cdc42-dependent Wiskott-Aldrich syndrome protein activation at the T cell-APC contact site.* The Journal of Immunology, 2003. **171**(3): p. 1360-1368.
199. Zhu, J., H. Yamane, and W.E. Paul, *Differentiation of effector CD4 T cell populations.* Annual review of immunology, 2010. **28**(1): p. 445-489.
200. Miller, J.F., *Immunological function of the thymus.* The Lancet, 1961. **278**(7205): p. 748-749.
201. Cantor, H. and E.A. Boyse, *Functional subclasses of T-lymphocytes bearing different Ly antigens. I. The generation of functionally distinct T-cell subclasses is a differentiative process independent of antigen.* The Journal of experimental medicine, 1975. **141**(6): p. 1376-1389.
202. Mosmann, T.R., et al., *Two types of murine helper T cell clone. I. Definition according to profiles of lymphokine activities and secreted proteins.* Journal of Immunology (Baltimore, MD.: 1950), 1986. **136**(7): p. 2348-2357.
203. Szabo, S.J., et al., *A novel transcription factor, T-bet, directs Th1 lineage commitment.* Cell, 2000. **100**(6): p. 655-669.
204. Hsu, H., J. Xiong, and D.V. Goeddel, *The TNF receptor 1-associated protein TRADD signals cell death and NF-κB activation.* Cell, 1995. **81**(4): p. 495-504.
205. Boehm, U., et al., *Cellular responses to interferon-γ.* Annual review of immunology, 1997. **15**(1): p. 749-795.
206. Cooper, A.M., et al., *Disseminated tuberculosis in interferon gamma gene-disrupted mice.* The Journal of experimental medicine, 1993. **178**(6): p. 2243-2247.

207. Kotenko, S.V., et al., *Interaction between the components of the interferon γ receptor complex.* Journal of Biological Chemistry, 1995. **270**(36): p. 20915-20921.
208. Borrow, P., et al., *CD40L-deficient mice show deficits in antiviral immunity and have an impaired memory CD8+ CTL response.* The Journal of experimental medicine, 1996. **183**(5): p. 2129-2142.
209. Milburn, M.V., et al., *A novel dimer configuration revealed by the crystal structure at 2.4 Å resolution of human interleukin-5.* Nature, 1993. **363**(6425): p. 172-176.
210. Wills-Karp, M., et al., *Interleukin-13: central mediator of allergic asthma.* Science, 1998. **282**(5397): p. 2258-2261.
211. Kuperman, D.A., et al., *Direct effects of interleukin-13 on epithelial cells cause airway hyperreactivity and mucus overproduction in asthma.* Nature medicine, 2002. **8**(8): p. 885-889.
212. Yamaguchi, Y., et al., *Purified interleukin 5 supports the terminal differentiation and proliferation of murine eosinophilic precursors.* The Journal of experimental medicine, 1988. **167**(1): p. 43-56.
213. Takaki, S., et al., *Molecular cloning and expression of the murine interleukin-5 receptor.* The EMBO journal, 1990. **9**(13): p. 4367-4374.
214. Langrish, C.L., et al., *IL-23 drives a pathogenic T cell population that induces autoimmune inflammation.* The Journal of experimental medicine, 2005. **201**(2): p. 233-240.
215. Veldhoen, M., et al., *TGFβ in the context of an inflammatory cytokine milieu supports de novo differentiation of IL-17-producing T cells.* Immunity, 2006. **24**(2): p. 179-189.
216. Ivanov, I.I., et al., *The orphan nuclear receptor RORγt directs the differentiation program of proinflammatory IL-17+ T helper cells.* Cell, 2006. **126**(6): p. 1121-1133.
217. Durant, L., et al., *Diverse targets of the transcription factor STAT3 contribute to T cell pathogenicity and homeostasis.* Immunity, 2010. **32**(5): p. 605-615.
218. Fossiez, F., et al., *T cell interleukin-17 induces stromal cells to produce proinflammatory and hematopoietic cytokines.* The Journal of experimental medicine, 1996. **183**(6): p. 2593-2603.
219. Liu, R., et al., *IL-17 promotes neutrophil-mediated immunity by activating microvascular pericytes and not endothelium.* The Journal of Immunology, 2016. **197**(6): p. 2400-2408.
220. Wolk, K., et al., *IL-22 increases the innate immunity of tissues.* Immunity, 2004. **21**(2): p. 241-254.
221. Nagata, S., et al., *Molecular cloning and expression of cDNA for human granulocyte colony-stimulating factor.* Nature, 1986. **319**(6052): p. 415-418.
222. Taub, D.D., et al., *T lymphocyte recruitment by interleukin-8 (IL-8). IL-8-induced degranulation of neutrophils releases potent chemoattractants for human T lymphocytes both in vitro and in vivo.* The Journal of clinical investigation, 1996. **97**(8): p. 1931-1941.
223. Nurieva, R.I., et al., *Bcl6 mediates the development of T follicular helper cells.* Science, 2009. **325**(5943): p. 1001-1005.
224. Eto, D., et al., *IL-21 and IL-6 are critical for different aspects of B cell immunity and redundantly induce optimal follicular helper CD4 T cell (Tfh) differentiation.* PloS one, 2011. **6**(3): p. e17739.
225. Choi, Y.S., et al., *Cutting edge: STAT1 is required for IL-6–mediated Bcl6 induction for early follicular helper cell differentiation.* The Journal of Immunology, 2013. **190**(7): p. 3049-3053.
226. Ozaki, K., et al., *A critical role for IL-21 in regulating immunoglobulin production.* Science, 2002. **298**(5598): p. 1630-1634.
227. Fontenot, J.D., M.A. Gavin, and A.Y. Rudensky, *Foxp3 programs the development and function of CD4+ CD25+ regulatory T cells.* Nature immunology, 2003. **4**(4): p. 330-336.
228. Hori, S., T. Nomura, and S. Sakaguchi, *Control of regulatory T cell development by the transcription factor Foxp3.* Science, 2003. **299**(5609): p. 1057-1061.
229. Asseman, C., et al., *An essential role for interleukin 10 in the function of regulatory T cells that inhibit intestinal inflammation.* The Journal of experimental medicine, 1999. **190**(7): p. 995-1004.

230. Fiorentino, D.F., et al., *IL-10 inhibits cytokine production by activated macrophages.* The Journal of immunology, 1991. **147**(11): p. 3815-3822.
231. de Waal Malefyt, R., et al., *Interleukin 10 (IL-10) and viral IL-10 strongly reduce antigen-specific human T cell proliferation by diminishing the antigen-presenting capacity of monocytes via downregulation of class II major histocompatibility complex expression.* The Journal of experimental medicine, 1991. **174**(4): p. 915-924.
232. Tivol, E.A., et al., *Loss of CTLA-4 leads to massive lymphoproliferation and fatal multiorgan tissue destruction, revealing a critical negative regulatory role of CTLA-4.* Immunity, 1995. **3**(5): p. 541-547.
233. Waterhouse, P., et al., *Lymphoproliferative disorders with early lethality in mice deficient in Ctla-4.* Science, 1995. **270**(5238): p. 985-988.
234. Sakaguchi, S., et al., *Immunologic self-tolerance maintained by activated T cells expressing IL-2 receptor alpha-chains (CD25). Breakdown of a single mechanism of self-tolerance causes various autoimmune diseases.* Journal of immunology (Baltimore, Md.: 1950), 1995. **155**(3): p. 1151-1164.
235. Curtsinger, J.M., et al., *Inflammatory cytokines provide a third signal for activation of naive CD4+ and CD8+ T cells.* The Journal of Immunology, 1999. **162**(6): p. 3256-3262.
236. Freeman, G.J., et al., *Engagement of the PD-1 immunoinhibitory receptor by a novel B7 family member leads to negative regulation of lymphocyte activation.* The Journal of experimental medicine, 2000. **192**(7): p. 1027-1034.
237. Chemnitz, J.M., et al., *SHP-1 and SHP-2 associate with immunoreceptor tyrosine-based switch motif of programmed death 1 upon primary human T cell stimulation, but only receptor ligation prevents T cell activation.* The Journal of Immunology, 2004. **173**(2): p. 945-954.
238. Barber, D.L., et al., *Restoring function in exhausted CD8 T cells during chronic viral infection.* Nature, 2006. **439**(7077): p. 682-687.
239. Zhu, C., et al., *The Tim-3 ligand galectin-9 negatively regulates T helper type 1 immunity.* Nature immunology, 2005. **6**(12): p. 1245-1252.
240. Huang, Y.-H., et al., *CEACAM1 regulates TIM-3-mediated tolerance and exhaustion.* Nature, 2015. **517**(7534): p. 386-390.
241. Ito, M., et al., *Killer cell lectin-like receptor G1 binds three members of the classical cadherin family to inhibit NK cell cytotoxicity.* The Journal of experimental medicine, 2006. **203**(2): p. 289-295.
242. Schluns, K.S., et al., *Interleukin-7 mediates the homeostasis of naive and memory CD8 T cells in vivo.* Nature immunology, 2000. **1**(5): p. 426-432.
243. Sallusto, F., et al., *Two subsets of memory T lymphocytes with distinct homing potentials and effector functions.* Nature, 1999. **401**(6754): p. 708-712.
244. Kumar, B.V., et al., *Human tissue-resident memory T cells are defined by core transcriptional and functional signatures in lymphoid and mucosal sites.* Cell reports, 2017. **20**(12): p. 2921-2934.
245. Baaten, B.J., et al., *CD44 regulates survival and memory development in Th1 cells.* Immunity, 2010. **32**(1): p. 104-115.
246. Gerberick, G.F., et al., *Selective modulation of T cell memory markers CD62L and CD44 on murine draining lymph node cells following allergen and irritant treatment.* Toxicology and applied pharmacology, 1997. **146**(1): p. 1-10.
247. Banerjee, A., et al., *Cutting edge: The transcription factor eomesodermin enables CD8+ T cells to compete for the memory cell niche.* The Journal of Immunology, 2010. **185**(9): p. 4988-4992.
248. Scott, A.C., et al., *TOX is a critical regulator of tumour-specific T cell differentiation.* Nature, 2019. **571**(7764): p. 270-274.
249. Alfei, F., et al., *TOX reinforces the phenotype and longevity of exhausted T cells in chronic viral infection.* Nature, 2019. **571**(7764): p. 265-269.

250. Khan, O., et al., *TOX transcriptionally and epigenetically programs CD8+ T cell exhaustion.* Nature, 2019. **571**(7764): p. 211-218.
251. Jeannet, G., et al., *Essential role of the Wnt pathway effector Tcf-1 for the establishment of functional CD8 T cell memory.* Proceedings of the National Academy of Sciences, 2010. **107**(21): p. 9777-9782.
252. Xu, B., et al., *Crystal structure of a γδ T-cell receptor specific for the human MHC class I homolog MICA.* Proceedings of the National Academy of Sciences, 2011. **108**(6): p. 2414-2419.
253. Adams, E.J., Y.-H. Chien, and K.C. Garcia, *Structure of a γδ T cell receptor in complex with the nonclassical MHC T22.* Science, 2005. **308**(5719): p. 227-231.
254. You, H., et al., *γδ T-cell autoresponses to ectopic membrane proteins: a new type of pattern recognition.* Cellular & Molecular Immunology, 2025. **22**(4): p. 356-370.
255. Mallevaey, T., et al., *A molecular basis for NKT cell recognition of CD1d-self-antigen.* Immunity, 2011. **34**(3): p. 315-326.
256. Coquet, J.M., et al., *Diverse cytokine production by NKT cell subsets and identification of an IL-17–producing CD4− NK1. 1− NKT cell population.* Proceedings of the National Academy of Sciences, 2008. **105**(32): p. 11287-11292.
257. Waldman, A.D., J.M. Fritz, and M.J. Lenardo, *A guide to cancer immunotherapy: from T cell basic science to clinical practice.* Nature Reviews Immunology, 2020. **20**(11): p. 651-668.
258. Lowin, B., et al., *Cytolytic T-cell cytotoxicity is mediated through perforin and Fas lytic pathways.* Nature, 1994. **370**(6491): p. 650-652.
259. Zimmerer, J.M., et al., *Cytotoxic effector function of CD4-independent, CD8+ T cells is mediated by TNF-α/TNFR.* Transplantation, 2012. **94**(11): p. 1103-1110.
260. Peters, P.J., et al., *Cytotoxic T lymphocyte granules are secretory lysosomes, containing both perforin and granzymes.* The Journal of experimental medicine, 1991. **173**(5): p. 1099-1109.
261. Dotiwala, F., et al., *Killer lymphocytes use granulysin, perforin and granzymes to kill intracellular parasites.* Nature medicine, 2016. **22**(2): p. 210-216.
262. Grujic, M., et al., *Serglycin-deficient cytotoxic T lymphocytes display defective secretory granule maturation and granzyme B storage.* Journal of Biological Chemistry, 2005. **280**(39): p. 33411-33418.
263. Alimonti, J.B., et al., *Granzyme B induces BID-mediated cytochrome c release and mitochondrial permeability transition.* Journal of Biological Chemistry, 2001. **276**(10): p. 6974-6982.
264. Stinchcombe, J.C., et al., *Centrosome polarization delivers secretory granules to the immunological synapse.* Nature, 2006. **443**(7110): p. 462-465.
265. Tartaglia, L.A., et al., *The two different receptors for tumor necrosis factor mediate distinct cellular responses.* Proceedings of the National Academy of Sciences, 1991. **88**(20): p. 9292-9296.
266. Geltink, R.I.K., R.L. Kyle, and E.L. Pearce, *Unraveling the Complex Interplay Between T Cell Metabolism and Function.* Annu Rev Immunol, 2018. **36**: p. 461-488.
267. Chang, C.H., et al., *Posttranscriptional control of T cell effector function by aerobic glycolysis.* Cell, 2013. **153**(6): p. 1239-51.
268. Buck, M.D., et al., *Mitochondrial Dynamics Controls T Cell Fate through Metabolic Programming.* Cell, 2016. **166**(1): p. 63-76.
269. Bengsch, B., et al., *Bioenergetic Insufficiencies Due to Metabolic Alterations Regulated by the Inhibitory Receptor PD-1 Are an Early Driver of CD8(+) T Cell Exhaustion.* Immunity, 2016. **45**(2): p. 358-73.
270. Mak, T.W., et al., *Glutathione Primes T Cell Metabolism for Inflammation.* Immunity, 2017. **46**(4): p. 675-689.
271. Lang, P.A., et al., *Reactive oxygen species delay control of lymphocytic choriomeningitis virus.* Cell Death Differ, 2013.

272. Yu, Y.R., et al., *Disturbed mitochondrial dynamics in CD8(+) TILs reinforce T cell exhaustion.* Nat Immunol, 2020. **21**(12): p. 1540-1551.
273. Vardhana, S.A., et al., *Impaired mitochondrial oxidative phosphorylation limits the self-renewal of T cells exposed to persistent antigen.* Nat Immunol, 2020. **21**(9): p. 1022-1033.
274. Delaney, G., et al., *The role of radiotherapy in cancer treatment: estimating optimal utilization from a review of evidence-based clinical guidelines.* Cancer: Interdisciplinary International Journal of the American Cancer Society, 2005. **104**(6): p. 1129-1137.
275. Mackall, C.L., et al., *Lymphocyte depletion during treatment with intensive chemotherapy for cancer.* 1994.
276. Nanayakkara, A.K., et al., *Targeted inhibitors of P-glycoprotein increase chemotherapeutic-induced mortality of multidrug resistant tumor cells.* Scientific reports, 2018. **8**(1): p. 967.
277. Lopez, J.A., et al., *Perforin forms transient pores on the target cell plasma membrane to facilitate rapid access of granzymes during killer cell attack.* Blood, The Journal of the American Society of Hematology, 2013. **121**(14): p. 2659-2668.
278. Klinger, M., et al., *Immunopharmacologic response of patients with B-lineage acute lymphoblastic leukemia to continuous infusion of T cell–engaging CD19/CD3-bispecific BiTE antibody blinatumomab.* Blood, The Journal of the American Society of Hematology, 2012. **119**(26): p. 6226-6233.
279. Grillo-Lopez, A., et al., *Rituximab the first monoclonal antibody approved for the treatment of lymphoma.* Current pharmaceutical biotechnology, 2000. **1**(1): p. 1-9.
280. Hamann, P.R., et al., *Gemtuzumab ozogamicin, a potent and selective anti-CD33 antibody–calicheamicin conjugate for treatment of acute myeloid leukemia.* Bioconjugate chemistry, 2002. **13**(1): p. 47-58.
281. Zhang, W.-W., et al., *The first approved gene therapy product for cancer Ad-p53 (Gendicine): 12 years in the clinic.* Human gene therapy, 2018. **29**(2): p. 160-179.
282. Sharma, P. and J.P. Allison, *The future of immune checkpoint therapy.* Science, 2015. **348**(6230): p. 56-61.
283. Leach, D.R., M.F. Krummel, and J.P. Allison, *Enhancement of antitumor immunity by CTLA-4 blockade.* Science, 1996. **271**(5256): p. 1734-1736.
284. Collins, A.V., et al., *The interaction properties of costimulatory molecules revisited.* Immunity, 2002. **17**(2): p. 201-210.
285. Krummel, M.F. and J.P. Allison, *CD28 and CTLA-4 have opposing effects on the response of T cells to stimulation.* The Journal of experimental medicine, 1995. **182**(2): p. 459-465.
286. Miyatake, S., et al., *Src family tyrosine kinases associate with and phosphorylate CTLA-4 (CD152).* Biochemical and biophysical research communications, 1998. **249**(2): p. 444-448.
287. Schneider, H. and C.E. Rudd, *Tyrosine phosphatase SHP-2 binding to CTLA-4: absence of direct YVKM/YFIP motif recognition.* Biochemical and biophysical research communications, 2000. **269**(1): p. 279-283.
288. Baroja, M.L., et al., *Inhibition of CTLA-4 function by the regulatory subunit of serine/threonine phosphatase 2A.* The Journal of Immunology, 2002. **168**(10): p. 5070-5078.
289. Marengère, L.E., et al., *Regulation of T cell receptor signaling by tyrosine phosphatase SYP association with CTLA-4.* Science, 1996. **272**(5265): p. 1170-1173.
290. Marasco, M., et al., *Molecular mechanism of SHP2 activation by PD-1 stimulation.* Science advances, 2020. **6**(5): p. eaay4458.
291. Patsoukis, N., et al., *PD-1 alters T-cell metabolic reprogramming by inhibiting glycolysis and promoting lipolysis and fatty acid oxidation.* Nature communications, 2015. **6**(1): p. 6692.
292. Taube, J.M., et al., *Colocalization of inflammatory response with B7-h1 expression in human melanocytic lesions supports an adaptive resistance mechanism of immune escape.* Science translational medicine, 2012. **4**(127): p. 127ra37-127ra37.
293. Chen, X., et al., *Expression of B7-H1 protein in human pancreatic carcinoma tissues and its clinical significance.* Ai Zheng, 2009. **28**(12): p. 1328-1332.

294. Shi, S.-J., et al., *B7-H1 expression is associated with poor prognosis in colorectal carcinoma and regulates the proliferation and invasion of HCT116 colorectal cancer cells.* PloS one, 2013. **8**(10): p. e76012.
295. Dong, H., et al., *Tumor-associated B7-H1 promotes T-cell apoptosis: a potential mechanism of immune evasion.* Nature medicine, 2002. **8**(8): p. 793-800.
296. Iwai, Y., et al., *Involvement of PD-L1 on tumor cells in the escape from host immune system and tumor immunotherapy by PD-L1 blockade.* Proceedings of the National Academy of Sciences, 2002. **99**(19): p. 12293-12297.
297. Tumeh, P.C., et al., *PD-1 blockade induces responses by inhibiting adaptive immune resistance.* Nature, 2014. **515**(7528): p. 568-571.
298. Herbst, R.S., et al., *Predictive correlates of response to the anti-PD-L1 antibody MPDL3280A in cancer patients.* Nature, 2014. **515**(7528): p. 563-567.
299. Hamid, O., et al., *Safety and tumor responses with lambrolizumab (anti–PD-1) in melanoma.* New England journal of medicine, 2013. **369**(2): p. 134-144.
300. Zaretsky, J.M., et al., *Mutations associated with acquired resistance to PD-1 blockade in melanoma.* New England Journal of Medicine, 2016. **375**(9): p. 819-829.
301. Tirosh, I., et al., *Dissecting the multicellular ecosystem of metastatic melanoma by single-cell RNA-seq.* Science, 2016. **352**(6282): p. 189-196.
302. Hugo, W., et al., *Genomic and transcriptomic features of response to anti-PD-1 therapy in metastatic melanoma.* Cell, 2016. **165**(1): p. 35-44.
303. Choi, J. and S.Y. Lee, *Clinical characteristics and treatment of immune-related adverse events of immune checkpoint inhibitors.* Immune network, 2020. **20**(1): p. e9.
304. Wang, Z., et al., *CAR-T therapy dilemma and innovative design strategies for next generation.* Cell Death & Disease, 2025. **16**(1): p. 211.
305. Gross, G., T. Waks, and Z. Eshhar, *Expression of immunoglobulin-T-cell receptor chimeric molecules as functional receptors with antibody-type specificity.* Proceedings of the National Academy of Sciences, 1989. **86**(24): p. 10024-10028.
306. Hombach, A., A. Hombach, and H. Abken, *Adoptive immunotherapy with genetically engineered T cells: modification of the IgG1 Fc 'spacer'domain in the extracellular moiety of chimeric antigen receptors avoids 'off-target'activation and unintended initiation of an innate immune response.* Gene therapy, 2010. **17**(10): p. 1206-1213.
307. Kochenderfer, J.N., et al., *Construction and preclinical evaluation of an anti-CD19 chimeric antigen receptor.* Journal of immunotherapy, 2009. **32**(7): p. 689-702.
308. Hudecek, M., et al., *The nonsignaling extracellular spacer domain of chimeric antigen receptors is decisive for in vivo antitumor activity.* Cancer immunology research, 2015. **3**(2): p. 125-135.
309. Alabanza, L., et al., *Function of novel anti-CD19 chimeric antigen receptors with human variable regions is affected by hinge and transmembrane domains.* Molecular Therapy, 2017. **25**(11): p. 2452-2465.
310. Milone, M.C., et al., *Chimeric receptors containing CD137 signal transduction domains mediate enhanced survival of T cells and increased antileukemic efficacy in vivo.* Molecular therapy, 2009. **17**(8): p. 1453-1464.
311. Futagawa, T., et al., *Expression and function of 4-1BB and 4-1BB ligand on murine dendritic cells.* International immunology, 2002. **14**(3): p. 275-286.
312. Zheng, C., et al., *Crystal structures of the TRAF2: cIAP2 and the TRAF1: TRAF2: cIAP2 complexes: affinity, specificity, and regulation.* Molecular cell, 2010. **38**(1): p. 101-113.
313. Mahoney, D., et al., *Both cIAP1 and cIAP2 regulate TNFα-mediated NF-κB activation.* Proceedings of the National Academy of Sciences, 2008. **105**(33): p. 11778-11783.
314. Vallabhapurapu, S., et al., *Nonredundant and complementary functions of TRAF2 and TRAF3 in a ubiquitination cascade that activates NIK-dependent alternative NF-κB signaling.* Nature immunology, 2008. **9**(12): p. 1364-1370.

315. Ea, C.-K., et al., *Activation of IKK by TNFα requires site-specific ubiquitination of RIP1 and polyubiquitin binding by NEMO.* Molecular cell, 2006. **22**(2): p. 245-257.
316. Lee, D.Y., et al., *4-1BB signaling activates the t cell factor 1 effector/β-catenin pathway with delayed kinetics via ERK signaling and delayed PI3K/AKT activation to promote the proliferation of CD8+ T Cells.* PloS one, 2013. **8**(7): p. e69677.
317. Chmielewski, M. and H. Abken, *CAR T cells releasing IL-18 convert to T-Bethigh FoxO1low effectors that exhibit augmented activity against advanced solid tumors.* Cell reports, 2017. **21**(11): p. 3205-3219.
318. Chmielewski, M. and H. Abken, *CAR T cells transform to trucks: chimeric antigen receptor–redirected T cells engineered to deliver inducible IL-12 modulate the tumour stroma to combat cancer.* Cancer Immunology, Immunotherapy, 2012. **61**(8): p. 1269-1277.
319. Kagoya, Y., et al., *A novel chimeric antigen receptor containing a JAK–STAT signaling domain mediates superior antitumor effects.* Nature medicine, 2018. **24**(3): p. 352-359.
320. Ma, L., et al., *Enhanced CAR–T cell activity against solid tumors by vaccine boosting through the chimeric receptor.* Science, 2019. **365**(6449): p. 162-168.
321. O'Leary, M.C., et al., *FDA approval summary: tisagenlecleucel for treatment of patients with relapsed or refractory B-cell precursor acute lymphoblastic leukemia.* Clinical Cancer Research, 2019. **25**(4): p. 1142-1146.
322. Maude, S.L., et al., *Chimeric antigen receptor T cells for sustained remissions in leukemia.* New England Journal of Medicine, 2014. **371**(16): p. 1507-1517.
323. Rickert, R.C., K. Rajewsky, and J. Roes, *Impairment of T-cell-dependent B-cell responses and Bl cell development in CD19-deficient mice.* Nature, 1995. **376**(6538): p. 352-355.
324. Maude, S.L., et al., *Tisagenlecleucel in children and young adults with B-cell lymphoblastic leukemia.* New England Journal of Medicine, 2018. **378**(5): p. 439-448.
325. Melenhorst, J.J., et al., *Decade-long leukaemia remissions with persistence of CD4+ CAR T cells.* Nature, 2022. **602**(7897): p. 503-509.
326. Rodriguez-Garcia, A., et al., *CAR-T cell-mediated depletion of immunosuppressive tumor-associated macrophages promotes endogenous antitumor immunity and augments adoptive immunotherapy.* Nature communications, 2021. **12**(1): p. 877.
327. Zebley, C.C., et al., *CD19-CAR T cells undergo exhaustion DNA methylation programming in patients with acute lymphoblastic leukemia.* Cell reports, 2021. **37**(9).
328. Anderson, N.D., et al., *Transcriptional signatures associated with persisting CD19 CAR-T cells in children with leukemia.* Nature medicine, 2023. **29**(7): p. 1700-1709.
329. Pircher, H., et al., *Tolerance induction in double specific T-cell receptor transgenic mice varies with antigen.* Nature, 1989. **342**(6249): p. 559-561.
330. Hogquist, K.A., et al., *T cell receptor antagonist peptides induce positive selection.* Cell, 1994. **76**(1): p. 17-27.
331. Seldin, M.F., et al., *Allelic variants of Ly-5 in inbred and natural populations of mice.* Immunogenetics, 1987. **26**: p. 74-78.
332. Liu, W., et al., *BAFF attenuates immunosuppressive monocytes in the melanoma tumor microenvironment.* Cancer research, 2022. **82**(2): p. 264-277.
333. Xu, H.C., et al., *Slow viral propagation during initial phase of infection leads to viral persistence in mice.* Communications Biology, 2021. **4**(1): p. 508.
334. Xu, H.C., et al., *Single MHC-I Expression Promotes Virus-Induced Liver Immunopathology.* Hepatology communications, 2022. **6**(7): p. 1620-1633.
335. Xu, H.C., et al., *Type I interferon protects antiviral CD8+ T cells from NK cell cytotoxicity.* Immunity, 2014. **40**(6): p. 949-60.
336. Xu, H.C., et al., *High-Affinity-Mediated Viral Entry Triggers Innate Affinity Escape Resulting in Type I IFN Resistance and Impaired T Cell Immunity.* J Immunol, 2024. **212**(9): p. 1457-1466.

337. Campos, C.G., et al., *New protocol based on UHPLC-MS/MS for quantitation of metabolites in xylose-fermenting yeasts.* Journal of The American Society for Mass Spectrometry, 2017. **28**(12): p. 2646-2657.
338. Marquis, B.J., et al., *A new derivatization reagent for HPLC–MS analysis of biological organic acids.* Chromatographia, 2017. **80**: p. 1723-1732.
339. Law, A.S., P.S. Hafen, and J.J. Brault, *Liquid chromatography method for simultaneous quantification of ATP and its degradation products compatible with both UV–Vis and mass spectrometry.* Journal of Chromatography B, 2022. **1206**: p. 123351.
340. Jones, A.E., et al., *A single LC-MS/MS analysis to quantify CoA biosynthetic intermediates and short-chain acyl CoAs.* Metabolites, 2021. **11**(8): p. 468.
341. Wicks, E.E. and G.L. Semenza, *Hypoxia-inducible factors: cancer progression and clinical translation.* J Clin Invest, 2022. **132**(11).
342. Prevost-Blondel, A., et al., *Tumor-infiltrating lymphocytes exhibiting high ex vivo cytolytic activity fail to prevent murine melanoma tumor growth in vivo.* J Immunol, 1998. **161**(5): p. 2187-94.
343. Liu, W., et al., *BAFF Attenuates Immunosuppressive Monocytes in the Melanoma Tumor Microenvironment.* Cancer Res, 2022. **82**(2): p. 264-277.
344. Koukourakis, M.I., et al., *Hypoxia-inducible factor (HIF1A and HIF2A), angiogenesis, and chemoradiotherapy outcome of squamous cell head-and-neck cancer.* International Journal of Radiation Oncology* Biology* Physics, 2002. **53**(5): p. 1192-1202.
345. Bannoud, N., et al., *Hypoxia supports differentiation of terminally exhausted CD8 T cells.* Frontiers in immunology, 2021. **12**: p. 660944.
346. Wu, H., et al., *Mitochondrial dysfunction promotes the transition of precursor to terminally exhausted T cells through HIF-1α-mediated glycolytic reprogramming.* Nature communications, 2023. **14**(1): p. 6858.
347. Cunha, P.P., et al., *Oxygen levels at the time of activation determine T cell persistence and immunotherapeutic efficacy.* Elife, 2023. **12**: p. e84280.
348. Palazon, A., et al., *An HIF-1alpha/VEGF-A Axis in Cytotoxic T Cells Regulates Tumor Progression.* Cancer Cell, 2017. **32**(5): p. 669-683 e5.
349. Wittenberg, J.B. and B.A. Wittenberg, *Myoglobin function reassessed.* J Exp Biol, 2003. **206**(Pt 12): p. 2011-20.
350. Kondadi, A.K., R. Anand, and A.S. Reichert, *Cristae Membrane Dynamics - A Paradigm Change.* Trends Cell Biol, 2020. **30**(12): p. 923-936.
351. Giacomello, M., et al., *The cell biology of mitochondrial membrane dynamics.* Nat Rev Mol Cell Biol, 2020. **21**(4): p. 204-224.
352. Cogliati, S., et al., *Mitochondrial cristae shape determines respiratory chain supercomplexes assembly and respiratory efficiency.* Cell, 2013. **155**(1): p. 160-71.
353. Green, A., T. Hossain, and D. Eckmann, *Mitochondrial dynamics involves molecular and mechanical events in motility, fusion and fission. Frontiers in cell and developmental biology, 10, 1010232*. 2022.
354. Chen, H. and D.C. Chan, *Physiological functions of mitochondrial fusion.* Annals of the New York Academy of Sciences, 2010. **1201**(1): p. 21-25.
355. Youle, R.J. and A.M. Van Der Bliek, *Mitochondrial fission, fusion, and stress.* Science, 2012. **337**(6098): p. 1062-1065.
356. Chen, W., H. Zhao, and Y. Li, *Mitochondrial dynamics in health and disease: mechanisms and potential targets.* Signal transduction and targeted therapy, 2023. **8**(1): p. 333.
357. Shadel, G.S. and T.L. Horvath, *Mitochondrial ROS signaling in organismal homeostasis.* Cell, 2015. **163**(3): p. 560-9.
358. Meister, A., *Selective modification of glutathione metabolism.* Science, 1983. **220**(4596): p. 472-7.

359. HARDIE, D.G., et al., *AMP-activated protein kinase: an ultrasensitive system for monitoring cellular energy charge.* Biochemical Journal, 1999. **338**(3): p. 717-722.
360. Miller, B.C., et al., *Subsets of exhausted CD8+ T cells differentially mediate tumor control and respond to checkpoint blockade.* Nature immunology, 2019. **20**(3): p. 326-336.
361. Li, J., et al., *High levels of Eomes promote exhaustion of anti-tumor CD8+ T cells.* Frontiers in immunology, 2018. **9**: p. 2981.
362. Pircher, H., et al., *Tolerance induction in double specific T-cell receptor transgenic mice varies with antigen.* Nature, 1989. **342**(6249): p. 559-61.
363. Xu, S., et al., *Uptake of oxidized lipids by the scavenger receptor CD36 promotes lipid peroxidation and dysfunction in CD8(+) T cells in tumors.* Immunity, 2021. **54**(7): p. 1561-1577 e7.
364. Clarke, S.R., et al., *Characterization of the ovalbumin-specific TCR transgenic line OT-I: MHC elements for positive and negative selection.* Immunology and cell biology, 2000. **78**(2): p. 110-117.
365. Kuburich, N.A., et al. *Vimentin and cytokeratin: Good alone, bad together*. in *Seminars in cancer biology*. 2022. Elsevier.
366. Gao, T.A. and Y.Y. Chen, *Engineering next-generation CAR-T cells: overcoming tumor hypoxia and metabolism.* Annual review of chemical and biomolecular engineering, 2022. **13**(1): p. 193-216.
367. Liu, G., et al., *Enhancing CAR-T cell efficacy in solid tumors by targeting the tumor microenvironment.* Cellular & Molecular Immunology, 2021. **18**(5): p. 1085-1095.
368. Liu, Y.-N., et al., *Hypoxia induces mitochondrial defect that promotes T cell exhaustion in tumor microenvironment through MYC-regulated pathways.* Frontiers in immunology, 2020. **11**: p. 1906.
369. Wu, Q., et al., *Hypoxia-inducible factors: master regulators of hypoxic tumor immune escape.* Journal of hematology & oncology, 2022. **15**(1): p. 77.
370. Lequeux, A., et al., *Targeting HIF-1 alpha transcriptional activity drives cytotoxic immune effector cells into melanoma and improves combination immunotherapy.* Oncogene, 2021. **40**(28): p. 4725-4735.
371. Semenza, G.L., et al., *Transcriptional regulation of genes encoding glycolytic enzymes by hypoxia-inducible factor 1.* J Biol Chem, 1994. **269**(38): p. 23757-63.
372. Semenza, G.L., et al., *Hypoxia response elements in the aldolase A, enolase 1, and lactate dehydrogenase A gene promoters contain essential binding sites for hypoxia-inducible factor 1.* J Biol Chem, 1996. **271**(51): p. 32529-37.
373. Phan, A.T., et al., *Constitutive Glycolytic Metabolism Supports CD8(+) T Cell Effector Memory Differentiation during Viral Infection.* Immunity, 2016. **45**(5): p. 1024-1037.
374. Ordway, G.A. and D.J. Garry, *Myoglobin: an essential hemoprotein in striated muscle.* J Exp Biol, 2004. **207**(Pt 20): p. 3441-6.
375. Sukumar, M., et al., *Inhibiting glycolytic metabolism enhances CD8+ T cell memory and antitumor function.* The Journal of clinical investigation, 2013. **123**(10): p. 4479-4488.
376. Cappel, D.A., et al., *Pyruvate-carboxylase-mediated anaplerosis promotes antioxidant capacity by sustaining TCA cycle and redox metabolism in liver.* Cell metabolism, 2019. **29**(6): p. 1291-1305. e8.
377. Ma, K., et al., *Succinate preserves CD8+ T cell fitness to augment antitumor immunity.* Immunity, 2025. **58**(10): p. 2505-2523. e8.
378. Xiao, B., et al., *Structure of mammalian AMPK and its regulation by ADP.* Nature, 2011. **472**(7342): p. 230-233.
379. Mangalhara, K.C., et al., *Manipulating mitochondrial electron flow enhances tumor immunogenicity.* Science, 2023. **381**(6664): p. 1316-1323.
380. Harel, M., et al., *Proteomics of melanoma response to immunotherapy reveals mitochondrial dependence.* Cell, 2019. **179**(1): p. 236-250. e18.

381. Liikanen, I., et al., *Hypoxia-inducible factor activity promotes antitumor effector function and tissue residency by CD8+ T cells.* J Clin Invest, 2021. **131**(7).
382. Wang, X., et al., *TOX promotes the exhaustion of antitumor CD8+ T cells by preventing PD1 degradation in hepatocellular carcinoma.* Journal of hepatology, 2019. **71**(4): p. 731-741.
383. Simon, S. and N. Labarriere, *PD-1 expression on tumor-specific T cells: Friend or foe for immunotherapy?* Oncoimmunology, 2018. **7**(1): p. e1364828.
384. Roussel, M., et al., *Functional characterization of PD1+ TIM3+ tumor-infiltrating T cells in DLBCL and effects of PD1 or TIM3 blockade.* Blood Advances, 2021. **5**(7): p. 1816-1829.
385. Li, J., et al., *Tumor-infiltrating Tim-3+ T cells proliferate avidly except when PD-1 is co-expressed: evidence for intracellular cross talk.* Oncoimmunology, 2016. **5**(10): p. e1200778.
386. Krishna, C., et al., *Single-cell sequencing links multiregional immune landscapes and tissue-resident T cells in ccRCC to tumor topology and therapy efficacy.* Cancer cell, 2021. **39**(5): p. 662-677. e6.
387. Van der Leun, A.M., D.S. Thommen, and T.N. Schumacher, *CD8+ T cell states in human cancer: insights from single-cell analysis.* Nature Reviews Cancer, 2020. **20**(4): p. 218-232.
388. Salti, S.M., et al., *Granzyme B regulates antiviral CD8+ T cell responses.* The Journal of Immunology, 2011. **187**(12): p. 6301-6309.
389. Zheng, W.-p. and R.A. Flavell, *The transcription factor GATA-3 is necessary and sufficient for Th2 cytokine gene expression in CD4 T cells.* Cell, 1997. **89**(4): p. 587-596.
390. Mulvey, A., et al., *Novel strategies to manage CAR-T cell toxicity.* Nature Reviews Drug Discovery, 2025: p. 1-19.
391. Bhaskar, S.T., et al., *Chimeric antigen receptor T-cell therapy yields similar outcomes in patients with and without cytokine release syndrome.* Blood advances, 2023. **7**(17): p. 4765-4772.
392. Shin, B., et al., *Mitochondrial oxidative phosphorylation regulates the fate decision between pathogenic Th17 and regulatory T cells.* Cell reports, 2020. **30**(6): p. 1898-1909. e4.

9. Acknowledgements

First, I want to thank especially Prof. Dr. Philipp Lang for his guidance and leadership throughout my research, which has been crucial for the completion of this work. His scientific foresight played a decisive role in helping to further develop this project.

Further, I want to thank my second supervisor Prof. Dr. Ingo Drexler for his helpful input and for agreeing to serve as the second reviewer for this thesis.

I want to thank Dr. Mitrajit Ghosh, who guided me and provided invaluable support, helping me shaping my work even further.

I want to thank Dr. Haifeng Xu for his incredible input, expertise and guidance throughout this study.

I want to thank Dr. Michał Gorzkiewicz for his support in and outside the laboratory. It was a pleasure working with you.

I further want to thank all my colleges for every incredible moment we shared both inside and outside the laboratory. Working alongside you has been truly enjoyable and was a great experience. Your support and friendship made this journey unforgettable.

Last, I want to thank my family and friends for their understanding, encouragement and their support in every situation. I am truly grateful for having you.

10. Statutory Declaration

I hereby swear under oath that the dissertation submitted here, entitled ‘Myoglobin expression improves T-cell metabolism and antitumor effector function’, was written independently by me and without impermissible external help, in accordance with the ‘Principles for Ensuring Good Scientific Practice at Heinrich Heine University Düsseldorf’. This work has not been submitted to any other examination authority in the same or a similar form.

_____ _____

(place, date) (signature)